

INFORMATION TO USERS

This manuscript has been reproduced from the microfilm master. UMI films the text directly from the original or copy submitted. Thus, some thesis and dissertation copies are in typewriter face, while others may be from any type of computer printer.

The quality of this reproduction is dependent upon the quality of the copy submitted. Broken or indistinct print, colored or poor quality illustrations and photographs, print bleedthrough, substandard margins, and improper alignment can adversely affect reproduction.

In the unlikely event that the author did not send UMI a complete manuscript and there are missing pages, these will be noted. Also, if unauthorized copyright material had to be removed, a note will indicate the deletion.

Oversize materials (e.g., maps, drawings, charts) are reproduced by sectioning the original, beginning at the upper left-hand corner and continuing from left to right in equal sections with small overlaps. Each original is also photographed in one exposure and is included in reduced form at the back of the book.

Photographs included in the original manuscript have been reproduced xerographically in this copy. Higher quality 6" x 9" black and white photographic prints are available for any photographs or illustrations appearing in this copy for an additional charge. Contact UMI directly to order.

UMI

**A Bell & Howell Information Company
300 North Zeeb Road, Ann Arbor MI 48106-1346 USA
313/761-4700 800/521-0600**

University of Alberta

**Morphology Development and Compatibilization
in Immiscible Polymer Blend Systems**

by

Parag G. Ghodgaonkar



A thesis submitted to the Faculty of Graduate Studies and Research
in partial fulfillment of the requirements for the degree of

MASTER OF SCIENCE

Department of Chemical and Materials Engineering

Edmonton, Alberta

Spring 1997



National Library
of Canada

Acquisitions and
Bibliographic Services

395 Wellington Street
Ottawa ON K1A 0N4
Canada

Bibliothèque nationale
du Canada

Acquisitions et
services bibliographiques

395, rue Wellington
Ottawa ON K1A 0N4
Canada

Your file *Votre référence*

Our file *Notre référence*

The author has granted a non-exclusive licence allowing the National Library of Canada to reproduce, loan, distribute or sell copies of his/her thesis by any means and in any form or format, making this thesis available to interested persons.

The author retains ownership of the copyright in his/her thesis. Neither the thesis nor substantial extracts from it may be printed or otherwise reproduced with the author's permission.

L'auteur a accordé une licence non exclusive permettant à la Bibliothèque nationale du Canada de reproduire, prêter, distribuer ou vendre des copies de sa thèse de quelque manière et sous quelque forme que ce soit pour mettre des exemplaires de cette thèse à la disposition des personnes intéressées.

L'auteur conserve la propriété du droit d'auteur qui protège sa thèse. Ni la thèse ni des extraits substantiels de celle-ci ne doivent être imprimés ou autrement reproduits sans son autorisation.

0-612-21166-5

University of Alberta
Library Release Form

Name of Author : Parag G. Ghodgaonkar
Title of Thesis : Morphology Development and Compatibilization in
Immiscible Polymer Blend Systems
Degree : Master of Science
Year This Degree Granted : 1997

Permission is hereby granted to the University of Alberta Library to reproduce single copies of this thesis and to lend or sell such copies for private, scholarly, or scientific research purposes only.

The author reserves all other publications and other rights in association with the copyright in the thesis, and except as hereinbefore provided, neither the thesis nor any substantial thereof may be printed or otherwise reproduced in any material form whatever without the author's written permission.



11025, Saskatchewan Drive
Edmonton, Alberta
T6G 2B4
Canada

January 28, 1997

UNIVERSITY OF ALBERTA

FACULTY OF GRADUATE STUDIES AND RESEARCH

The undersigned certify that they have read, and recommended to the Faculty of Graduate Studies and Research for acceptance, a thesis entitled **MORPHOLOGY DEVELOPMENT AND COMPATIBILIZATION IN IMMISCIBLE POLYMER BLEND SYSTEMS** submitted by **PARAG GHODGAONKAR** in partial fulfillment of the requirements for the degree of **MASTER OF SCIENCE**.




Dr. U. Sundararaj (Supervisor)



Dr. S. E. Wanke



Dr. M. C. Williams



Dr. M. L. Wayman

Date : JANUARY 21, 1997

ABSTRACT

This thesis investigates aspects of morphology development during polymer blending. The final mechanical and chemical properties of a polymer blend depend on the size of the dispersed phase. An attempt was made to predict this dispersed phase diameter from a simple force balance using the viscoelastic properties of the polymers. The elasticities of the two homopolymers influence breakup and are incorporated into the force balance. The predictions are compared with experimental data for non-reactive systems : PS/PP, PS/EPMA, PS/PE, PS/PA and reactive systems : PS-O α /EPMA and PSMA/PA. The model best describes the behavior for low dispersed phase concentrations (2 wt%) since the force balance is for a single drop in a polymer matrix. The PS/PP system exhibits a minimum in drop diameter with increasing shear rate (observed at 162.5 s⁻¹) and the force balance predicts it.

An externally added copolymer can compatibilize an immiscible polymer blend system. The order in which the components are added affects the compatibilization efficiency. Different addition orders were used for the compatibilization of two polymer blend systems (PS/PMMA and PS/LLDPE). Three symmetrical copolymers were used for the PS/PMMA system ($M_w = 50K$; 100K and 160K). Two triblock copolymers ($M_w = 75K$ and 275K) and a diblock copolymer ($M_w = 207K$) were used for the PS/LLDPE system. The best dispersions were obtained when the copolymer block molecular weight was comparable to that of the homopolymers.

The morphology development was visualized using a glass front plate designed for the Haake mixer. The systems studied were PA330/PS (reactive and non-reactive), PA330/EPMA and PC/PEI. The polymer pellets breakup into sheets which breakup to form holes. Colored pellets enabled better visualization of the breakup process. The effect of several parameters like shear rate, temperature ramping rate and weight fraction of the dispersed phase on phase inversion - phenomenon of switching of phases during melting - was studied.

Acknowledgments

I am grateful to Dr. Uttandaraman Sundararaj for his guidance and support throughout the course of this program. His patience and supervision during the different stages of this thesis is truly appreciated.

I would like to thank Dr. Michael C. Williams for allowing me the use of the RMS-800 and the DSC instruments in his lab. Special thanks to Wei-Yan Wang, Moin Muhammad and Ibnelwaleed Hussien for showing me the use of these instruments.

I thank Dr. Michael L. Wayman for letting me use the Scanning Electron Microscope for analyzing my polymer blend samples. I am extremely grateful to Tina Barker for accommodating me and helping me learn the SEM machine.

Assistance given by Walter Boddez of the Chemical and Materials Engineering Department is truly appreciated. I thank Keith Faulder and the Chemical Engineering Machine Shop for building the mixer front plate for the Haake mixer.

I value the help given by Jarrod Beztilyn, a summer student who performed many of the experiments whose results were used in Chapter 4 of this thesis. I appreciate the suggestions and ideas given by Mr. Manav Lahoti and Mr. Nikhil Rao, my research associates, for my experiments.

I gratefully acknowledge the Natural Sciences and Engineering Research Council of Canada for funding this project.

Finally, I wish to thank my parents, who have helped me at every stage of my life. My father, mother, and brother have been a source of inspiration and love for me. I also thank all my friends, for their support and love.

Table of Contents

Chapter 1. Introduction	1
1.1 Importance of Polymer Blends	1
1.2 Miscibility of Polymers	2
1.3 Mixing of Polymers	5
1.4 Compatibilization of Blends	8
1.5 Visualization	12
1.6 Survey of Thesis	12
1.7 References	13
Chapter 2. Prediction of the Dispersed Phase Drop Diameter in polymer blends	16
2.1 Introduction	16
2.2 Analysis	23
2.2.1 Theory behind the force balance	23
2.2.2 Particle Size Prediction	25
2.3 Experimental	27
2.3.1 Materials	27
2.3.2 Experiments	28
2.4 Results	31
2.5 Discussion	36
2.6 Conclusions	50
2.7 References	51
Chapter 3. Effect of Order of Addition on Compatibilization	53
3.1 Introduction	53
3.2 Experimental	55
3.2.1 Materials	55

3.2.2	Experimental Procedure	56
3.3	Results	61
3.4	Discussion	73
3.5	Conclusions	91
3.6	References	92
Chapter 4.	Visualization of Polymer Mixing	94
4.1	Introduction	94
4.2	Background	94
4.3	Experimental	96
4.3.1	Design of the Glass Plate	96
4.3.2	Material and Description of Runs	98
4.3.3	Procedure	100
4.4	Results	103
4.5	Discussion	122
4.6	Conclusions	129
4.7	References	130
Chapter 5.	Future Work and Recommendations	129
5.1	Future Experiments	132
5.1.1	Prediction of Polymer blend morphology	132
5.1.2	Factorial Design to predict particle diameter	132
5.1.3	Partial Least Squares	135
5.1.4	Extensional Flow	136
5.1.5	Compatibilization Studies	137
5.2	Recommendations	138
5.2.1	Image Analysis	138
5.2.2	Visualization Experiments	138
5.2.3	General Procedural Modifications	139

5.3	References	139
Appendix A	Calculation of Sample Weight	140
Appendix B	Calculation of Average Particle Diameter of the Dispersed Phase	144
Appendix C	Calculation of Shear rate in the mixer	149
Appendix D	Material properties of the polymers	151

LIST OF TABLES

Table 2.1	Properties of Materials Used	28
Table 2.2	Experimental Runs, T=200°C	29
Table 2.3	Shear rate, diameter measured (in microns) and specific energy input (KJ/Kg) for the systems studied	35
Table 3.1	Properties of Materials used	57
Table 3.2	Experimental Runs. (Temperature for all runs = 200°C)	59
Table 3.3	Results for the PS/PMMA system (with symmetrical PS/PMMA diblock copolymers)	63
Table 3.4	Results for the PS/LLDPE system	67
Table 4.1	Properties of Polymers	99
Table 4.2	PA/PS(MA) Runs (Reactive and Non-reactive)	102
Table 4.3	PA330/EPMA runs	102
Table 4.4	PC/PEI run (Non - Phase Inverting)	103
Table 5.1	Experimental model of a 2³ factorial design for a PE/PS system	134
Table B1	Area and Average diameter of each particle measured from Fig B2	146

LIST OF FIGURES

Fig 1.1	Phase diagram of a polymer blend showing temperature versus blend composition(%).	4
Fig 1.2	Schematic diagram of a Haake Rheocord batch mixer.	6
Fig 1.3	Tensile strength versus weight percent PS for a blend of PS and PP.[<i>adapted from Han (1981)</i>]	9
Fig 1.4	Effect of interfacial reaction on the normalized impact energy of PP/NBR blends [<i>adapted from Liu and Baker (1994)</i>]	10
Fig 2.1 (a)	Average diameter of PE dispersed in PS versus the volume fraction of PE. The temperature used was 200°C and the blending time was 300 s. The curves were obtained for a range of rotation speeds. [<i>Adapted from Huneault et al. (1985)</i>]	21
Fig 2.1 (b)	Average diameter of PE dispersed in PS versus shear rate. The diameter exhibits a minimum for nearly all volume fractions.	22
Fig 2.2	Effect of shear rate on the dispersed phase diameter for the PS/PP blend at different weight fractions of the dispersed PP phase. The 2%, 5% and 8% curves exhibit a minimum in diameter at a critical shear rate (162.5 s ⁻¹).	23
Fig 2.3	The shear and normal forces acting on a single block of polymer [<i>Adapted from Macosko, 1994</i>]	24
Fig 2.4	A schematic to explain the four main forces acting on a single polymer drop in a polymer matrix.	26
Fig 2.5	SEM micrographs of the PS/PP blend. All the micrographs are for 8 wt% dispersed phase . The pictures show the effect of shear rate on the drop diameter; (a) 52 s ⁻¹ , (b) 162.5 s ⁻¹ , and (c) 195 s ⁻¹ . It is observed that diameter goes through a minimum at around 162.5s ⁻¹ .	32
Fig 2.6	Effect of concentration on the dispersed phase diameter for the PS/PP blend. The micrographs are at the same shear rate (260 s ⁻¹) but different weight fractions; (a) 2% and (b) 20%. The diameter for the 20% sample is much higher than that for the 2% sample.	33
Fig 2.7 (a)	Comparison of experimentally observed drop diameter for the 2 wt% PP in PS system with the force balance predictions [equations 2.8 and 2.10]. Both experiments and models show a minimum in drop diameter at a critical shear rate.	37
Fig 2.7 (b)	Comparison of the experimentally observed drop diameter for 2% PS/PP with the predictions given by Taylor [equation 2.2] and Wu	38

	[equation 2.3].	
Fig 2.8 (a)	Effect of shear rate on the dispersed phase drop diameter for the non - reactive PS/EPMA system and the reactive PS-Ox/EPMA system (2 wt% EPMA). The diameter predicted from the force balance [equation 2.10] is also shown.	40
Fig 2.8 (b)	Comparison of the experimental drop diameters with Wu's correlation [equation 2.3] for the PS/EPMA system. Taylor's equation [2.2] predicts no breakup will occur.	42
Fig 2.9 (a)	Effect of shear rate on the dispersed phase drop diameter for the PS/PE system (2% and 5% PE). No minimum is observed for this system. The predicted values also suggest that there should be no minimum diameter for this shear rate range.	43
Fig 2.9 (b)	Comparison of the experimental drop diameters with Taylor's prediction [Equation 2.2] and with Wu's correlation [Equation 2.3] for the PS/PE system (2% and 5%).	44
Fig 2.10 (a)	Effect of shear rate on the dispersed phase drop diameter for the PS/PA330 system (2% PA330). Equation 2.10 cannot be used to predict drop diameter for this high viscosity ratio system. The effect of reaction on blend morphology is also studied for this system by blending PSMA5/PA330.	45
Fig 2.10 (b)	Comparison of the experimental drop diameters with Wu's correlation [Equation 2.3]. Taylor predicts no breakup will occur in this system for simple shear flow.	46
Fig 2.11	The diameter of the dispersed phase versus the specific energy input (kJ/kg). The curves followed a trend similar to that observed by varying shear rates [Figs 2.4, 2.8 (a) and 2.9(a)]. (a) PS666D/PP3050 (b) PS666D/EPMA (c) PS666D/PE752.	49
Fig 3.1	Average diameter of the dispersed PMMA phase (for a blend of 10 wt% PMMA in PS666D) versus PS-PMMA diblock concentration ($M_w=80K-80K$) (weight % of the dispersed phase). The temperature was 200°C and the rotation rate was 50 rpm. The critical diblock concentration to reach equilibrium was 4% of the dispersed phase (0.4% of the total blend).	62
Fig 3.2	Average diameter of the dispersed PMMA phase (for the 90:10 PS/PMMA system) versus PS-PMMA diblock molecular weight. The temperature for all blends was 200°C and the rotation speed was 50 rpm. The graph is plotted for the several different orders of addition. The diameters for each diblock are staggered to enable proper	64

	observation of the graph.	
Fig 3.3 (a)	Effect of order of addition of the components on the average dispersed phase particle diameter for the PS/PMMA system (compatibilizer is PS-PMMA diblock having $M_w=25K-25K$).	66
Fig 3.3 (b)	Torque profiles for the different orders of addition for the PS/PMMA system (PS-PMMA diblock $M_w = 25K - 25K$).	68
Fig 3.4 (a)	Effect of order of addition of the components on the average dispersed phase particle diameter for the PS/PMMA system (compatibilizer is PS-PMMA diblock having $M_w=50K-50K$).	69
Fig 3.4 (b)	Torque profiles for the different orders of addition for the PS/PMMA system (PS-PMMA diblock $M_w = 50K - 50K$).	70
Fig 3.5 (a)	Effect of order of addition of the components on the average dispersed phase particle diameter for the PS/PMMA system (compatibilizer is PS-PMMA diblock having $M_w=80K-80K$).	71
Fig 3.5 (b)	Torque profiles for the different orders of addition for the PS/PMMA system (PS-PMMA diblock $M_w = 80K - 80K$).	72
Fig 3.6	Average diameter of the dispersed LLDPE phase (for the 90:10 PS/LLDPE system) versus total compatibilizer molecular weight. The temperature for all blends was 200°C and the rotation speed was 50 rpm. The graph is plotted for the several different orders of addition. The diameters for each diblock are staggered to enable proper observation of the graph.	74
Fig 3.7	Effect of order of addition of the components on the average dispersed phase particle diameter for the PS/LLDPE system (compatibilization done by triblock having $M_w = 75 K$).	75
Fig 3.8	Effect of order of addition of the components on the average dispersed phase particle diameter for the PS/LLDPE system (compatibilization done by triblock having $M_w = 207 K$).	77
Fig 3.9	Effect of order of addition of the components on the average dispersed phase particle diameter for the PS/LLDPE system (compatibilization done by triblock having $M_w = 275 K$).	78
Fig 3.10	SEM micrographs showing the dispersed PMMA drops in a matrix of PS for the “emulsification” curve [Fig 3.1] of 90:10 PS:PMMA blend with the PS-PMMA 80K-80K diblock added at the following compositions: (a) 0.5 wt%, (b) 1 wt%, (c) 5 wt% and (d) 15 wt% of the dispersed phase concentration.	80
Fig 3.11	SEM micrographs showing the effect of molecular weight of the PS-PMMA diblock compatibilizer on the 90:10 PS/PMMA blend.	84

	All the micrographs are for the same order of addition (#4) using different diblock molecular weights (a) 25K-25K, (b) 50K-50K and (c) 80K-80K.	
Fig 3.12	SEM micrographs showing the effect of order of addition of the PS-PMMA diblock compatibilizer ($M_w = 80K-80K$) on the dispersed phase drop diameter for the PS/PMMA system. All the pictures are for the same diblock but represent the following orders of addition (a) no diblock, (b) order #1, (c) order #2, (d) order #3 and (e) order #4.	87
Fig 3.13	SEM micrographs showing the effect of molecular weight of the compatibilizer on the dispersed phase drop diameter for the 90:10 PS/LLDPE system. All the pictures are for the same order of addition [order #4] but the compatibilization is done using the following compatibilizers: (a) no compatibilizer, (b) $M_w = 75K$, (c) $M_w = 207K$ and (d) $M_w = 275K$.	89
Fig. 3.14	Formation of micelles for the case of (a) P(S-EP) diblock, and (b) P(S-EB-S) triblock. The compatibilizer in both (a) and (b) was added to the dispersed phase (LLDPE) first (addition order 2).	91
Fig 4.1 (a)	Design of the metal front plate used for the visualization purposes. The figure shows the orthographic views of the front plate of the mixer, (a) Front view and (b) Side view. The glass slab had the dimensions of the oval hole in the metal plate.	97
Fig. 4.1 (b)	The back plate (used to protect the glass plate) and the glass plate.	97
Fig 4.2	Torque and temperature profiles for the PAR/PS blend (80/20). The mixing was done at 50 rpm and with a ramp from 220 - 300°C at a rate of 5°C/min.	104
Fig 4.3.	Snapshots of the mixer window showing the different physical regimes as written below. The system is PAR/PS (80/20 blend) mixed at 50 rpm with a temperature ramp from 220-300°C at a rate of 5°C/min.	105
Fig 4.4	Morphology of the PAR/PS blend (80/20). The mixing was done at 50 rpm and with a ramp from 220 - 300°C at a rate of 5°C/minute. The final structure consists of PS drops dispersed in a matrix of PAR.	107
Fig 4.5	Effect of reaction. The torque is plotted versus the time for the 80:20 PA330/PS666D and the PA330/PSMA5% blends. The mixing was done at 125 rpm and the temperature was ramped from 80 to 180°C at 5°C/min. The reactive system shows a higher torque peak which occurs at a later time.	108

Fig 4.6	Effect of reaction. The torque is plotted versus the temperature for the 80:20 PA330/PS666D and the PA330/PSMA5% blends. The mixing was done at 125 rpm with a ramp from 80 - 180°C at 5°C/minute.	109
Fig 4.7	A non-reactive and reactive blend of PA330 and PS666D. The weight fraction of PS is 20% and the mixer was rotating at 125 rpm. (a) non-reactive and (b) reactive PA/PS. The SEM scans were taken at the end of the run, i.e. when the torque attained a constant value.	111
Fig 4.8.	PS morphology at different times after dissolving out the PA330 from the blend sample. The blend studied was PA330/PS=80:20 mixed at 125 rpm. The PA was dissolved using 95% formic acid (HCOOH).	112
Fig 4. 9.	PA morphology at different times after dissolving out PS from the blend sample. The blend is PA330:PS=80:20. The PS is dissolved using methylene chloride (CH ₃ Cl).	113
Fig. 4. 10	Snapshots of the mixer glass window showing the different physical regimes of the phase inversion process. The system shown is PA/PS (80/20 blend) mixed at 125 rpm with the temperature ramped from 80 - 180°C at a rate of 5°C/min.	114
Fig. 4. 11	Snapshots of the mixer glass window showing the different physical regimes of the phase inversion process. The system shown is PA/PSMA (80/20 blend) mixed at 125 rpm with the temperature ramped from 80 - 180°C at a rate of 5°C/min.	115
Fig 4.12 (a)	Effect of ramping. The torque versus time curves for the 80:20 PA330/PS666D blends mixed at three different ramps. The temperature was ramped from 80-180°C at rates of 1, 2, and 5°C/min. and the rotor was kept at 50 rpm.	117
Fig 4.12 (b)	Effect of ramping. The torque versus temperature curves for the 80:20 PA330/PS666D blends mixed at three different ramps. The temperature was ramped from 80-180°C at rates of 1, 2, and 5°C/min. and the rotor was kept at 50 rpm.	118
Fig 4.13 (a)	Effect of shear rate. The torque versus time profile for 80/20 PA330/PS blends mixed at four different rotation rates and ramped from 80-180°C at a rate of 5°C/min.	119
Fig 4.13 (b)	Effect of shear rate. The torque versus temperature profile for 80/20 PA330/PS blends mixed at four different rotation rates and ramped from 80-180°C at a rate of 5°C/min.	120
Fig 4.14	Torque profile for the PA330/EPMA blends. The effect of weight fraction of the dispersed phase was studied by changing EPMA	121

	concentration. All blends were made at 50 rpm and by ramping the temperature from 90 - 160°C at a rate of 2°C/min.	
Fig 4.15	Torque and temperature profiles for the PC/PEI blend (80/20). The mixing was done at 10 rpm and the temperature ramped from 200 to 300°C at a rate of 2°C/minute.	122
Fig 4.16	Snapshots of the glass front plate during mixing of an 80:20 PC/PEI blend. The mixing is done at 10 rpm and the temperature ramped from 200-300°C at a rate of 2°C/min.	123
Fig 5.1	Normal Plot for PE/PS system showing the interaction effects.	135
Fig B1	SEM micrograph of a 92:08 PS666D/PP3050 blend prepared at 200 °C in a mixer rotating at 75 rpm.	144
Fig B2	Picture showing the particles marked out from Fig B1.	145
Fig C1	Mixer barrel showing the velocity profile used to calculate the shear rate.	149
Fig D1	Complex viscosity versus frequency for PS666D and PP3050. The strain used was 10% and the temperature used was 200°C.	152
Fig D2	Elastic Moduli (G') versus frequency for PS666D and PP3050. The strain used was 10% and the temperature used was 200°C.	153

Chapter 1

INTRODUCTION

1.1 Importance of Polymer Blends

New polymers are constantly being synthesized to meet stricter requirements and needs. However, industrial demands are not fulfilled completely and successfully by these new materials. Additionally, the development and commercialization of these new polymers involves enormous costs (Sundararaj *et al.*, 1992). Polymer blends offer an attractive option to get the same enhanced properties in a more economical and simpler manner. A polymer blend is defined as a mixture of two or more polymers, each having a weight fraction of at least 2% (Utracki, 1995). Current research focuses on developing materials having good thermal and mechanical properties (Utracki, 1989).

Blends constitute an important aspect of the plastics industry and are expected to grow at a rate of 10% per annum (Favis, 1988; Utracki, 1995). The number of polymer blend patents has been increasing every year, and in the year 1995, there were about 4000 patents on polymer blends. However, the polymer blend industry is still relatively new and has yet to reach industrial maturity. The only commercial polymer blend so far which shows a steady sales is Cycovin from GE Plastics (Utracki, 1995). This is a PVC/ABS (polyvinylchloride/acrylonitrile butadiene styrene copolymer) blend. Blending can also extend the life of a product. It can also be used to recycle process scrap and post-consumer goods, which is very important today (Utracki, 1983).

1.2 Miscibility of polymers

One drawback (or perhaps benefit in some cases) associated with common polymer blends is that polymers are generally not miscible. Miscibility is a term used to describe the thermodynamics between the polymers (Verhoogt, 1992). Miscibility is used when the polymers mix on a microscopic level and form a single phase. The phase behavior of polymer blends is described by the Gibbs free energy of mixing, ΔG_m . The condition for miscibility is that the Gibbs free energy of mixing should be less than zero.

$$\Delta G_m = \Delta H_m - T\Delta S_m \quad (1.1)$$

where ΔH_m = Heat of mixing (J);

ΔS_m = Entropy of mixing (J/K);

T = Temperature (K).

This is a necessary but not a sufficient condition for miscibility. The additional condition that has to be satisfied is

$$\left(\frac{\partial^2 \Delta G_m}{\partial \phi_i^2} \right)_{T,P} > 0 \quad (1.2)$$

where ϕ_i = volume fraction of component i.

P = pressure (Pa).

Polymers are extremely large molecules and hence are not very mobile. Their high molecular weight reduces their freedom; i.e. the entropy of the polymer chains. Thus, the

entropy of mixing is generally low. Additionally, polymer-polymer mixing is usually endothermic, i.e. there is a positive heat of mixing. As a result, a polymer mixture is likely to be immiscible due to the positive ΔG_m . The miscibility can be increased only through the presence of certain interactions between the polymers which can result in a negative ΔG_m .

Polymer blends immiscible at low temperatures may be miscible at elevated temperatures. Fig 1.1 shows a phase diagram of temperature versus the percent composition of one phase of a polymer blend. A polymer blend exhibits two - phase behavior at low temperatures and one - phase behavior at elevated temperatures. At the temperatures where blending was done in this thesis, the blend behavior is two - phase. Operating at elevated temperatures to make the blend miscible is not beneficial. The polymers usually degrade if they are kept for prolonged times at higher temperatures and this will affect the final morphology as well as the mechanical properties. In addition, it is not always desirable to have a single phase. There are instances when the two - phase structure is preferred.

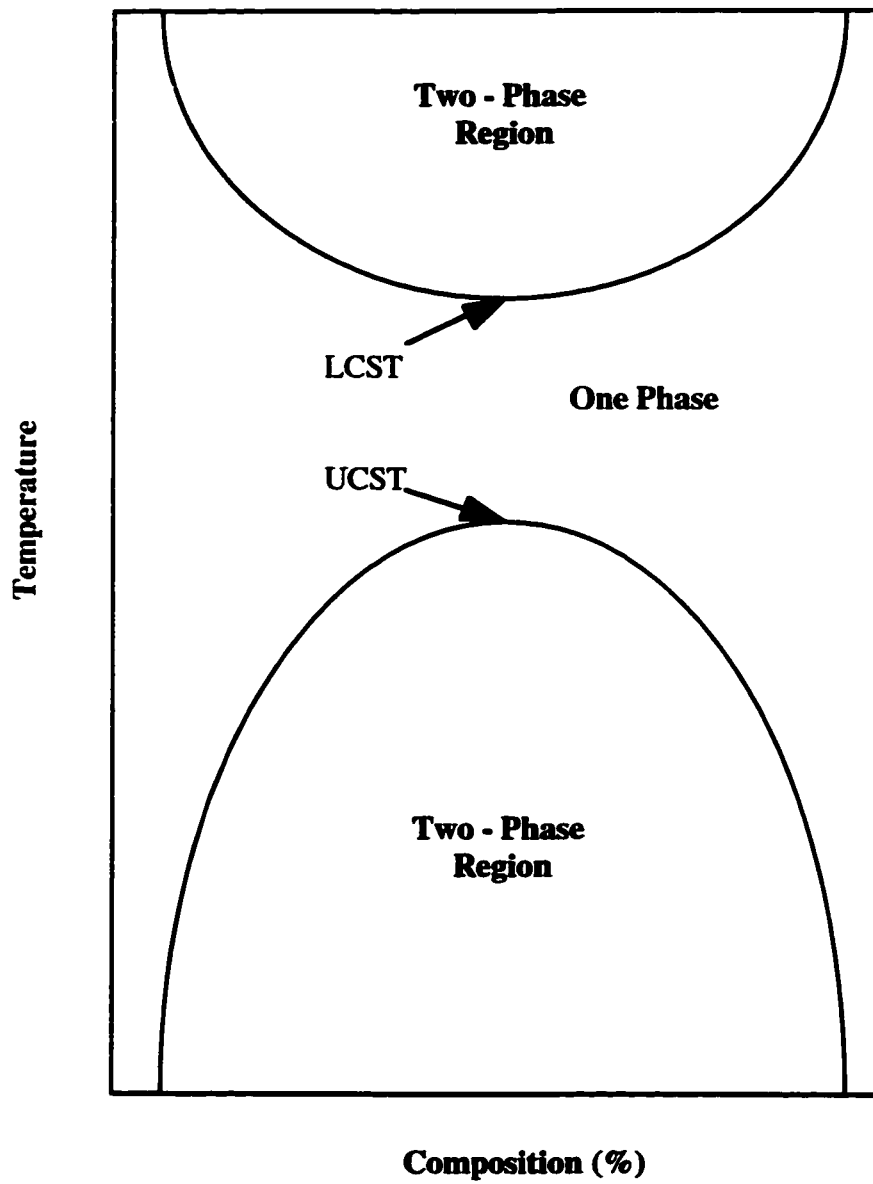


Fig 1.1
Phase diagram of a polymer blend showing temperature versus blend composition (%).
LCST : Lower Critical Solution Temperature
UCST : Upper Critical Solution Temperature

1.3 Mixing of Polymers

The mixing of polymers to obtain better mechanical and chemical properties has been studied by several researchers. The properties of a final polymer blend are dependent on the morphology which includes the size of the dispersed phase, the shape of the dispersed phase drops and the size distribution. Most blends are prepared by mechanically dispersing one polymer inside another. The dispersed phase size is a good measure of the efficiency of the mixing process. The blending is usually performed in a twin-screw extruder. Several researchers (Schreiber, 1983; Plochocki, *et al.*, 1990; Favis, 1990) have observed that after a certain initial time period, there is no significant change in the morphology of a blend made in a batch mixer. The effect of time in a batch mixer is equivalent to the effect of length in a twin-screw extruder (Sundararaj *et al.*, 1992). All the blends were made in a Haake Rheocord batch mixer. Fig. 1.2 shows a picture of the batch mixer with the roller blades. The experimental procedure is described in detail in the following chapters. The major reduction in the dispersed phase takes place within the first few minutes of mixing in a batch mixer (Scott and Macosko, 1994).

A mixing operation involves two basic mechanisms: mixing by dispersion and mixing by distribution (Huneault *et al.*, 1995). Dispersion is a process by which the dispersed phase is broken down by the shearing action to form a number of smaller particles. Distributive mixing is defined as the uniform distribution of the particles throughout the matrix or major phase. Dispersion involves the reduction of size of the particles and distribution involves their homogenization among the major phase.

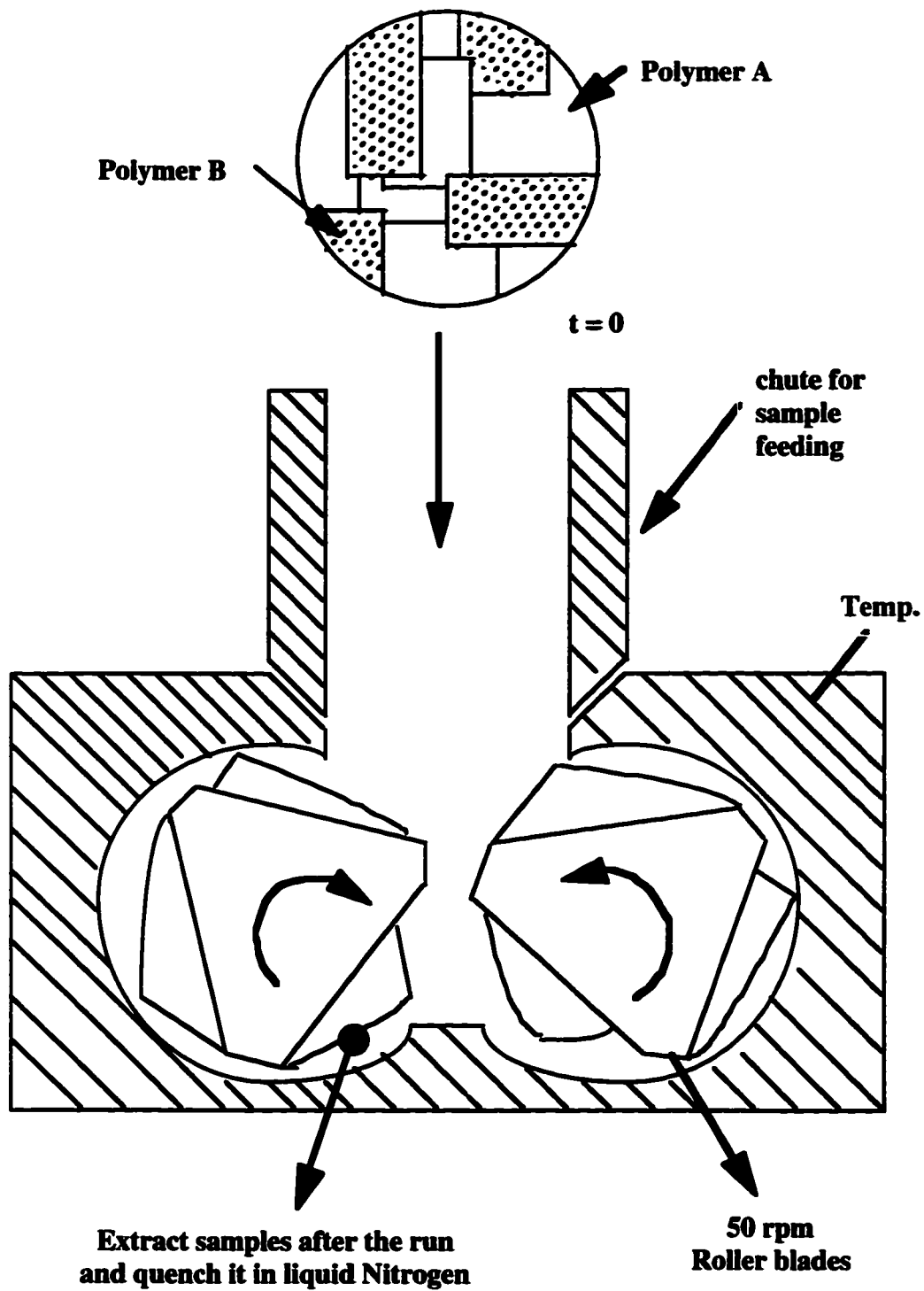


Fig 1.2
Schematic diagram of a Haake Rheocord batch mixer.

The size and shape of the pellets of polymer added to the mixer at the start are very important in controlling the final dispersion.

The pioneering work in studying the deformation of a drop in a matrix has been done by Taylor (1932). He studied the deformation in shear flow of a Newtonian drop in a Newtonian matrix and modeled the drop diameter based on the viscosity ratio and the Capillary number (Ca):

$$Ca \equiv \frac{\dot{\gamma} \eta_m D}{2\Gamma} \quad (1.3)$$

where $\dot{\gamma}$ is the shear rate; η_m is the matrix phase viscosity; D is the diameter of the drop; and Γ is the interfacial tension. He reported that for a Newtonian system, no deformation takes place beyond a viscosity ratio of 2.5. For polymer systems, the deformation process is much more complex (Scott and Macosko, 1991; Huneault *et al.*, 1995; Sundararaj *et al.*, 1992; Sundararaj *et al.*, 1995).

The critical Capillary number relations (when the drop breaks) are different than those for Newtonian systems and thus, the breakup can occur at viscosity ratios above 2.5 (Chapter 2 of this thesis). The flow field in a batch mixer or an extruder is complex and combines the shear as well as extensional deformation. Hence, prediction of the morphology development is extremely challenging. Several researchers have tried to model the morphology development during mixing (Huneault *et al.*, 1995; Sundararaj *et al.*, 1995; van Oene, 1972). The polymer deforms by forming sheets (Scott and Macosko, 1991; Sundararaj *et al.*, 1995). These sheets develop holes inside them which grow and

coalesce and thus, break the sheets into ligaments. These ligaments elongate up to a point and then break up into small domains by Rayleigh-type instabilities. The amount of deformation depends on the system parameters like interfacial tension. Plochocki (1990) has postulated a mechanism of abrasion for the morphology development in the initial melting stage. The final dispersed phase drop size is determined by a dynamic equilibrium between the breakup and coalescence (Roland and Böhm, 1984; Elmendorp, 1986). Coalescence has been reported to depend on several factors like concentration of the dispersed phase, mobility of the interface and the time of collision between drops.

One of the important factors neglected while studying morphology development is the elasticity of the polymer (van Oene, 1972). Polymers differ from Newtonian liquids in their elastic behavior. The elasticity of the polymer offers a resistance to the deformation and thus stabilizes the drop.

1.4 Compatibilization of blends

Polymers are generally incompatible with each other. Fig. 1.3 gives an example of the incompatibility of two polymers, polystyrene (PS) and polypropylene (PP) (Han, 1981). The figure shows a graph of tensile strength versus weight percent of the PS. The homopolymers display better tensile strengths (for 0 and 100% PS) than the blends.

The effect of compatibilization on mechanical properties is shown in Fig. 1.4. The figure shows the Notched Izod Impact energy versus the number average particle diameter for a blend of polypropylene (PP) and acrylonitrile-*co*-butadiene-*co*-acrylic acid rubber (NBR) (Liu and Baker, 1993). The normalized impact energy for the reactive

blend is definitely higher than that for the non-reactive blend, for the same dispersed rubber particle size. Thus, compatibilization leads to improved mechanical properties.

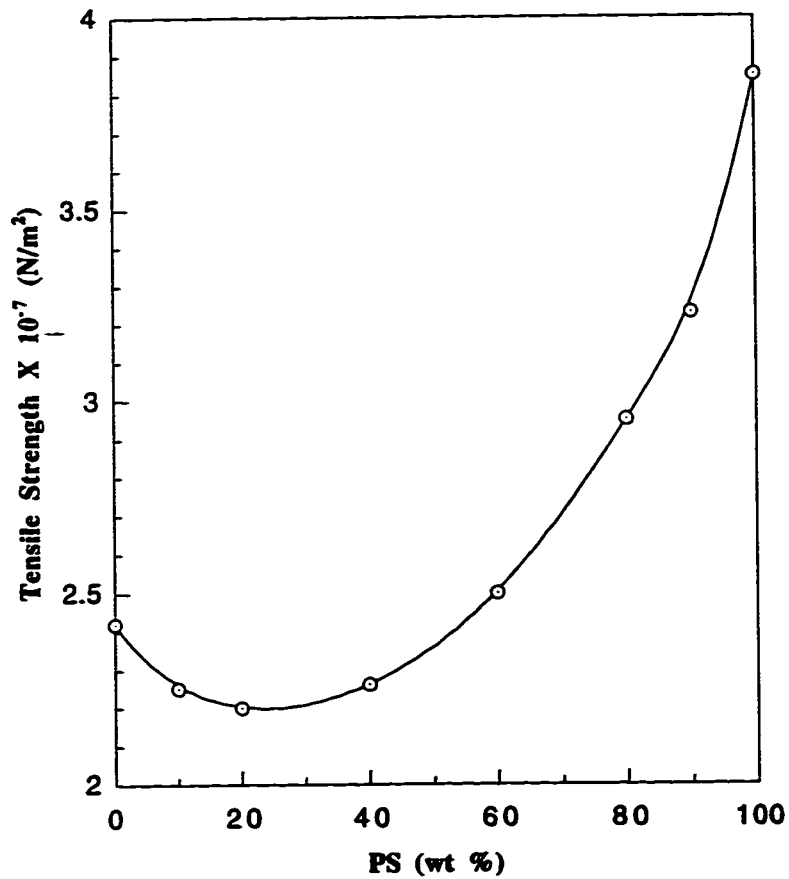


Fig 1.3
Tensile strength versus weight percent PS for a blend of PS and PP.[*adapted from Han (1981)*]

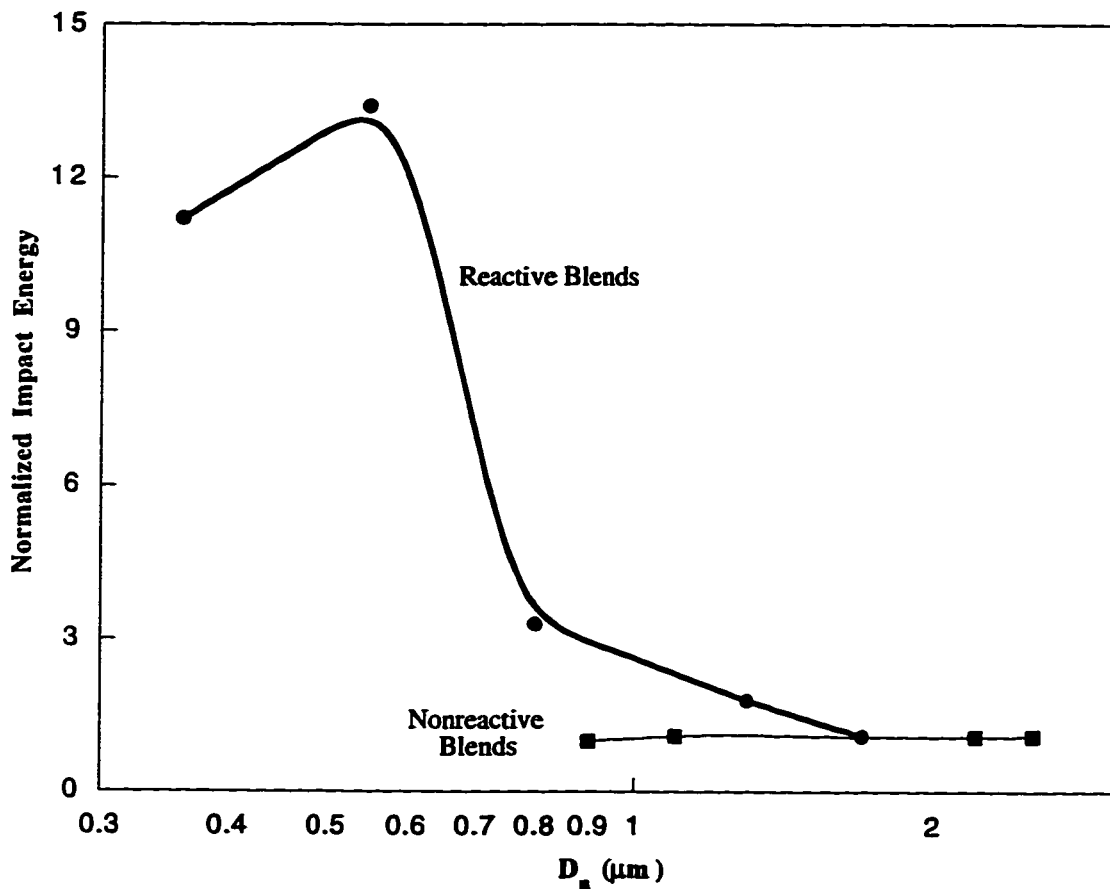


Fig 1.4
 Effect of interfacial reaction on the normalized impact energy of PP/NBR blends [*adapted from Liu and Baker (1994)*]

Compatibilization of the interface between polymers has been studied in detail (Locke and Paul, 1973; Liu and Baker, 1992). The compatibilization can be done either by adding an external modifier or by stabilizing the interface by forming a copolymer *in situ*. The compatibilizer forms a third phase between the two polymers thereby

increasing the adhesion between the two phases. Usually, the compatibilizer is either a diblock or a triblock having blocks which are of the same material as the homopolymers.

It has been shown (Wu, 1985) that as the dispersed particle size decreases, there is an increase in the mechanical property (Notched Izod impact strength) of a nylon and rubber blend. The reactive system of nylon and rubber had smaller particle diameter and showed even better impact strength. Thus, the general rule is that a smaller dispersed phase diameter leads to improved mechanical properties. As a result, compatibilization becomes even more important as it leads to smaller dispersed phase diameters.

It has been reported that adding a compatibilizer lowers the interfacial tension between homopolymers and stabilizes the interface against coalescence (Anastasiadis *et al.*, 1989; Elemans *et al.*, 1990). The coalescence can be almost eliminated by forming a copolymer *in situ* during blending (Nakayama *et al.*, 1993; Sundararaj and Macosko, 1995). The effect is pronounced at higher weight fractions of the dispersed phase. When an external diblock or triblock is added to the system, the diblock may not diffuse to the interface (Sundararaj and Macosko, 1995; Nakayama, 1993). The long molecules cannot diffuse to the interface and hence, the stabilization is not complete. Also, in some cases, the compatibilizer may be stuck in one of the phases in the form of micelles. Thermodynamically, the compatibilizer always prefers to be at the interface (Leibler, 1988). However, when the molecules are very large, the shear forces may not break the micellar structure and no compatibilizer reaches the interface. Since diffusion is extremely important for an externally compatibilized system, the order in which the several components are added to the mixer is critical.

1.5 Visualization

In industry, blends are usually prepared using an extruder. The only polymer that can be seen visually is the final product that comes out of the extruder. The steps that a polymer goes through while shearing are very important in understanding the final structure. Work has been done by several researchers (Scott and Macosko, 1991; Sundararaj *et al.*, 1992) in observing the breaking mechanism of a polymer. Another interesting phenomenon observed is that of phase inversion (Shih, 1992; Sundararaj *et al.*, 1996). This happens for the case where the minor phase has a melting transition below that of the major phase. The minor phase melts first and envelops the major phase. As the major phase melts, more and more of the polymer goes into the molten state. This leads to an inversion in continuity as the major phase becomes the continuous phase. The polymer mixing was visualized by constructing a glass front plate and recording the mixing using a video camera and VCR.

1.6 Survey of the Thesis

The following chapters deal with some of the key factors which determine the morphology of a polymer blend during mixing. The objective of this thesis is to bring together the knowledge about these factors to better understand the morphology in polymer blends. The contents of each chapter are mentioned briefly below.

Chapter 2 deals with the effect of elasticity in predicting the dispersed phase drop diameter in a polymer blend. A force balance is used and an equation is proposed to predict the dispersed phase drop diameter. The force balance is tested for several systems and the results are compared with experimentally observed diameters. The

equation is able to qualitatively predict the drop diameter for several systems. It was also able to explain the minimum observed when the drop diameter was plotted with shear rate for some systems. Some of the drawbacks of the balance are also presented.

Chapter 3 deals with the effect of order of addition of the several components on the degree of compatibilization for two polymer blend systems. Four orders of addition were studied. It has been shown that the addition order plays a crucial role in the compatibilization process. The best dispersion was achieved when all the components were premelted before mixing and an explanation for this is given. The effects of compatibilizer molecular weight and compatibilizer concentration are also studied.

In Chapter 4, visualization is done during polymer blending and the video images help in understanding the torque profile, and hence, the morphology development. A glass plate was built onto the front part of the batch mixer and the mixing process was observed. The phenomenon of phase inversion was also studied. The melting torque peaks of the two homopolymers were resolved by slowly ramping the temperature. In the final chapter, recommendations for future work are presented.

1.5 References

- Anastasiadis, S. J.; Gancarz, I.; Koberstein, J. T., *Macromolecules*, **22**, 1449 (1989).
- Elemans, P. H. M.; Janssen, J. H. M.; Meijer, H. E. H., *J. Rheol.*, **34**, 1311 (1990).
- Elmendorp, J. J.; Vegt, A. K. van der, *Polym. Eng. Sci.*, **26**, 1332 (1986).
- Favis, B. D.; Chalifoux, J. P., *Polymer*, **29**, 1761 (1988).
- Favis, B. D., *J. Appl. Polym. Sci.*, **39**, 285 (1990).

- Han, C. D., in "Multiphase Flow in Polymer Processing", Ch.1, Academic Press, 1981.
- Huneault, M. A.; Champagne, M. F.; Daigneault, L. E.; and Dumoulin, M. M., *Annual Technical Conference, Society of Plastics Engineers (SPE), ANTEC '95*, 2020 (1995).
- Leibler, L., *Makromol. Chem., Macromol. Symp.*, **16**, 1 (1988).
- Liu, N. C.; Baker, W. E., *Polym. Eng. Sci.*, **32**, 1695 (1992).
- Liu, N. C.; Baker, W. E., *Polymer*, **35**, 988 (1994).
- Locke, C. E.; Paul, D. R., *J. Appl. Polym. Sci.*, **17**, 2791 (1973).
- Nakayama, A.; Guegan, P.; Hirao, A.; Inoue, T.; Macosko, C. W., *Polym. Prepr. (Am. Chem. Soc., Div. Polym. Chem.)*, **34** (2), 840 (1993).
- Paul, D. R.; Newman, S., in "Polymer Blends", Vol. 1, Ch. 1, Academic Press, New York (1978).
- Plochocki, A. P.; Dagli, S. S.; Andrews, R. D., *Polym. Eng. Sci.*, **30**, 741 (1990).
- Roland, C. M.; Böhm, G. G. A., *J. Polym. Sci.: Polym. Phys.*, **22**, 79 (1984).
- Schreiber, H. P.; Olguin, A., *Polym. Eng. Sci.*, **23**, 129 (1983).
- Scott, C. E.; Macosko, C. W., *Polym. Bull.*, **26**, 341 (1991).
- Scott, C. E.; Macosko, C. W., *Polymer*, **35**, 5422 (1994).
- Scott, C. E.; Macosko, C. W., *Polymer*, **36**, 461 (1995).
- Shih, C. K.; Tynan, D. G.; Denelsbeck, D. A., *Polym. Eng. Sci.*, **31**, 1670 (1991).
- Shih, C. K., *Adv. Polym. Tech.*, **11**, 223 (1992).
- Sundararaj, U.; Macosko, C. W.; Rolando, R. J.; Chan, H. T., *Polym. Eng. Sci.*, **32**, 1814 (1992).
- Sundararaj, U., Ph. D. Thesis, University of Minnesota, Minneapolis, MN (1994).
- Sundararaj, U.; Macosko, C. W., *Macromolecules*, **28**, 2647 (1995).

Sundararaj, U.; Macosko, C. W.; Shih, C. K., *Polym. Eng. Sci.*, **36**, 1769 (1996).

Taylor, G. I., *Proc. R. Soc. London*, **A138**, 41 (1932).

Utracki, L. A., *Polym. Eng. Sci.*, **23**, 602 (1983).

Utracki, L. A., in "Polymer Alloys and Blends", Ch.1, Hanser Publishers, Munich (1989).

Utracki, L. A., *Polym. Eng. Sci.*, **35**, 2 (1995).

van Oene, H., *J. Colloid Interface Sci.*, **40**, 448 (1972).

Verhoogt, H., Ph. D. Thesis, Delft University, 1992.

Wu, S., *Polymer*, **26**, 1855 (1985).

Chapter 2

PREDICTION OF THE DISPERSED PHASE DROP DIAMETER IN POLYMER BLENDS

2.1 Introduction

Polymer blends have emerged as one of the most efficient means of obtaining new materials having improved mechanical properties (Paul, 1978; Utracki, 1989; Fayt *et al.*, 1989). The morphology obtained by compounding or processing of polymer blends cannot be easily predicted and poses a great challenge for both industrial and academic researchers. The blend morphology can control the final properties of the polymer. Hence, a predictive model for morphology development as a function of polymer properties, operational parameters and flow geometry is very useful for blend design.

A neutrally buoyant, initially spherical droplet suspended in another liquid and subjected to shear or extensional stress experiences deformation and then breaks up into smaller droplets. Taylor (1932, 1934) performed the pioneering work on the dispersion of a single Newtonian liquid droplet in another Newtonian liquid subjected to a planar simple shear. He modeled drop size using viscosity ratio, $\eta_r = \eta_d/\eta_m$, and capillary number, Ca:

$$Ca \equiv \frac{\dot{\gamma} \eta_m D}{2\Gamma} \quad (2.1)$$

where $\dot{\gamma}$ is the shear rate; η_m is the matrix phase viscosity; η_d is the dispersed phase viscosity; D is the diameter of the drop; and Γ is the interfacial tension. The Capillary number is equivalent to an effective shear rate. At a certain critical value of Capillary number, the droplet breaks.

For simple shear flow, Taylor balanced the interfacial forces and the shear forces and obtained a relation for the maximum drop size which would be stable:

$$D = \frac{4\Gamma(\eta_r + 1)}{\dot{\gamma} \eta_m (\frac{19}{4}\eta_r + 4)} \quad \eta_r < 2.5 \quad (2.2)$$

However his theory was based on several simplifying assumptions. He assumed that the drop remained spherical and that there was no slip at the surface of the drop. Taylor predicted that no drop breakup occurs when $\eta_r > 2.5$. Drop breakup was investigated further by several researchers (Cox, 1969; Acrivos and Lo, 1978; Chin and Han, 1979,1980; Flumerfelt, 1980; Hinch and Acrivos, 1980; Rallison; 1981; Bentley and Leal, 1986 a & b). In extensional flow, it has been shown (Acrivos and Lo, 1978; Chin and Han, 1979; Rallison, 1981; Grace, 1982; Bentley and Leal, 1986; deBruijn, 1989) that the critical Capillary number is lower than that in case of simple shear flow. Grace (1982) has performed a study of drop breakup in Newtonian mixtures for both simple shear and extensional flows. It was shown experimentally that drop breakup is possible in pure extensional flow at all viscosity ratios but is impossible in simple shear flow above $\eta_r = 4$. Polymer melts are non-Newtonian and polymer mixers have flow patterns consisting of a mixture of simple shear flow and extensional flow. Hence, the modeling of polymer systems is more complicated than Newtonian systems.

For Newtonian drops suspended in a viscoelastic fluid and subjected to an extensional flow field, Flumerfelt (1980) reported that there is a minimum drop size below which breakup cannot be achieved. This minimum drop size value is larger when the medium is elastic; that is, elasticity tends to stabilize the droplets.

Molten polymers are viscoelastic liquids at processing conditions. In polymer-polymer systems, the droplets not only experience dissipative (viscous) forces, but also the deformation resisting forces around the droplet arising from elasticity (Utracki and Shi, 1992). Therefore, the mechanism of drop deformation and breakup is quite different in viscoelastic systems than that in Newtonian systems. The droplet elasticity tends to

stabilize the drop during deformation. Drop deformation is mainly influenced by the ratio of shear stress, τ , (which is exerted by the external flow field) and the stabilizing interfacial stress, Γ/R (where Γ is the interfacial tension and R is the radius). This ratio is defined as the Capillary number. There is usually a critical Capillary number for a drop beyond which it will break up. When the $Ca \gg Ca_{crit}$, the dispersed phase particles extend into threads. When $Ca \ll 1$, coalescence is observed.

When both the droplets and suspending medium are viscoelastic liquids, it is generally believed that the viscosity ratio should be close to 1 to obtain the finest dispersion (Wu, 1987). Wu (1987) reported that viscoelastic drops can breakup during extrusion even at high viscosity ratios; $\eta_r > 4$. He obtained a correlation relating Capillary number (which he mistakenly termed as Weber number) to viscosity ratio for twin-screw extruded polymer blends. He obtained an expression for the final particle diameter as:

$$D = \frac{4 \Gamma \eta_r^{\pm 0.84}}{\dot{\gamma} \eta_m} \quad (2.3)$$

where the (+) sign in the exponent applies for $\eta_r > 1$ and the (-) sign applies for $\eta_r < 1$. This relation cannot be related to the Taylor limit (single drop breakup) because all the blends used had a dispersed phase concentration of 15 wt%. In addition, the complex nature of deformation during the flow through an extruder makes it difficult to fully understand the breakup phenomenon. Wu suggested that as the viscosity ratio increases above unity or decreases below unity, the dispersed particles become larger. Similar results were obtained by Favis and Chalifoux (1987). It should be noted that these researchers used mixers which had a complex combination of shear and extensional flows. No comments were made on the effects of polymer viscoelasticity.

Van Oene (1972) reported that the elasticity of the polymers plays an important role in deformability of drops in addition to viscosity ratio and the interfacial tension. He developed a relation for the dynamic interfacial tension coefficient:

$$\Gamma_{12} = \Gamma_{12}^o + (D/12)[N_{1,d} - N_{1,m}] \quad (2.4)$$

where Γ_{12}^o is the interfacial tension in a quiescent polyblend, $N_{1,d}$ is the first normal stress difference of the dispersed phase and $N_{1,m}$ is the first normal stress difference of the matrix phase. The equation predicted that higher elasticity of the dispersed phase results in larger drops. However, the equation can give a negative interfacial tension value which is nonsensical.

Roland and Bohm (1984) studied the influence of coalescence in two-phase polymeric fluids. They reported that coalescence in polymer blend systems is caused by drop collisions as well as Brownian motion. They found that as the shear rate is increased, there is an increase in coalescence which is opposite to the result expected. Tokita (1977) suggested that equilibrium drop diameter in blending originates from continuous breakup and coalescence of the dispersed particles. He assumed that the coalescence is proportional to the number of collisions. He proposed an equation for the equilibrium drop size which predicts that the equilibrium particle size is smaller when the stress field increases, the interfacial tension decreases, and when the volume fraction of the dispersed phase decreases. However, the values predicted from the theory did not compare well with experimental data. Several other researchers have studied the effect of coalescence on the final equilibrium drop diameter (Elmendorp and der Vegt, 1986; Plochocki *et al.*, 1990; Sundararaj and Macosko, 1995; Huneault *et al.*, 1995). During mixing, Plochocki *et al.* (1990) observed that the diameter of the dispersed phase decreases progressively until a minimum droplet size is achieved beyond which the droplet size increases at higher shear rates.

M. A Huneault *et al.* (1995) reported that the average diameter of polyethylene (PE) dispersed in a matrix of polystyrene (PS) phase increases with the volume fraction of the dispersed polyethylene phase for a range of rotation rates (Fig. 2.1a). They plotted the average particle diameter versus the volume fraction of the dispersed phase. They assumed that the rotation rates had little effect on morphology. An interesting phenomenon which the authors did not note was that as the rotation rate increased, the particle diameter decreases first and after a certain critical rotation rate, the diameter increases again. The drop diameter versus shear rate for the different concentrations has been replotted in Fig.2.1(b). The curves exhibit minima at a critical shear rate for all concentrations of PE.

Similar results were obtained when a system of PS and polypropylene (PP) was blended. The results are shown in Fig. 2.2. These results were reproducible for all the concentrations chosen. In this chapter, an attempt is made to explain this phenomenon and a general equation is proposed which predicts the particle size using a simple force balance. The forces that deform a droplet are the shear forces and the matrix first normal force. These forces are balanced by the forces that resist deformation, the interfacial forces and the droplet first normal force. It should be noted that these forces are acting in different axes. However, this balance is used as a first approximation. From the balance, the diameter of the dispersed phase is expressed in terms of the rheological properties of the two polymers. The calculation is compared with the experimental data. The effects of using reactive blends on drop size will also be shown. In this case, the interface between the two polymers is stabilized by reaction and coalescence is eliminated (Sundararaj and Macosko, 1995).

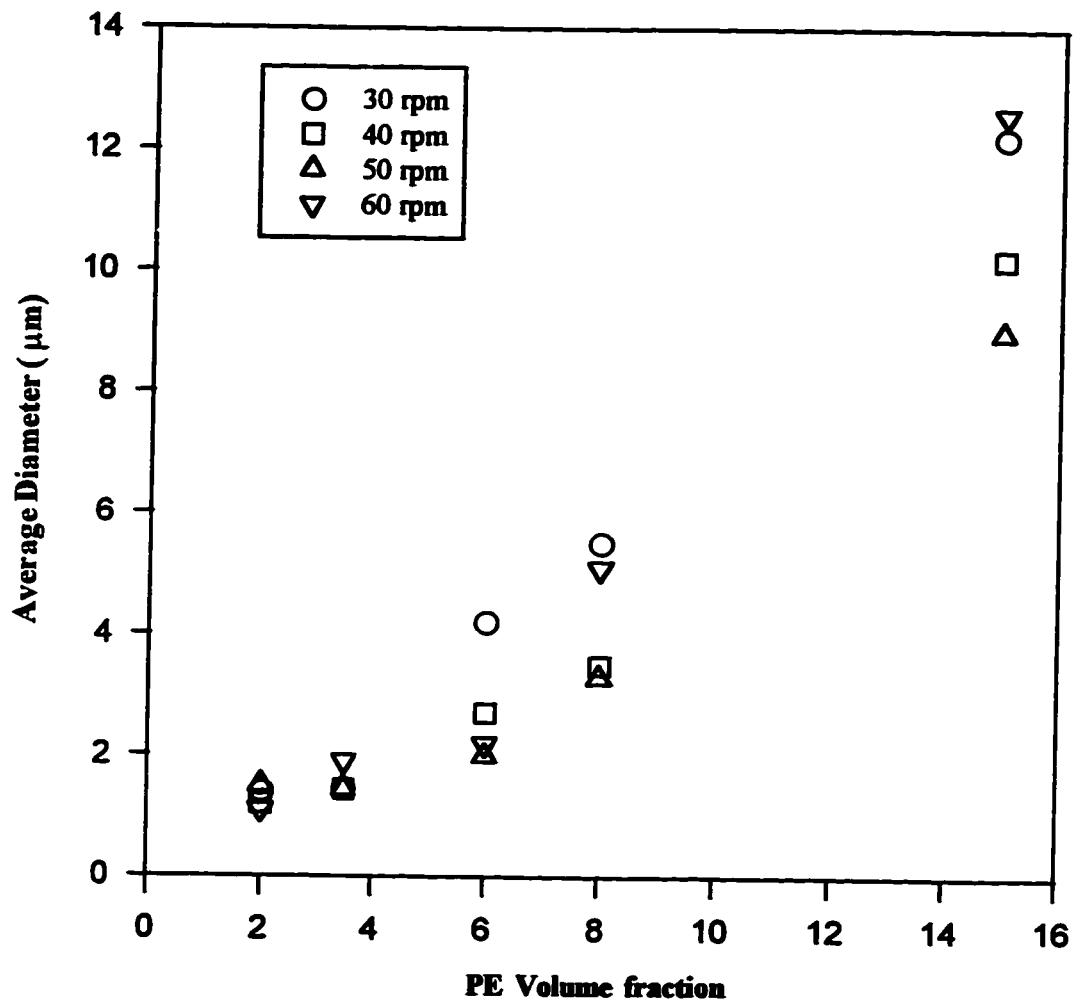


Fig 2.1 (a)
 Average diameter of PE dispersed in PS versus the volume fraction of PE. The temperature used was 200°C and the blending time was 300 s. The curves were obtained for a range of rotation speeds. [Adapted from Huneault et al. (1985)]

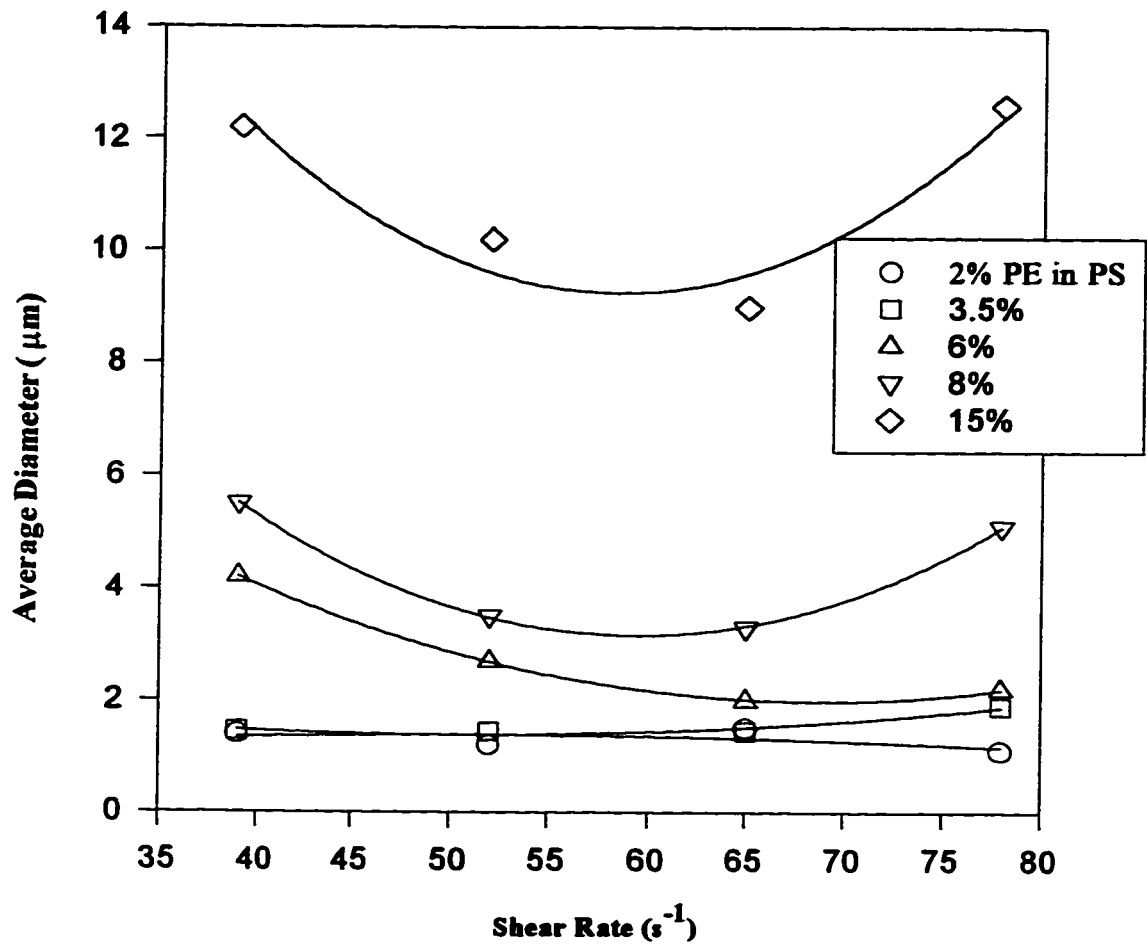


Fig 2.1 (b)
 Average diameter of PE dispersed in PS versus shear rate. The diameter exhibits a minimum for nearly all volume fractions.

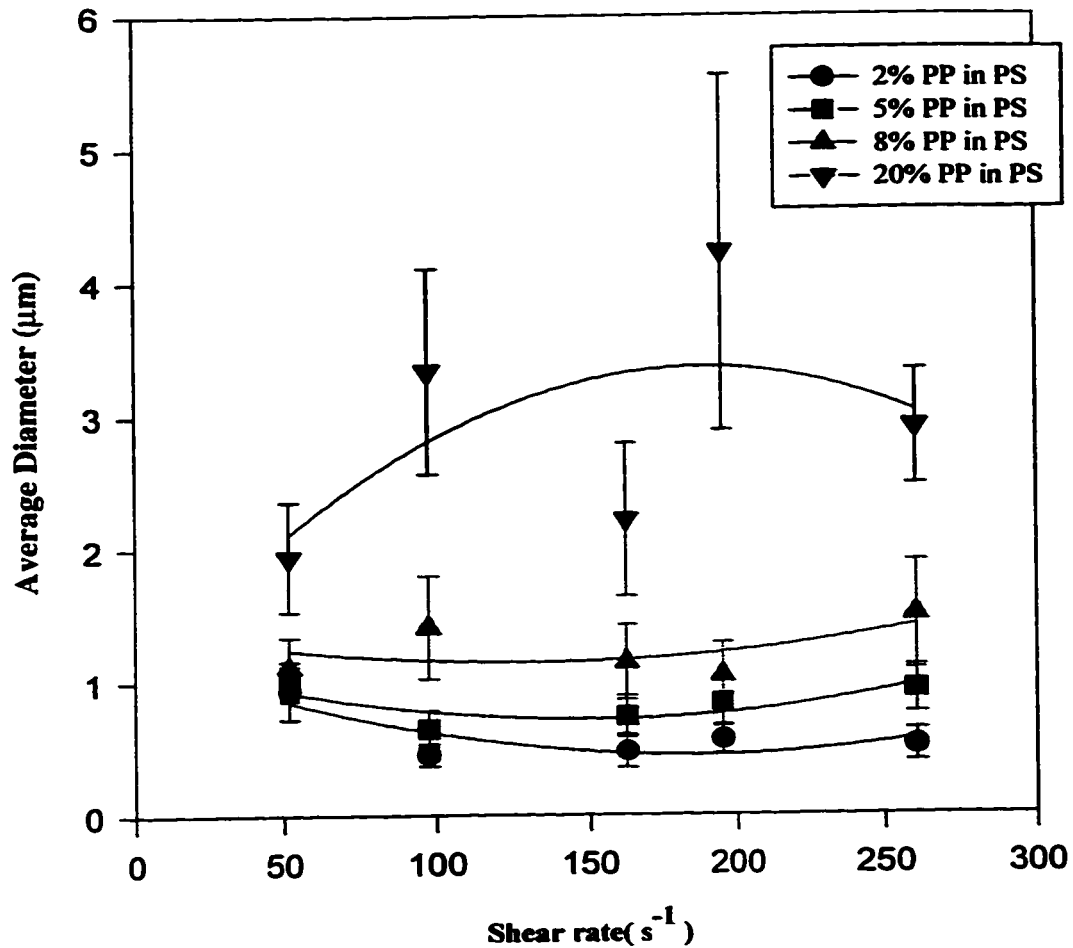


Fig 2.2
Effect of shear rate on the dispersed phase diameter for the PS/PP blend at different weight fractions of the dispersed PP phase. The 2%, 5% and 8% curves exhibit a minimum in diameter at a critical shear rate (162.5 s^{-1}).

2.2. Analysis

2.2.1 Theory behind the force balance

When two polymers are blended in a mixer, several complex phenomena take place. There is a combination of shear and extensional flows present in the mixer. As a first approximation, consider a single drop of polymer being deformed in a Newtonian flow field. There are several forces acting on the droplet. The equilibrium is attained when the forces that deform the drop are balanced by the forces that resist deformation. The shear

stress acting on the drop tries to deform it whereas the interfacial force tries to resist the deformation. The ratio of the two forces is defined as the Capillary number. Depending on the value of this dimensionless number, the drop either deforms or breaks. When the shear force is large compared to the interfacial force, the drop deforms to a large extent. As it elongates, there is a critical length beyond which the cylinder breaks due to Rayleigh type instabilities. This phenomenon has been studied extensively for Newtonian systems. In the case of a polymer drop, the droplet elasticity also resists deformation. A final equilibrium is attained when the forces balance each other. So the elasticity of the polymer phases must be incorporated into a model. Two ways to incorporate the elastic contribution were considered. One was to consider only the droplet's first normal stress and the other was to consider both the droplet normal stress and the matrix normal stress.

When a viscoelastic material is sheared, it experiences viscous stresses as well as normal stresses (Fig. 2.3).

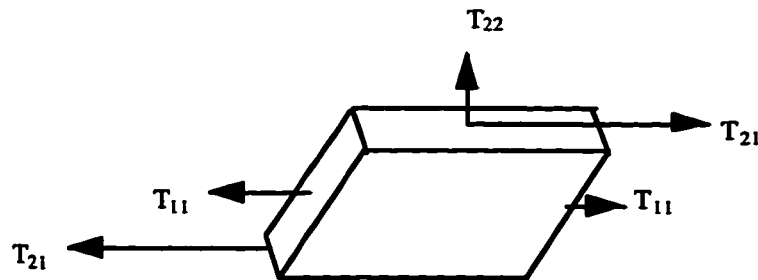


Fig 2.3
The shear and normal forces acting on a single block of polymer [Adapted from Macosko, 1994]

The first normal stress difference is defined as $N_1 \equiv T_{11} - T_{22}$ (where T_{11} and T_{22} are the tensile forces). For isotropic materials, N_1 is positive (unless it is zero). The first normal stress difference is proportional to the square of the shear rate, i.e. $N_1 \propto \dot{\gamma}^2$. The

constant of proportionality is called the first normal stress coefficient, ψ_1 . The force balance that is put forward is based on some simplifying assumptions which have been observed in polymer melts (Macosko, 1994). At low shear rates,

$$\psi_1(\dot{\gamma}) = \frac{2G'(\omega)}{\omega^2} \quad \text{for} \quad \omega = \dot{\gamma} \rightarrow 0 \quad (2.5)$$

This equation can be modified and written as

$$N_1 = \psi_1 * \dot{\gamma}^2 \equiv \psi_1 * \omega^2 \equiv 2 G'(\omega) \quad \text{for} \quad \omega = \dot{\gamma} \rightarrow 0 \quad (2.6)$$

2.2.2 Particle Size Prediction

For the first case where only the droplet first normal stress is considered, the proportionality obtained is (Sundararaj and Macosko, 1995):

$$\text{Shear forces} \propto \text{Interfacial forces} + \text{Droplet Elasticity (normal force)} \quad (2.7a)$$

$$\eta_m \dot{\gamma} \propto \frac{2\Gamma}{D} + 2 G'_d \quad (2.7b)$$

This deformation is resisted by the interfacial tension and the droplet's normal stress, $T_{11,d}$. Since T_{11} is much greater than T_{22} , we can approximate the difference $T_{11} - T_{22} \equiv T_{11}$. This difference is the first normal stress difference, N_1 . At low shear rates or frequency of rotation, the first normal stress difference can be approximated by $2G'$, where G' is the elastic modulus. At high shear rates, ($> 10 \text{ s}^{-1}$), $N_1 > 2G'$, but the two quantities are proportional to each other. If we use a proportionality of 1 with Equation 2.7b, we obtain an equation for drop diameter as

$$D = \frac{2\Gamma}{\eta_m \dot{\gamma} - 2 G'_d} \quad (2.8)$$

In the case of a polymer-polymer blend, we must consider the matrix. The matrix normal stress will try to deform the droplet (Sundararaj *et al.*, 1995). Hence, in the force proportionality, there is an additional force that tries to deform the drop. This force was

incorporated and Fig. 2.4 shows all the forces acting on a single drop. A force balance gives:

$$\text{Shear forces} + \text{Matrix Elasticity} \propto \text{Interfacial forces} + \text{Droplet Elasticity} \quad (2.9a)$$

Once again, we approximate the first normal stress difference by $2 G'$.

$$\eta_m \dot{\gamma} + 2 G'_m \propto \frac{2\Gamma}{D} + 2 G'_d \quad (2.9b)$$

The equation for drop diameter is obtained as

$$D = \frac{2\Gamma}{\eta_m \dot{\gamma} - 2(G'_d - G'_m)} \quad (2.10)$$

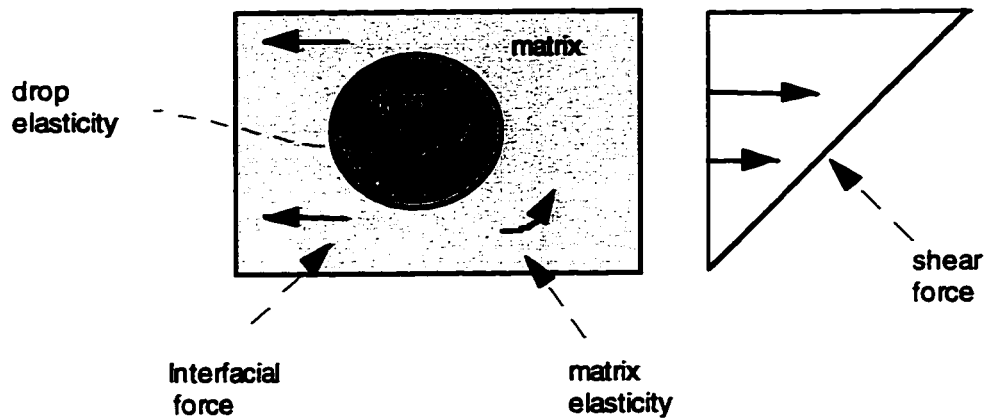


Fig 2.4
A schematic to explain the four main forces acting on a single polymer drop in a polymer matrix.

It should be emphasized that use of this force balance will give qualitative behavior; to obtain quantitative values, the proportionalities between these forces due to the effects of viscosity ratio, elasticity ratio, and direction of forces must be determined.

2.3 Experimental

2.3.1 Materials

The source, acronym, molecular weights and the magnitude of complex viscosity of the materials used are given in Table 2.1. All materials were provided in pellet form. The dynamic rheological characterizations were performed using the Rheometrics RMS 800 rheometer with 25 mm parallel plate fixtures at 10% strain. The measurement of these rheological properties has been described in detail in appendix D. The viscosity measured by the RMS is a dynamic complex viscosity whereas the viscosity used in the force balance is a steady shear viscosity. However, we can compare the two values by using an empirical relationship, called as the “Cox-Merz rule”, which holds true for nearly all shear rates (Macosko, 1994). The rule states that the shear rate dependence of the steady state viscosity η is equal to the frequency dependence of the linear viscoelastic viscosity η^* . Since the rheometrics spectrometer was operated in the linear viscoelastic regime, this rule is reliable. It can be written as:

$$\eta(\dot{\gamma}) \equiv |\eta^*(\omega)|; \text{ with } \dot{\gamma} \equiv \omega \quad (2.11)$$

The polystyrene used in the experiments was Dow Styron 666D (PS666D). It is reported to have a melt index of 7.5 and has a molecular weight $M_w = 200,000$. The polypropylene was PP 3050 obtained from Elf Atochem. The polyethylene used was LDPE 752 obtained from Dow Chemical. The nylon, Zytel 330(PA330) obtained from Dupont, is a partially aromatic, amorphous nylon. The EPMA (ethylene-propylene-maleic-anhydride) used was obtained from Exxon. It has a 0.7% MA graft and $M_w=84,000$. It is reported to have an ethylene content of 76%. The reactive polystyrenes were Arco poly(styrene-5wt% maleic anhydride) (PSMA5) and polystyrene-oxazoline (PS-Ox) obtained from Dow Chemical.

2.3.2 Experiments

Before blending, the pellets were dried overnight at a temperature of 80°C to remove any volatiles. The Haake Rheocord 90 rheometer with a 600 series batch mixer and roller blades was used for all experiments. The mixer was pre-heated to the starting temperature before adding the pellets through a feed chute with a ram having 5 kg mass. The rotation rate was varied from 40 to 200 rpm.

Table 2.1. Properties of Materials Used.

Polymer (abbrev)	Source (functionality)	M_w	viscosity η^* at 65 s ⁻¹ and 200°C (Pa.s)
Polystyrene (PS666D)	Dow Chemical	200,000	950
Polypropylene (PP3050)	Elf Atochem	60,000 (M_n)	840
Polyethylene (LDPE 752)	Dow Chemical	194,000	400
amorp. Polyamide (PA330)	Dupont (difunctional)		10,000
ethylene-propylene maleic-anhydride (EP-MA)	Exxon (0.7% MA graft)	84,000	2400
polystyrene-maleic anhydride (PSMA5)	Arco (5 wt% MA copolymer)		850
polystyrene-oxazoline (PS-Ox)	Dow Chemical (1.0% oxazoline)	200,000	900

Pellets of the components were dry mixed in a beaker before blending in the mixer. The component weights were calculated using the desired weight percents of each component and by requiring that the total melt volume of material be kept at 78% of the

mixer volume. This corresponds to a volume of 54 cm³. At this loading, there is optimum material exchange between the two chambers of the mixer and there were no stagnant areas in the mixer center due to overfilling. This has been shown by visual observation of the mixing chamber by using a glass front plate on the mixer (Sundararaj *et al.*, 1992). The densities were estimated using the data given by van Krevelen (1976). A sample calculation of the weights of polymer to be added to the mixer has been described in Appendix A.

In all the blending experiments, the mixer wall temperature was kept constant at 200°C. The runs are summarized in Table 2.2. For the PS/PP blends, the weight percentage of the dispersed phase (PP) was varied from 2 % to 20 %. The mixing time for all the runs was 10 minutes, and it was assumed that an equilibrium morphology was attained in the batch mixer for blend pairs at the conditions used (Scott, 1990). After 10 minutes, the motor was stopped and the front plate and the middle section of the mixer

Table 2.2. Experimental Runs, T=200°C

System (matrix/ dispersed)	Viscosity Ratio	Interfacial Tension # (10³ N.m)	D Taylor Limit (μm) 65s⁻¹
PS/PP	0.8700	4.6	0.013
PS/PE	0.4502	4.9	0.014
PS/EP-MA	4.9220	4.5	0.010
PS/PA	13.7400	18	0.047
PS-Ox/EPMA	2.7000	2.4	0.040
PSMA5%/PA	4.5400	18*	0.120

* Value for non-reactive system

Obtained using Breaking Thread method (Sundararaj, 1990)

barrel were removed exposing the mixer blades. Most of the material was attached to the blades and a sample was withdrawn from blade indents and immediately quenched in liquid nitrogen. The sample was withdrawn within 25 seconds of stopping the rotor. In many

cases, a fracture surface was created when the hot blend was immersed in liquid nitrogen as it imploded by rapid quenching. In cases where the sample did not implode in liquid nitrogen, it was cooled in liquid nitrogen and then broken using a hammer, creating the fracture surface. Using standard heat transfer calculations (Scott, 1990), it was found that the sample midline temperature cools below 100°C within 15 seconds of being dropped into liquid nitrogen. To determine the average particle size, the samples were analyzed using Scanning Electron Microscopy (SEM). A small sample was stuck onto a SEM stub which was then coated with a thin layer of gold. Microscopy was done using a HITACHI S-2700 SEM.

The diameter of the dispersed phase was measured using the image analysis software NIH Image 1.58b33, developed by the National Institute of Health. For image analysis, the particles in the SEM micrographs were outlined and the traced image was scanned and stored. The area of each particle was measured and the particle diameter was determined assuming that all the particle images are circles. The error associated with this assumption was negligible. Usually, the diameters of ca. 200-350 particles were measured and averaged to get a value closer to the exact one. A sample measurement of the average diameter of the dispersed phase has been described in Appendix B. It is important to note that the spherical particles are three-dimensional and they can be sectioned at any point. Therefore, the section may not pass through the center of each sphere. To account for this, a size correction was done using the Cruz-Orive method (Cruz-Orive, 1976), which is recommended by Russ (1986). The method has been described by Sundararaj *et al.* (1995). The corrected values were compared with the raw data and the difference in the average particle size was less than 10%. Therefore these corrections are neglected in the data presented.

Image analysis measured the cross-sectional area of all the particles present on the micrograph. The particle areas were converted to equivalent diameters using

$$d_{\text{equivalent}} = \sqrt{\frac{4(\text{area})}{\pi}} \quad (2.9)$$

The error bars shown for each point in the plots are one standard deviation in each direction for the particle sizes measured. The limits of the error bars can be used as a measure of the particle size distribution. A general observation for all measured diameters is that the breadths of distribution increase in size as the weight percentage of the dispersed phase increases and decrease in size as the shear rate increases.

2.4 Results

Plots of the dispersed phase diameters versus rotation rates were made for the blend pairs studied for all the concentrations. The systems are chosen so as to cover a range of viscosity ratios. The viscosity ratio is close to one for the PS666D/PP3050 system ($\eta_r = 0.87$). A viscosity ratio of unity has been reported to give the best dispersion (Wu, 1987). The viscosity ratio is 4.9 for the PS666D/EP-MA system, 13.7 for the PS666D/PA330 system and is 0.45 for the PS666D/PE system. Fig. 2.2 gives the particle size of the dispersed phase (PP) versus shear rate for a range of dispersed phase concentrations.

The shear rate used was the maximum shear rate obtained in the mixer. This was determined by assuming drag flow in the minimum gap between the mixer blades and the barrel. A no slip boundary condition at the barrel wall and the mixer blade surface was assumed. From this calculation, the shear rate is obtained by multiplying the rotation rate by 1.3. A detailed description of this calculation is given in appendix C.

For the PS/PP, the diameter exhibits a minimum at 125 rpm for the 2%, 5% and the 8% cases. For the 20% case, we observed a maximum at 125 rpm (which corresponds to a maximum shear rate of 162.5 s^{-1}). It may be that coalescence is more significant at this high dispersed phase weight fraction. Fig. 2.5 (a), (b) and (c) show the micrographs for the 92:08 PS/PP blend at shear rates of 52 s^{-1} , 162.5 s^{-1} and 195 s^{-1} . The drop diameter is at a minimum at a critical shear rate of 162.5 s^{-1} . Fig. 2.6 shows the effect of concentration on the drop diameter. The average drop diameter for the 20% PS in PP sample is much

larger than that for the 2% sample due to coalescence (Sundararaj and Macosko, 1995). All the data points were reproduced for this system and the validity of the results was verified.

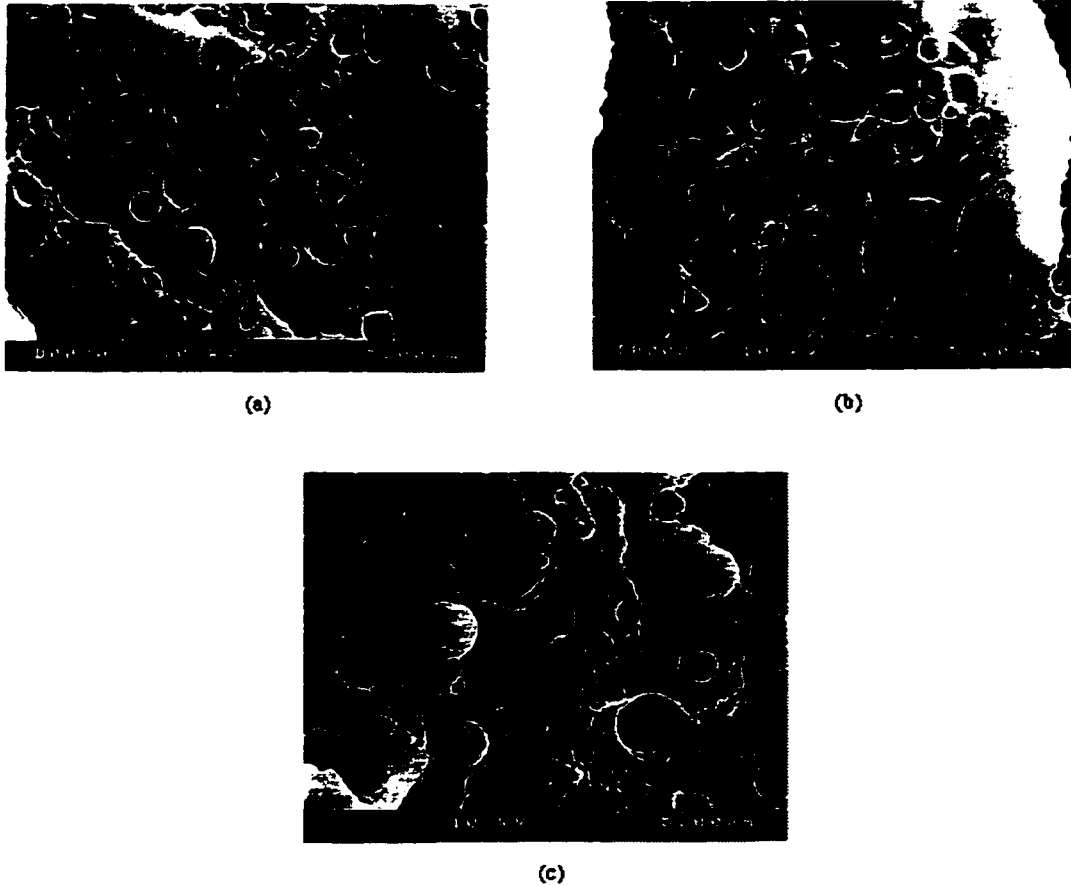
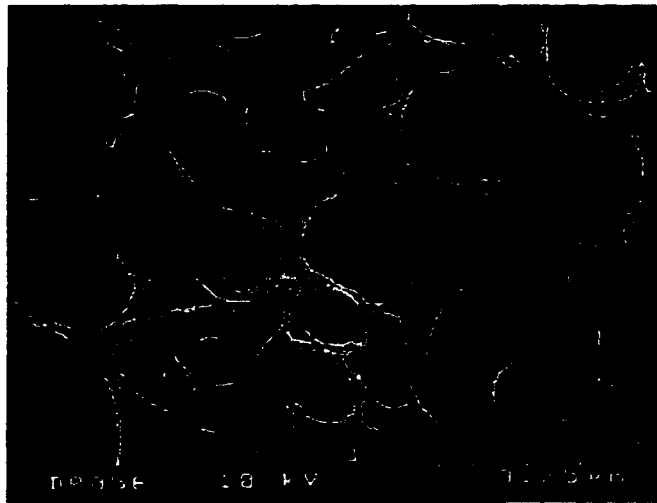


Fig 2.5
SEM micrographs of the PS/PP blend. All the micrographs are for 8 wt% dispersed phase. The pictures show the effect of shear rate on the drop diameter; (a) 52 s^{-1} , (b) 162.5 s^{-1} , and (c) 195 s^{-1} . It is observed that diameter goes through a minimum at around 162.5 s^{-1} .

Equations (2.8) and (2.10) were used to predict the diameter of the dispersed phase and the results are shown in Fig.2.7(a). Equation (2.10) is able to explain the minimum in the curve of diameter versus shear rate and is a closer approximation to the experimentally observed curve. The plot shows that the matrix normal stress has an important contribution to the final equilibrium size. Hence, the term $(G'_d - G'_m)$ in equation (2.10) plays a crucial role.



(a)



(b)

Fig 2.6
Effect of concentration on the dispersed phase diameter for the PS/PP blend. The micrographs are at the same shear rate (260 s^{-1}) but different weight fractions; (a) 2% and (b) 20%. The diameter for the 20% sample is much higher than that for the 2% sample.

In Fig. 2.7 (a), the experimental results are compared with the values predicted by equation (2.10) for the 2wt% PS/PP system. The prediction is for a single polymer drop in a polymer matrix; it should match the experimental results for dilute concentrations (the most dilute concentration used was 2 wt%). It can be seen that the critical shear rate is the same in both the experiment and the prediction (Equation 2.10). Fig.2.7(b) shows that the

diameters measured even at the lowest concentrations (2 wt%) were well above Taylor's limit for shear flow (equation 2.2) and lower than Wu's predicted value (Equation 2.3).

Fig. 2.8 (a) and (b) are similar plots for the PS/EP-MA system at 2 wt% EP-MA. The effect of reactive compatibilization (PS-Ox/EPMA) is also shown. The particle size is much smaller in the reactive case. For the lower shear rates, there is a large difference in droplet diameter between the reactive and the non-reactive blends. For the reactive system, the drop diameter decreases sharply and reaches a steady value at shear rates over 50 s^{-1} .

The decrease in particle size in the reactive case is rapid as compared to the non-reactive system which reaches a steady diameter only at $\sim 100 \text{ s}^{-1}$. At higher shear rates, the difference between the non-reactive and the reactive diameters is small but still significant. The diameters for the reactive blend are nearly identical at all shear rates indicating that reaction reduces coalescence via formation of *in situ* copolymers (Sundararaj and Macosko, 1995).

There is no minimum drop diameter in the PS/PE blend system, and the drop diameter continues to decrease up to the maximum shear rate of 260 s^{-1} for the 5% system (Fig 2.9(a)). The 2% PS/PE system does not show any trend but the dispersed diameter is nearly constant. However, the force balance also does not show any minimum in the curve of drop diameter versus shear rate. Thus, the force balance is still a good predictor (qualitatively) of the dispersed phase drop diameter.

Table 2.3. Shear rate, diameter measured (in microns) and specific energy input (KJ/Kg) for the systems studied.

System	shear rate (s⁻¹)	Actual Diameter (μm)	Specific Energy Input (KJ/Kg)
PS/PP (98:02)	52.0	0.9352	299.4
	97.5	0.4514	689.0
	162.5	0.4763	1129.0
	195.0	0.5643	1427.9
	260.0	0.5171	1757.0
PS/PP (95:05)	52.0	0.9888	290.2
	97.5	0.6470	666.5
	162.5	0.7384	1135.0
	195.0	0.8422	1478.8
	260.0	0.9360	1787.0
PS/PP (92:08)	52.0	1.1065	280.5
	97.5	1.4079	613.0
	162.5	1.1457	1060.8
	195.0	1.0430	1151.2
	260.0	1.4952	1777.9
PS/PP (80:20)	52.0	1.9396	214.8
	97.5	3.3305	455.0
	162.5	2.2143	785.0
	195.0	4.2182	982.8
	260.0	2.9082	1521.0
PS/EP-MA (98:02)	32.5	0.4465	165.8
	65.0	0.2579	453.19
	97.5	0.2003	721.39
	162.5	0.1227	1188.0
	195.0	0.2083	1422.5
PS/PE (95:05)	52.0	1.3246	190.9
	97.5	0.8450	439.0
	162.5	0.6252	757.3
	195.0	0.5431	896.0
PS/PA (98:02)	65.0	1.4783	-
	97.5	1.1847	-
	162.5	1.1052	-
	195.0	1.0584	-
	260.0	1.0821	-

The values of shear rate, average dispersed diameter and specific energy input (described later) for all the systems used are given in Table 2.3. Fig. 2.10 (a) and (b) show the results obtained for the PS/PA330 system. Again, the reactive system has a

lower dispersed phase particle size. For the reactive system, the matrix phase used was PSMA 5%, a polystyrene with maleic anhydride grafted onto the backbone. The MA reacts with the amino group of the polyamide to form a copolymer at the interface. Fig. 2.10 (a) shows no curve for the predicted diameter using the force balance (equation 2.10). The force balance for this system predicts a negative drop diameter. In other words, the force balance predicts that there is no drop breakup beyond a certain shear rate. This is a drawback of the force balance. Fig. 2.10 (b) shows the comparison between the experimental diameters and the diameters predicted using Wu's equation. For the PS/PA system, Taylor's equation predicts no breakup since the viscosity ratio is greater than 2.5 (10.5).

2.5 Discussion

The shear rate present in the Haake mixer was calculated using some simplifying assumptions. The velocity at the mixer wall is maximum and that at the rotor blades is zero. A steady maximum simple shear rate is calculated and the following relation is obtained:

$$\text{Shear rate} = \text{Rotor speed} \times 1.3$$

Since the Haake mixer has a very complex flow field which is a combination of shear and extensional flows, the diameter should, if anything, be lower than the value predicted for shear flow. This discrepancy is attributed to the fact that polymers are highly elastic and polymer drops tend to elongate significantly before breaking. Therefore, Taylor's theory cannot be used to predict particle diameter in polymer blends.

As shown in the analysis section (ζ 2.2), two equations were obtained to predict the dispersed phase drop diameter using simple rheological properties measured by the RMS instrument. Equation 2.8 does not include the matrix elasticity whereas Equation 2.10 does. The experimentally measured diameters are closer to the values predicted from Equation 2.10 and hence, the matrix elasticity is critical to the particle diameter prediction.

This can be seen clearly from Fig. 2.7 (a). Both equations show the minimum in particle diameter but Equation 2.10 is able to predict the diameters quantitatively better than Equation 2.8.

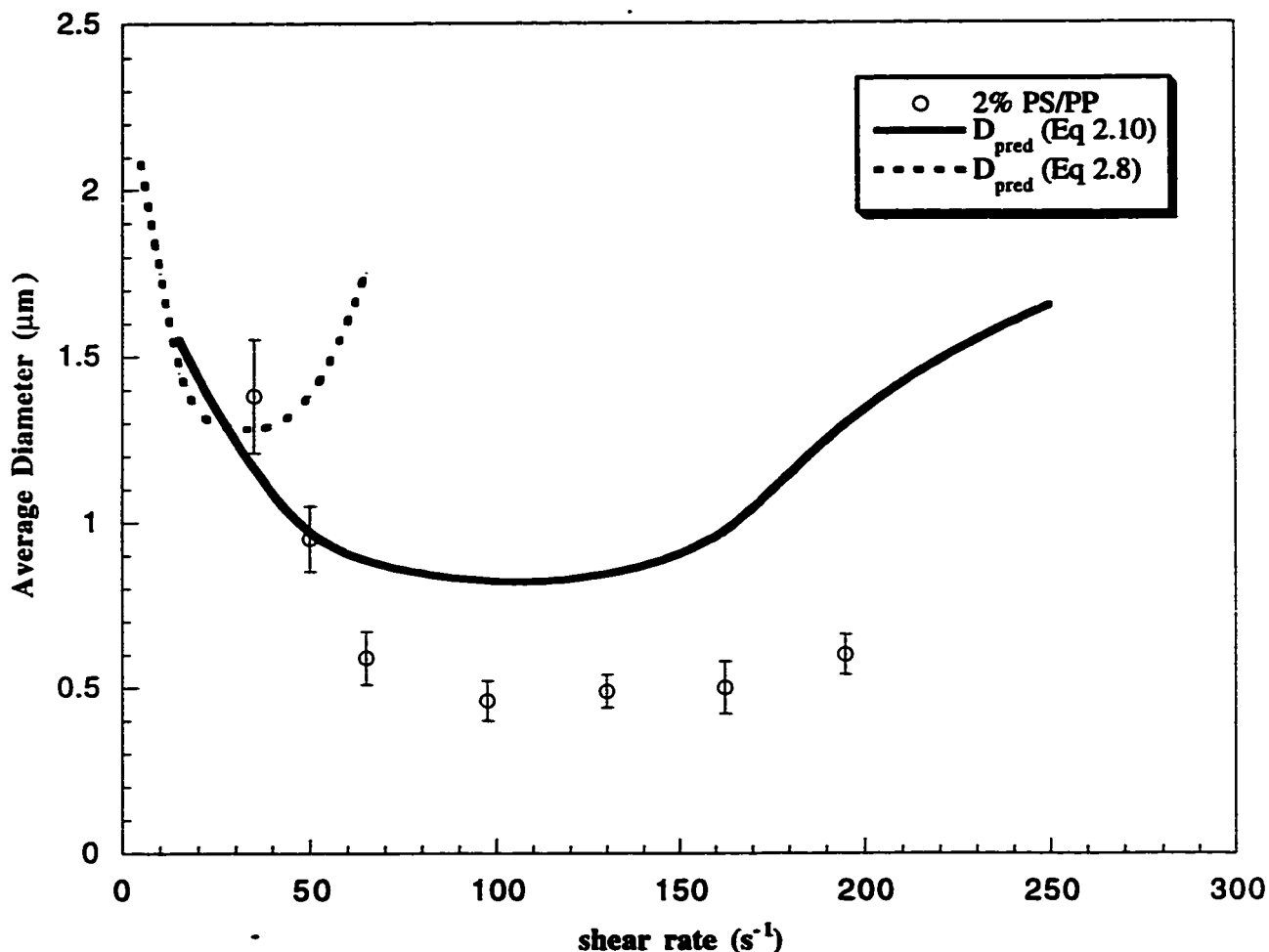


Fig 2.7 (a)
Comparison of experimentally observed drop diameter for the 2 wt% PP in PS system with the force balance predictions [equations 2.8 and 2.10]. Both experiments and model show a minimum in drop diameter at a critical shear rate.

Fig. 2.7 (b) compares the experimentally observed values for 2% PS/PP to Taylor's prediction for a single drop [equation 2.2] and to Wu's correlation for twin-screw extruded blends [Equation 2.3]. The experimental drop size is always greater than Taylor's result owing to polymer viscoelasticity. It is true that during polymer blending in a Haake

mixer, a simple shear analysis may not be adequate since the flow field includes extensional flows. Therefore, the particle size should be lower than what simple shear analysis predicts. Wu's correlation was obtained at 15 wt% concentration, where coalescence was important. Hence, the diameter predicted by Equation 2.3 is larger than the experimental value for a dilute system.

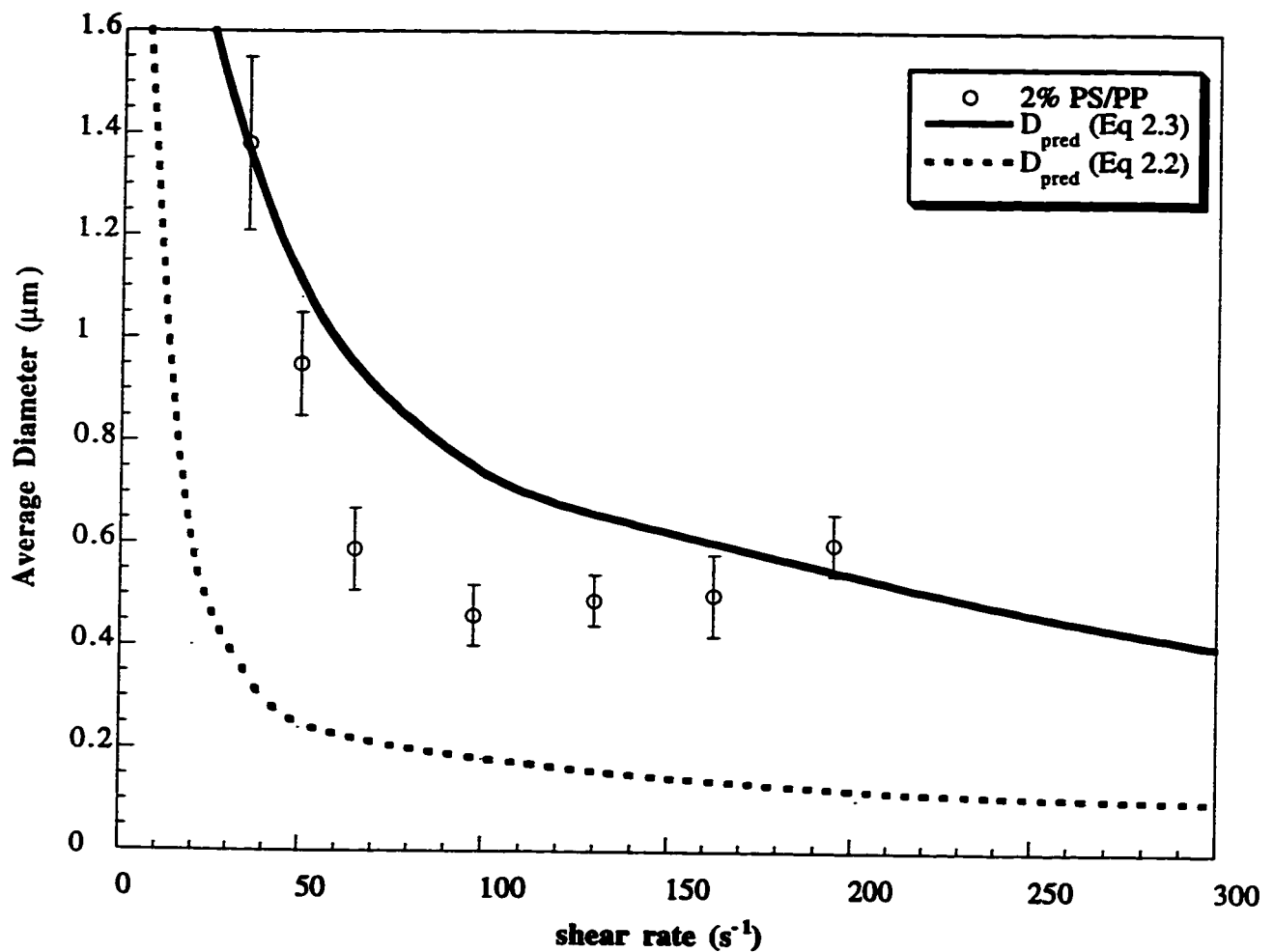


Fig 2.7 (b)
Comparison of the experimentally observed drop diameter for 2% PS/PP with the predictions given by Taylor [equation 2.2] and Wu [equation 2.3].

An explanation is suggested to account for this anomalous behavior of a minimum in the plot of diameter versus shear rate. The first normal stress difference, or equivalently

$2G'$ in Equation 2.10, depends on the shear rate. At low shear rate, the polymer behaves like a liquid. This means that the polymer chains can slide on one another easily. The polymer has a lower elastic modulus. At low shear rates, both the matrix and the dispersed phase G' 's are low and thus, the term $(G'_d - G'_m)$ in Equation 2.10 is negligible compared to $\eta_m \dot{\gamma}$. The shear stress ($\eta_m \dot{\gamma}$) is small, and thus, the predicted particle diameter is large since the denominator in Equation (2.10) is small. As the shear rate increases, the experimental drop diameter decreases initially. This is because the shear stress is increasing continuously with shear rate. The difference in the G' 's is still insignificant and does not affect the drop diameter. Thus, from Equation (2.10), the prediction is that there will be a decrease in the particle diameter. The shear forces are greater than the restoring forces and the drop breaks into smaller drops.

As the shear rate increases, the polymer tends to behave more and more like an elastic solid. The value of G' increases with increasing shear rates and the term $(G'_d - G'_m)$ becomes appreciable compared to $\eta_m \dot{\gamma}$. This is possible only when the two homopolymers being blended have different elastic responses. If the two polymers show the same or comparable elastic moduli, the difference $(G'_d - G'_m)$ is negligible even at high shear rates. At a critical point, a minimum drop diameter is reached when the term in the denominator reaches a maximum. Beyond this point, the difference in the elastic moduli can increase more rapidly than the increase in shear stress and the drop resists deformation and breakup. Thus, as the shear rate is increased beyond the critical shear rate, there is an increase in the diameter of the dispersed phase.

The force balance used to predict the drop diameter (Equation 2.10) is for a single drop. In all of the systems studied, the lowest weight fraction of dispersed phase used is 2%, where the condition of single drop is not strictly valid. Even at dispersed weight fraction of 2%, there will be some coalescence due to collisions between the drops.

Therefore, the force balance only gives a qualitative behavior of the drop diameter. Quantitatively, there is always a difference except for the case of a reactive system which will be discussed later.

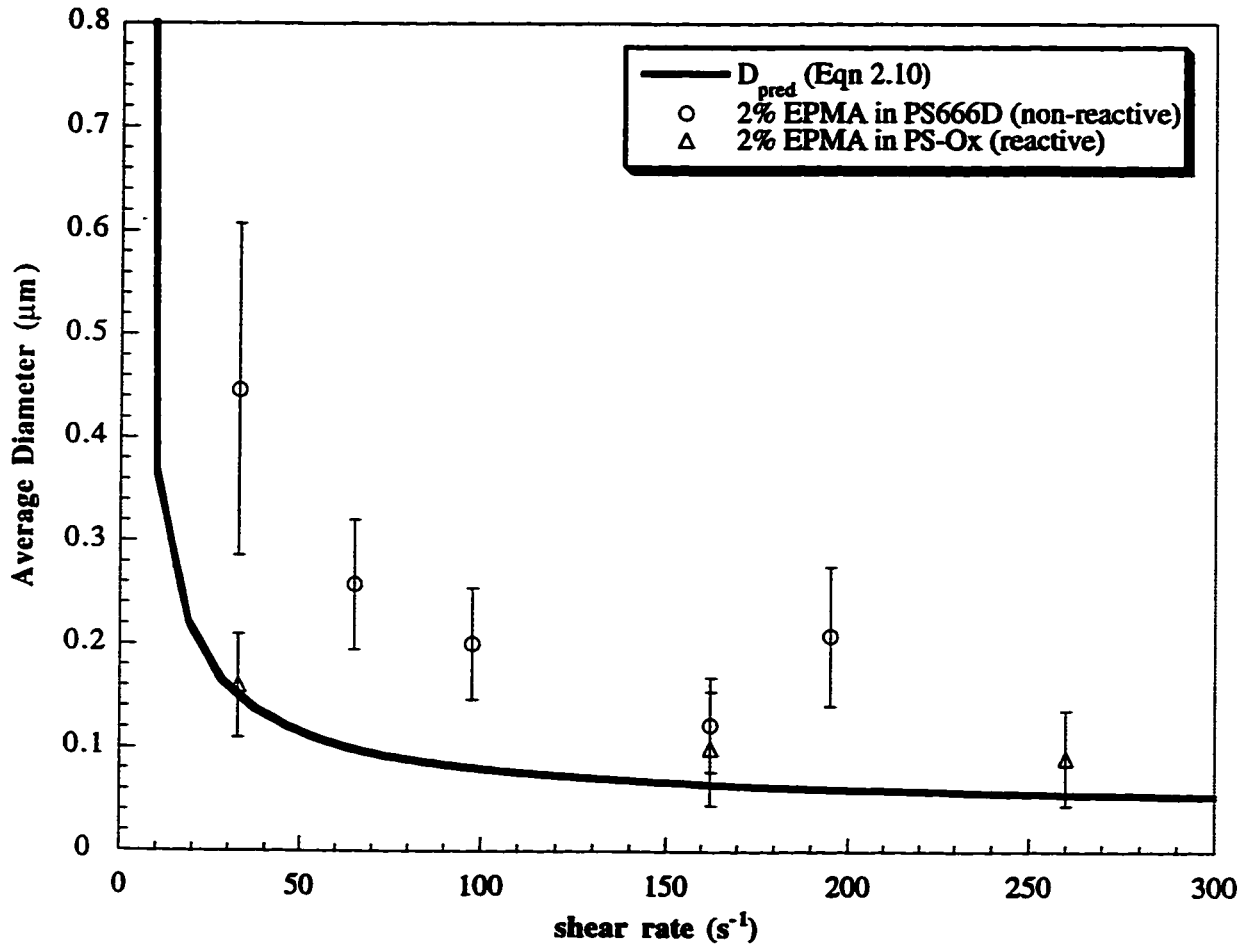


Fig 2.8 (a)
Effect of shear rate on the dispersed phase drop diameter for the non-reactive PS/EPMA system and the reactive PS-Ox/EPMA system (2 wt% EPMA). The diameter predicted from the force balance [equation 2.10] is also shown.

The reactive system (PS-Ox/EPMA) shows smaller particle diameter compared to the non-reactive system (Fig. 2.8 a). This is expected since reaction causes the *in situ* formation of copolymer at the interface leading to a stabilization of the dispersed phase drops. Thus, reaction reduces the drop diameter by the suppression of coalescence

(Sundararaj and Macosko, 1995). An interesting observation is that the drop diameter predicted from the force balance matches well with the diameter obtained for the reactive system (Fig. 2.8 a). The condition of a single drop in a matrix is satisfied to a greater extent in the reactive case than the non-reactive case. The reactively stabilized drops cannot coalesce due to the presence of the copolymer at the interface. Hence, at a weight fraction of 2%, the diameters obtained for the reactive system and those predicted by the force balance are comparable. It should be noted that for the reactive system prediction, the interfacial tension value used is the same as that for the non-reactive system. It is extremely difficult to measure an accurate interfacial tension value for reactive systems (Sundararaj, 1994). For the PS/EPMA system, the viscosity ratio is 2.5. Therefore, Taylor predicts no drop breakup. According to Taylor, there is no drop deformation beyond $\eta_r = 2.5$. However, since polymer systems are viscoelastic, there is drop deformation and breaking even at higher viscosity ratios. Fig. 2.8 (b) shows the comparison between the experimentally observed diameters and those predicted by Wu's equation. The experimental diameters for the 2% PS/EPMA system are smaller than the diameters predicted by Wu's equation. In all of Wu's (Wu, 1987) experiments, the weight fraction of the dispersed phase was 15% and thus, larger dispersed phase diameters are obtained using Wu's equation.

For the PS/PE system, the elastic moduli of both the homopolymers are comparable. There is a large difference quantitatively between the values of predicted and experimental diameters (Fig. 2.9 a). For the PS/PE system, a dispersed weight fraction of 5% was also investigated. At this weight fraction, the coalescence is more pronounced and higher dispersed phase particle size was obtained.

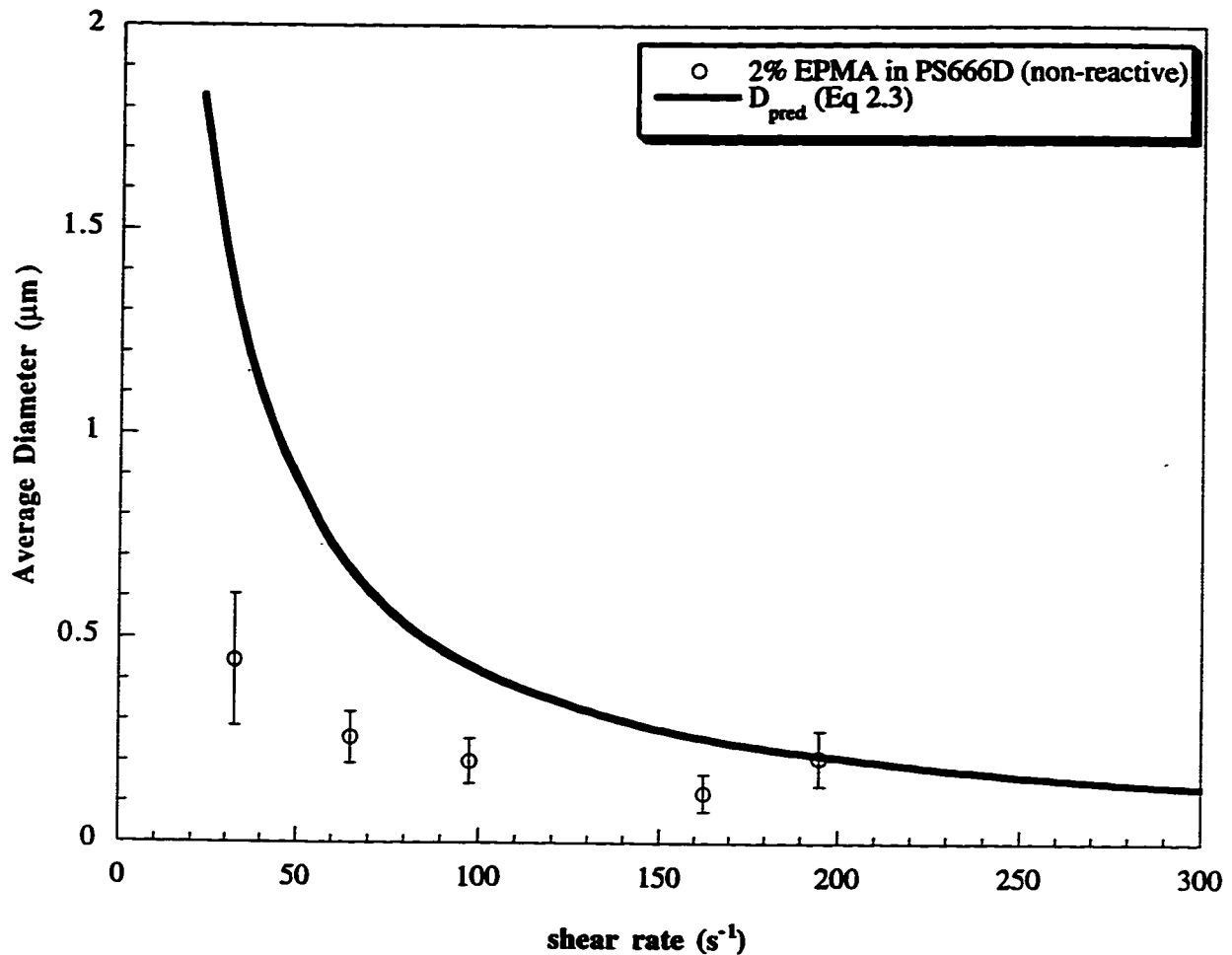


Fig 2.8 (b)
 Comparison of the experimental drop diameters with Wu's correlation [equation 2.3] for the PS/EPMA system. Taylor's equation [2.2] predicts no breakup will occur.

For PS and PE, the elastic moduli (G'_d and G'_m) are comparable at all shear rates. The elastic contribution ($G'_d - G'_m$) is less significant in Equation 2.10. The denominator in Equation 2.10 depends only on the shear stress for this system. The shear stress increases continuously with shear rate and, as a result, the denominator in Equation 2.10 increases (the shear stress continues to increase even for a shear-thinning power law fluid). Therefore, the drop diameter decreases with increase in shear rate. Both the predicted and the experimental curves show the same trends for this system. From Fig. 2.9 (b), it is

clear that the experimental diameter is higher than the diameter predicted by Taylor (Equation 2.2) and lower than that predicted by Wu (Equation 2.3) for the same shear rate.

In the case of the PS/PA system ($\eta_r = 10.5$) as shown in Fig. 2.10 (a), the value of $(G'_d - G'_m)$ becomes so large at high shear rates that the denominator in Equation (2.10) is negative. The equation predicts a negative drop diameter at high shear rates, which is

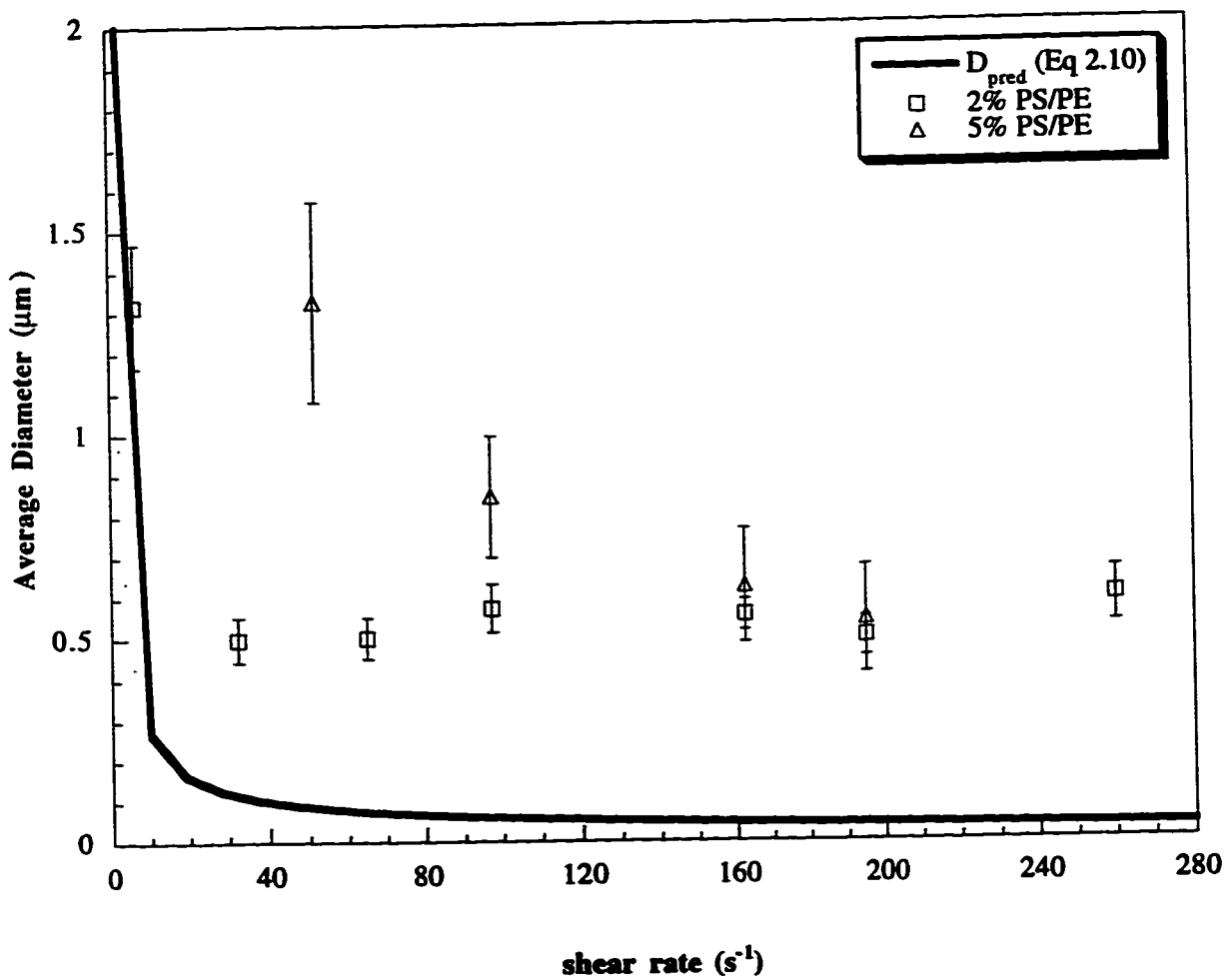


Fig 2.9 (a)
Effect of shear rate on the dispersed phase drop diameter for the PS/PE system (2% and 5% PE). No minimum is observed for this system. The predicted values also suggest that there should be no minimum diameter for this shear rate range.

nonsensical. PA330 has a large G' value compared to the G' value of PS666D. Hence, the force balance indicates that it is very difficult to deform a polyamide drop in a matrix of polystyrene and the PA330 drop acts more like an elastic solid. The balance indicates that when the difference $(G'_d - G'_m)$ is greater than $\eta_m \dot{\gamma}$, drop breakup is very difficult. Fig. 2.10 (a) is a plot of PA330 drop diameter versus the shear rate for the 2% weight fraction

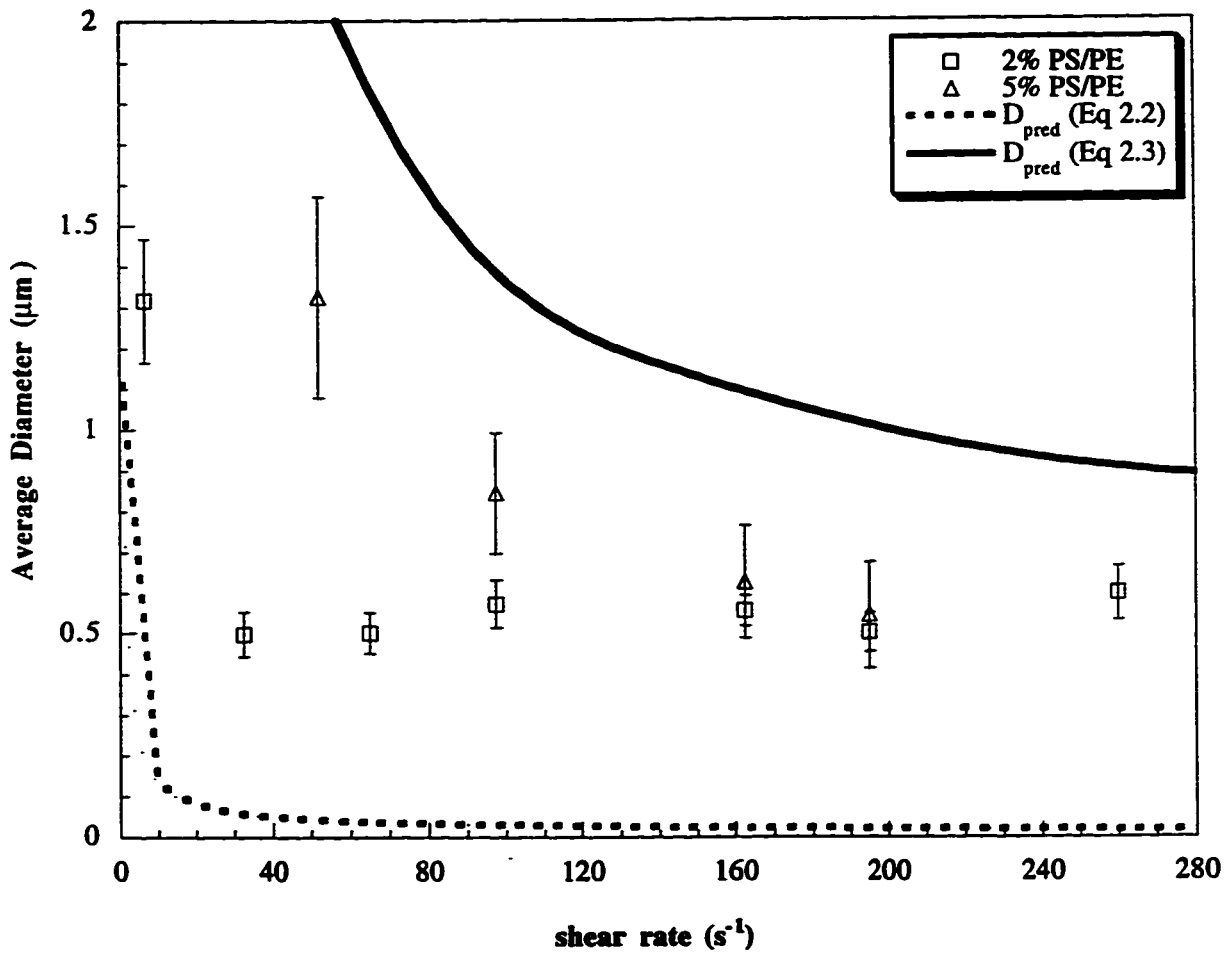


Fig 2.9 (b)
Comparison of the experimental drop diameters with Taylor's prediction [Equation 2.2] and with Wu's correlation [Equation 2.3] for the PS/PE system (2% and 5%).

of the dispersed phase. The effect of reaction on dispersed phase diameter was studied for this system (PSMA5/PA330). Once again, reaction stabilizes the drop and results in a finer dispersion than in the non-reactive system.

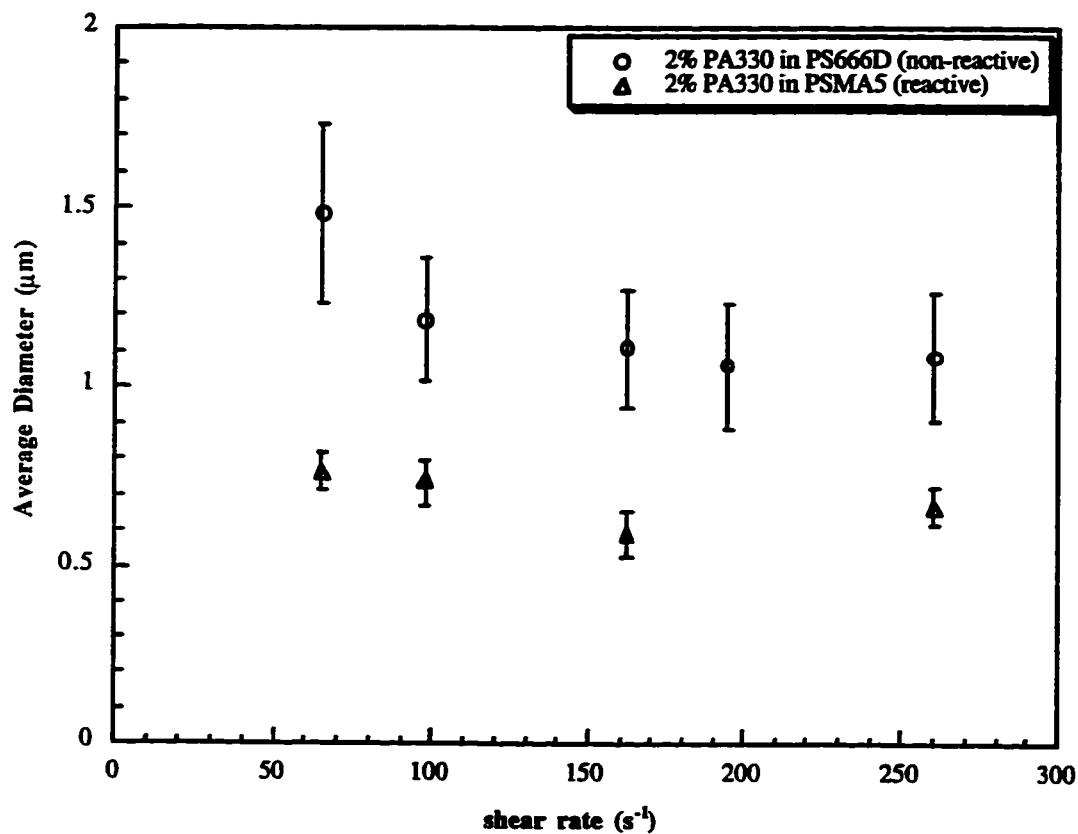


Fig 2.10 (a)
Effect of shear rate on the dispersed phase drop diameter for the PS/PA330 system (2% PA330). Equation 2.10 cannot be used to predict drop diameter for this high viscosity ratio system. The effect of reaction on blend morphology is also studied for this system by blending PSMA5/PA330.

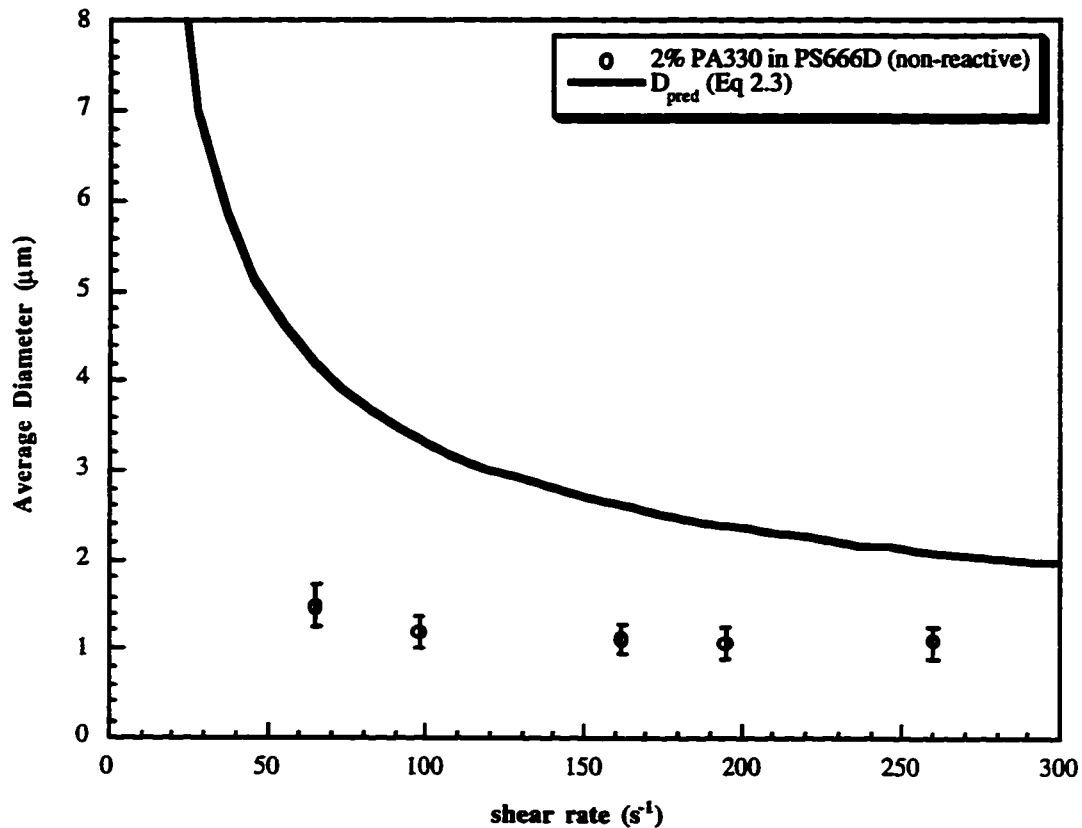


Fig 2.10 (b)
 Comparison of the experimental drop diameters with Wu's correlation [Equation 2.3].
 Taylor predicts no breakup will occur in this system for simple shear flow.

It has been reported by some researchers (Golba Jr. and Seeger, 1987; Liu and Baker, 1992) that a parameter called the specific energy input (or specific energy consumption) influences the diameter of the dispersed phase. The specific energy input is a measure of the amount of energy expended on the blend during processing. It is obtained by multiplying the integral of the area under the torque curve versus time by the shear rate per unit mass of blend materials (Liu and Baker, 1992). The results for the systems studied are shown in Fig 2.11. Fig 2.11 (a) is the plot of dispersed particle diameter

versus specific energy input for the PS/PP blends. The curves obtained are similar to the plots of diameter versus shear rate for the PS/PP system.

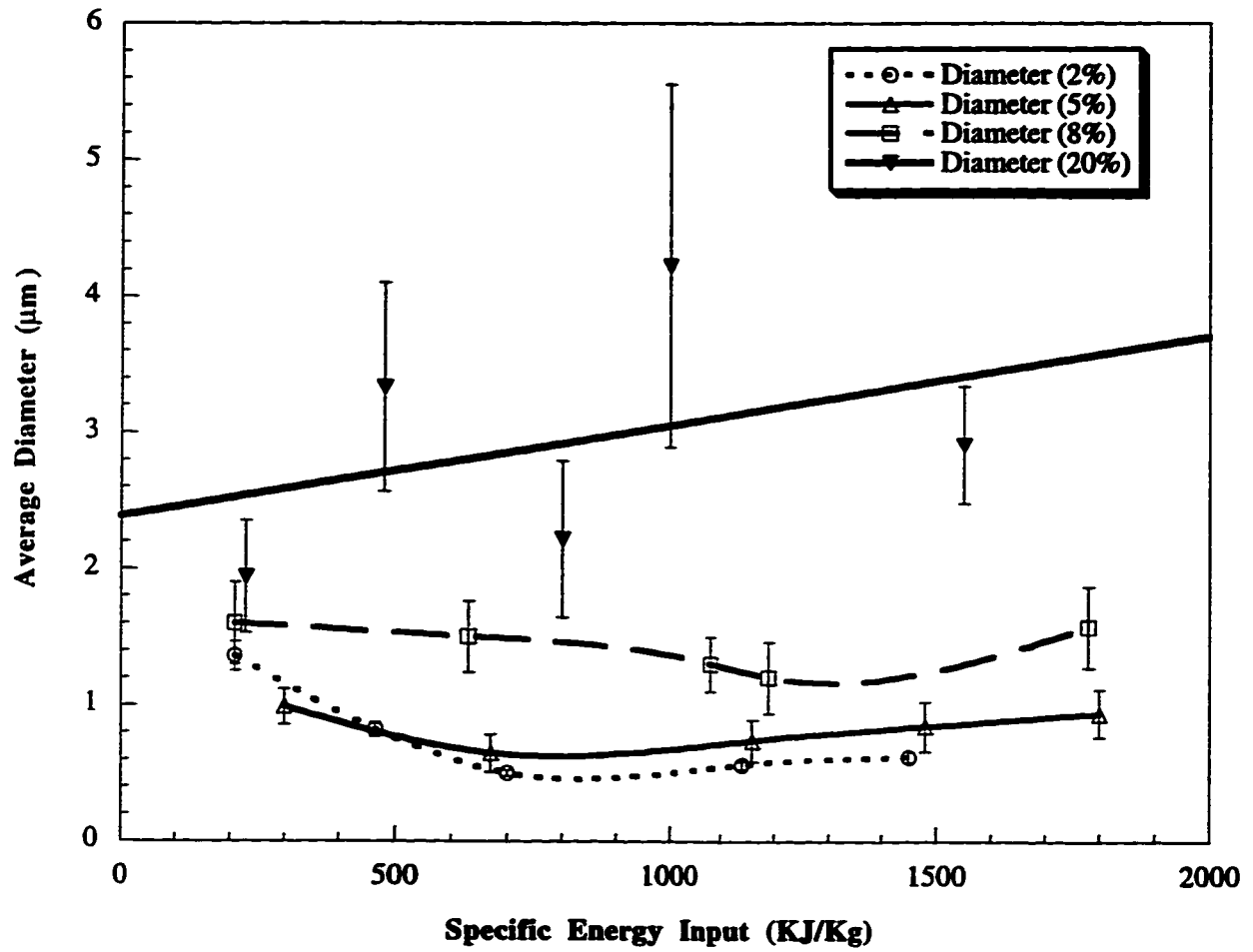


Fig 2.11 (a)

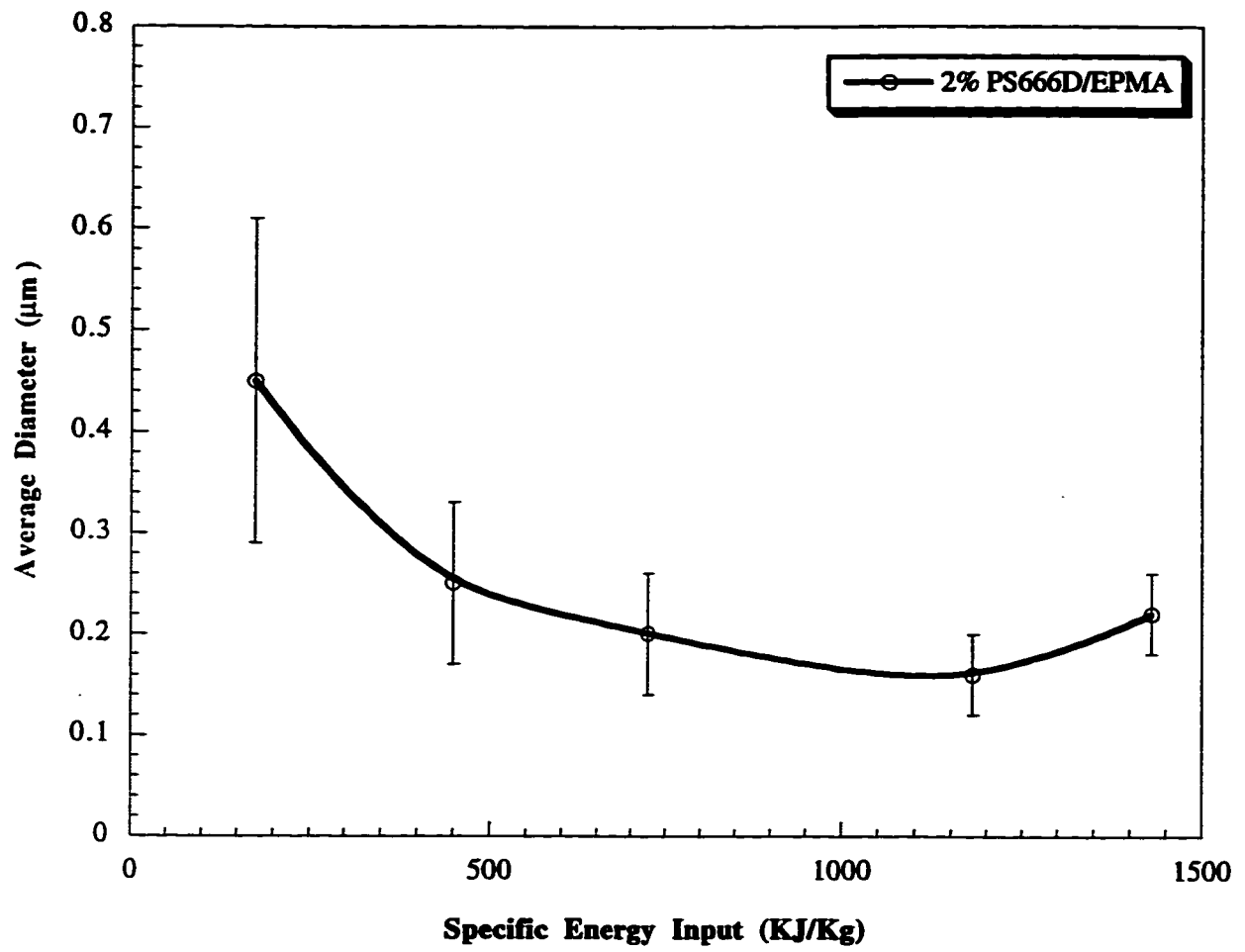
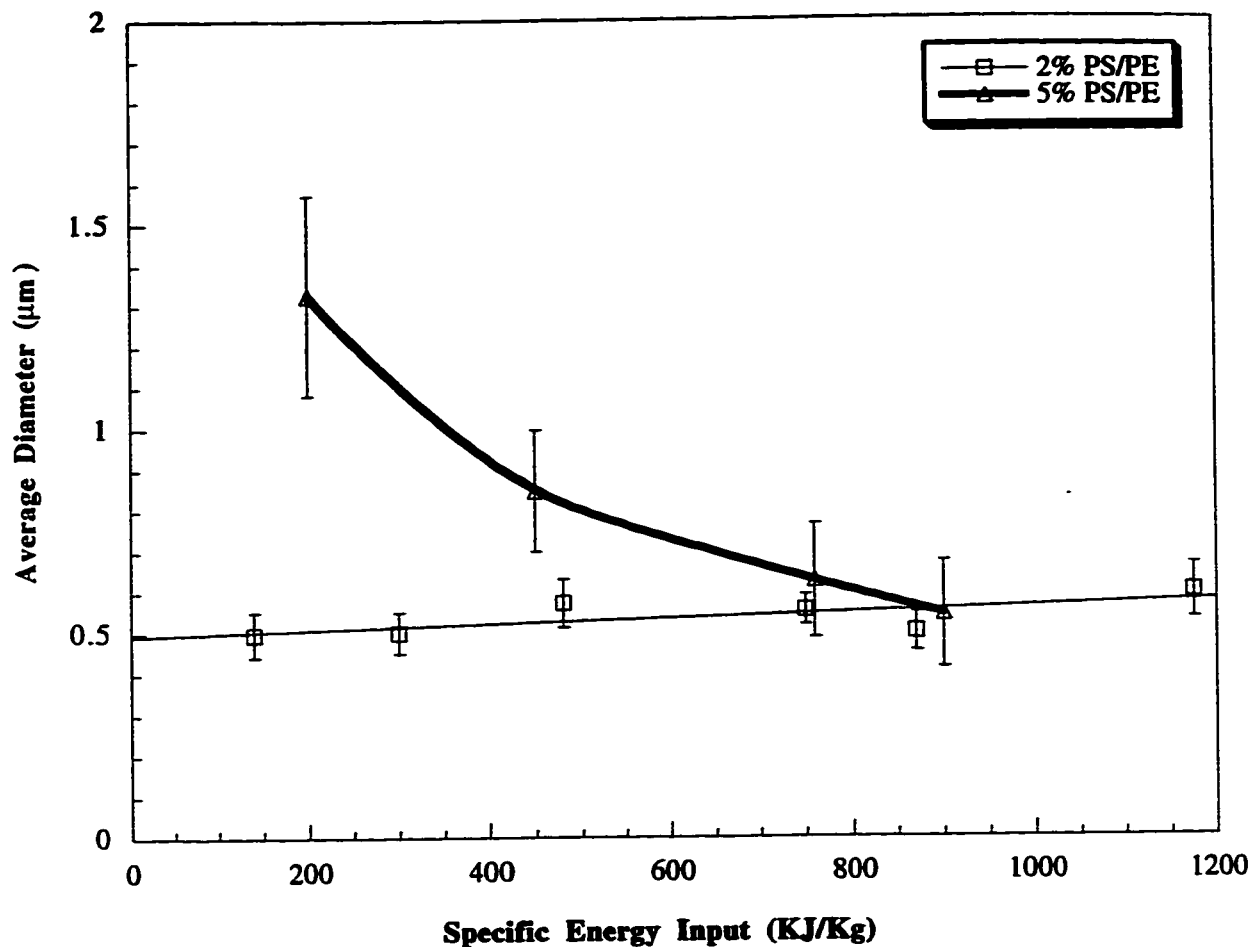


Fig 2.11 (b)



(c)

Fig 2.11

The diameter of the dispersed phase versus the specific energy input (kJ/kg). The trends were similar to that observed by varying shear rates [Figs 2.4, 2.8(a) and 2.9(a)]. (a) PS666D/PP3050 (b) PS666D/EPMA (c) PS666D/PE752.

This is because the integrals of the torque-time curves (in the definition of specific energy input), at different shear rates but the same concentration, are comparable in magnitude for every system. The mass of material used for different shear rates is identical. Therefore, the specific energy input increases almost linearly with shear rate. Thus, no additional information is obtained by using the specific energy input.

From Fig 2.4, it is observed that the diameter increases with increase in weight percentage of the dispersed phase. Between the 8% PP in PS and the 20% PP in PS blends, there is a large jump in particle size. This is due to the increased fraction of dispersed phase, which causes more collisions between the PP drops. It has been reported by Tokita (1977) that coalescence is directly proportional to the number of collisions taking place, and increasing shear rate may dramatically increase the number of collisions at this high concentration. This may be why there is an increase in drop diameter with shear rate for the 20% blend.

2.6 Conclusions

The diameter of the dispersed phase can be modeled qualitatively by the force balance (in Equation 2.10) for most of the systems studied. The predicted diameters are comparable to the experimentally determined diameters. The PS/PP system ($\eta_r=0.87$) shows a minimum drop diameter with shear rate. The diameter attains a minimum value at a shear rate of 162.5 s^{-1} and then increases at higher shear rates for the 2%, 5% and the 8% PP in PS blends. The minima were independent of the weight fraction of the dispersed phase. However, no minimum was observed for the 20% PP in PS blend. This may be due to greater coalescence at this high concentration. The model best predicts the behavior of the 2% PS/PP blend since the force balance is for a single polymer drop in a polymer matrix.

Not all systems show a minimum drop diameter. The PS/PE system shows a decreasing drop diameter with shear rate for shear rates up to 200 s^{-1} . A minimum may occur at a higher shear rate. The force balance predicts the same trend in drop diameter as the experimentally observed results. For systems where the drop normal stress is significantly greater than the matrix normal stress (PS/PA330), the model predicts a negative drop diameter at high shear rates which is nonsensical. When the normal stress of the dispersed phase is large, it is difficult to deform the droplet and the drop size should not change even if the shear rate is increased. Reaction stabilizes the interface and reduces

coalescence so that the drop diameter does not vary significantly over a range of shear rates.

2.7 References

- Acrivos, A.; Lo, T. S., *J. Fluid Mech.*, **86**, 641 (1978).
- Bentley, B. J.; Leal, L. G., *J. Fluid Mech.*, **167**, 219 (1986)^a.
- Bentley, B. J.; Leal, L. G., *J. Fluid Mech.*, **167**, 241 (1986)^b.
- Chin, H. B.; Han, C. D., *J. Rheol.*, **23**, 557 (1979).
- Chin, H. B.; Han, C. D., *J. Rheol.*, **24**, 1 (1980).
- Cox, R. G., *J. Fluid Mech.*, **37**, 601 (1969).
- Cruz-Orive, L. M., *J. Microsc.*, **107**, 235 (1976).
- De Bruijn, R. A., PhD thesis, Eindhoven University of Technology, Netherlands (1989).
- Elmendorp, J. J.; Van der Vegt, A. K., *Polym. Eng. Sci.*, **26**, 1332 (1986).
- Favis, B. D.; Chalifoux, J. P., *Polym. Eng. Sci.*, **27**, 1591 (1987).
- Fayt, R.; Jérôme, R.; Teyssié, P., "Multiphase Polymers: Blends and Ionomers", L. A. Utracki and R. A. Weiss, eds., ACS Symposium Series 395, American Chemical Society, Washington D. C. (1989).
- Flumerfelt, R. W., *J. Colloid Interface Sci.*, **76**, 330 (1980).
- Flumerfelt, R. W., *Ind. Eng. Chem. Fundam.*, **11**, 312 (1972).
- Golba Jr., J. C.; Seeger, G. T., *Plast. Engineering*, March issue, p57, (1987).
- Grace, H. P., *Chem. Eng. Commun.*, **14**, 225 (1982).
- Hinch, E. J.; Acrivos, A., *J. Fluid Mech.*, **98**, 305 (1980).
- Huneault, M. A.; Shi, Z. H.; Utracki, L. A.; *Polym. Eng. Sci.*, **35**, 115 (1995).
- Liu, N. C.; Baker, W. E., *Polym. Eng. Sci.*, **32**, 1695 (1992).
- Macosko, C. W., "Rheology Principles, Measurements, and Applications", VCH Publishers Inc., New York (1994).
- Paul, D. R., "Polymer Blends", Vol. 2, D. R. Paul and S. Newman, eds., Academic Press, New York (1978).
- Plochocki, A. P.; Dagli, S. S.; Andrews, R. D., *Polym. Eng. Sci.*, **30**, 741 (1990).
- Rallison, J. M., *J. Fluid Mech.*, **109**, 445 (1981).

- Roland, C. M.; Bohm, G. G., *J. Polym. Sci., Polym. Phys.*, **22**, 79 (1984).
- Russ, J. C., "Practical Stereology", Ch. 4, Plenum Press, New York (1986).
- Scott, C. E., PhD thesis, University of Minnesota (1990).
- Sundararaj, U.; Macosko, C. W.; Shih, C. K., *Soc. Plast. Eng. Tech. Papers*, **50**, 1802 (1992).
- Sundararaj, U., Ph. D. Thesis, University of Minnesota (1994).
- Sundararaj, U.; Macosko, C. W., *Macromolecules*, **28**, 2647 (1995).
- Sundararaj, U.; Dori, Y.; Macosko, C. W., *Polymer*, **36**, 1957 (1995).
- Taylor, G. I., *Proc. Roy. Soc. London*, **A138**, 41 (1932).
- Taylor, G. I., *Proc. Roy. Soc. London*, **A146**, 501 (1934).
- Tokita, N., *Rubber Chem. Technol.*, **50**, 292 (1977).
- Utracki, L. A., "Polymer Alloys and Blends", Ch. 1, Hanser Publishers, Munich (1989).
- Utracki, L. A.; Shi, Z. H., *Polym. Eng. Sci.*, **32**, 1824 (1992).
- van Krevelen, D. W., "Properties of Polymers", Elsevier, Amsterdam, (1976).
- Van Oene, H. J., *J. Colloid Interface Sci.*, **40**, 448 (1972).
- Wu, S., *Polym. Eng. Sci.*, **27**, 335 (1987).

Chapter 3

EFFECT OF ORDER OF ADDITION ON COMPATIBILIZATION

3.1 Introduction

The blending of two or more homopolymers to form immiscible blends having certain desired mechanical properties poses a challenge to both industry and academia. Most polymer pairs are not miscible and, therefore, the polymer chains cannot effectively transfer stresses across the interface. Poor adhesion exists between the phases and this leads to poor blend mechanical properties. Hence, there is a need to compatibilize the interface between the individual polymers (Locke and Paul, 1973; Wu, 1985; Borggreve *et al.*, 1989; Liu and Baker, 1992a). This can be done either by adding an external component which stabilizes the interface or by modifying the interface by reacting the components *in situ* (Subramanian, 1985; Scott and Macosko, 1991; Liu and Baker, 1992b; Sundararaj *et al.*, 1992a). Although many studies report ways to compatibilize various immiscible polymer blends, much remains to be understood about the role of compatibilizers.

When a compatibilizer is added to a polymer blend system, it may not always reach the interface or perhaps only a small fraction of it does. Due to large polymer chain lengths, entanglements exist in a polymer blend system and therefore there is a large diffusion barrier for a compatibilizer trying to reach the interface. Thus, there is a good possibility that a compatibilizer remains in the matrix or in the dispersed phase and does not reach the interface. A diblock copolymer may prefer to stay in micellar form in one of the two phases. If the shear forces are not strong enough to destroy this micellar structure, the interfacial stabilization efficiency of the compatibilizer is further reduced. The order of addition of the components may determine the copolymer location and therefore, the order of addition is important in controlling the efficacy of the modifier.

Fayt *et al.* (1986) used transmission electron microscopy (TEM) to directly observe poly-(hydrogenated butadiene-*b*-styrene) block copolymer (HPB-*b*-PIP-*b*-PS) added during melt blending of low density polyethylene (LDPE) and polystyrene (PS). They reported that the copolymer forms a 100 Å thick continuous shell around the dispersed phase but much of the copolymer is preferentially in the LDPE phase. This inclusion is independent of the blending conditions. They observed that the copolymer tends to form microdomains.

Fayt *et al.* (1986) did not consider the effect of diblock molecular weight on the degree of compatibilization. The rule of thumb as stated by Paul (1978) is that the molecular weight of the compatibilizer should be greater than that of the individual homopolymers. If this condition is not satisfied, then the homopolymer tends to form a distinct separate phase (Paul, 1978). However, this conclusion was observed only for the case of solution blends; melt blends were not studied. Fayt and Teyssie (1990) observed improvements in tensile and impact properties of blends of low density polyethylene (LDPE) and commercial high-impact polystyrene (HIPS) as a result of adding a suitable compatibilizer (HPB-*b*-PS). In all their experiments, the block copolymer was first mixed with the minor component before the major component was added.

Nakayama (1994) studied the effect of pre-made versus reactively formed block copolymers for the PS/PMMA system. For the pre-made diblock copolymers, two methods of copolymer addition were studied. In the first case, the diblock was mixed with the dispersed phase before adding the matrix phase, and in the second, all components were added simultaneously. The dispersion was better for the second case. It was found that small molecular weight diblocks cannot stabilize the dispersed phase drops. However, a very high molecular weight diblock has a high diffusion barrier and is unable to reach the interface (Nakayama, 1994). Yang *et al.* (1995) performed work on the effect of order of addition on the final morphology. The system studied was a blend of linear low density polyethylene (LLDPE) and polystyrene (PS), and the compatibilizers used were a diblock

(styrene-ethylene/propylene) (S/EP) and a triblock (styrene-ethylene/butylene-styrene) (S-EB-S). In Yang *et al.*'s work, the different orders of addition consisted only of changing the time when the compatibilizer was added. It was reported that the addition of the copolymer resulted in the formation of an interlocked structure (Yang *et al.*, 1995) and that this structure depended on the time of diblock addition. Schwarz *et al.* (1989) studied the compatibilizing effect of S-EB-S (triblock) and S-EB (diblock) on the blends of high density polyethylene and polystyrene (HDPE/PS), and HDPE/PS with an additional polymer, polyether copolymer (PEC). The formation of a compatibilizer interface was studied using dynamic mechanical thermal analysis (DMTA). They observed a distinct T_g for the compatibilizer in the blend which suggested the presence of a separate phase.

Favis (1994) studied the relationship between the dispersed phase size and the concentration of the compatibilizer or "emulsifier". The dispersed phase size decreases rapidly with emulsifier concentration. This result was attributed to the decrease in interfacial tension. They suggested that there was a critical concentration of the emulsifier (C_{crit}) after which there was no significant change in the size. He has related this C_{crit} value to the interfacial area of the dispersed phase. Tremblay *et al.* (1995) have tried to use scanning transmission electron microscopy (STEM) and electron energy-loss spectroscopy (EELS) to detect and locate the modifier in a polymer blend system. They showed that when the modifier (dimethylamino ethanol) was added to the dispersed phase (bromobutyl rubber) in a two-step mixing procedure, it tended to remain in that phase alone and thus, gave poor emulsification.

3.2 Experimental

3.2.1 Materials

All homopolymers were provided in pellet form. The copolymers used were in powder form. The source, acronym, molecular weight, and the magnitude of the complex viscosity of the materials used are given in Table 3.1. The measurement of the rheological properties like complex viscosity has been described in detail in appendix D. The

polystyrene used in the experiments was Dow Styron 666D (PS666D) which is reported to have a melt index of 7.5 and has a molecular weight $M_w = 200,000$. The poly (methyl methacrylate) (PMMA) was obtained from Rohm and Haas and it has a M_w of 110,000. The synthesis procedure for the PS-PMMA diblocks has been given in an article by Guegan *et. al.* (1993). The diblocks have molecular weights $M_w = 80K-80K$ (160,000), 50K-50K (100,000) and 25K-25K (50,000). The linear low density polyethylene (LLDPE) was Novapol PF-0118-F obtained from Novacor. It has a melt index of 1.0 and has a molecular weight of approximately $M_w = 108,000$. Three compatibilizers were used for the PS/LLDPE system. The diblock used was poly-(styrene/ethylene propylene) obtained from Shell. It has a molecular weight of $M_w = 207,000$ and a styrene content of 27.6 weight% (WRC 0019-89). The two triblocks used were poly-(styrene-ethylene/butylene-styrene) and were obtained from Shell. The triblock WRC 0023-19 has a molecular weight of $M_w = 275,000$ and a styrene content of 32.9 weight%. The triblock CAP75G has a molecular weight of $M_w = 75,000$ and a styrene content of 30 weight%.

3.2.2 Experimental Procedure

Before blending, the pellets were dried overnight in an oven at 80°C to remove traces of any volatiles. The Haake Rheocord 90 torque rheometer with a 600 series batch mixer and roller blades was used for all experiments. The rotation rate was kept constant at 50 rpm. The component weights were calculated using the desired weight percentages of each component. Sundararaj *et. al.* (1992b) used a glass front plate on the mixer to perform visualization of the mixing process. They concluded that when the total melt volume of material comprises 78% of the mixer volume, there is optimum material exchange between the two chambers of the mixer and there are no stagnant areas in the mixer center due to overfilling. This 78% loading corresponds to a melt volume of 54 cm³. The density of each component was estimated using the data given by van Krevelen (1976). In all the blending experiments, the mixer wall temperature was kept constant at 200°C and the rotor speed was set at 50 rpm.

Table 3.1. Properties of Materials used.

Polymer (abbrev.)	Source (functionality)	M_w	T_g (°C)	viscosity η^* at 65 s⁻¹ and 200°C (Pa.s)
Polystyrene (PS666D)	Dow Chemical	200,000	100	950
Polymethyl Methacrylate (PMMA)	Rohm and Hass	110,000	117	11000
PS-PMMA Diblock #1	-	50,000	105	-
PS-PMMA Diblock #2	-	100,000	101	-
PS-PMMA Diblock #3	-	160,000	106	-
Linear Low Density Polyethylene (LLDPE)	Novacor	108,000		4200
Diblock (S-EP) WRC 0019-89	Shell	207,000		-
Triblock (S-EB-S) WRC 0023-89	Shell	275,000		-
Triblock (S-EB-S) CAP 75G	Shell	75,000		-

For the PS/PMMA blends, the weight fraction of the dispersed phase was kept constant at 10%. The copolymer weight percent was kept at 10% of the dispersed phase (that is 1% of the total blend). The ratio of dispersed to matrix phase concentration was the same as that in the uncompatibilized blend-for “x%” dispersed phase, the blend ratio (major:minor:copolymer) would be (100-y) : 0.9y : 0.1y, where “y%” = “x%”/(0.9 + 0.001 “x%”).

Order of Addition

Four different orders of addition were studied, as described below:

1. (#1) The mixer was preheated to the starting temperature (200°C). The rotor blades were rotating at the set rate (50 rpm). Pellets of the minor and major phase components and the compatibilizer powder were dry mixed in a beaker. The components were then added to the mixer through a feed chute pushed with a ram with a 5 kg mass.
2. (#2) The mixer was preheated to the starting temperature. The block copolymer and the dispersed phase were first added to the rotating mixer. The torque peaked and then decreased indicating that the dispersed phase had melted completely. The matrix phase was added through the feed chute.
3. (#3) The mixer was preheated to the starting temperature. The block copolymer and the matrix phase were added to the rotating mixer at the same time. This addition was completed within 25 seconds of starting the run. The torque peaked and then decreased as the matrix phase melted. After the matrix had melted, the dispersed phase was added to the chamber.
4. (#4) The mixer was kept at room temperature. The dispersed phase pellets, the diblock copolymer powder, and the matrix phase pellets were added to the cold mixer. The temperature of the mixer was raised to 200°C. When the components melted, the diblock powder was at the interface. Once the mixer wall reached 200°C, the rotor was started.

To observe the effect of compatibilizer molecular weight, three different PS/PMMA diblocks with different molecular weights were used (25K-25K, 50K-50K and 80K-80K). To calculate the minimum amount of emulsifier required to compatibilize the PS/PMMA system, the blends were prepared at different concentrations of the 80K-80K PS-PMMA diblock (1% to 15% of the dispersed phase concentration).

Table 3.2. Experimental Runs. (Temperature for all runs = 200°C)

System (Matrix/Dispersed)	Viscosity Ratio at 65 s⁻¹ and 200°C	Shear Rate (s⁻¹)	Orders of Addition used^b
PS/PMMA (uncompatibilized)	11.6	65	-
PS/PMMA (compatibilized with diblock)	11.6*	65	#1, #2, #3, #4.
PS/LLDPE (uncompatibilized)	4.4	65	-
PS/LLDPE (compatibilized using a. diblock. b. triblock.)	4.4*	65	#1, #2, #3, #4.

^b Refer to the Experimental Section.

* Same as for the uncompatibilized system.

The runs are summarized in Table 3.2. The mixing time for all the blends was 10 minutes, and it was assumed that stable morphology was reached for blend pairs at the conditions used (Scott, 1990). During the run, the Rheocord program measured the torque and the melt temperature in the batch mixer. After 10 minutes, the motor was stopped and the front plate and the middle section of the mixer barrel were removed exposing the roller blades. Most of the material was attached to the blades and a sample was removed from the blade indents and immediately quenched in liquid nitrogen. The sample was withdrawn within 25 seconds of stopping the motor. In many cases, a fracture surface was created when the hot blend imploded by rapid quenching in liquid nitrogen. In cases where the sample did not implode in liquid nitrogen, the sample was cooled in liquid nitrogen and

then broken using a hammer. The sample was then prepared for scanning electron microscopy (SEM) by adhering it to a SEM stub and coating with carbon. A HITACHI S-2700 SEM instrument was used for observation.

The diameter of the dispersed phase was measured using the image analysis software NIH Image 1.58b33, developed by the National Institute of Health (NIH). For image analysis, the particles from the SEM micrographs were outlined and the tracing was scanned. The software calculated the area of each particle and the diameter was calculated assuming that the particles were spherical. Around 200-250 particle diameters were measured for each blend and the average and standard deviation were calculated for each case. A size correction was done to account for the error in the measured diameter due to the fact that the section does not necessarily pass through the center of each sphere,. The Cruz-Orive method (Cruz-Orive, 1976), recommended by Russ (1986) was used. The use of this method for polymer blends has been described by Sundararaj *et. al.* (1995). However, the difference between the corrected and measured diameter was less than 10% and therefore, these corrections were neglected. The error bars shown for each point in the plots are one standard deviation in each direction for the particle sizes measured. The limits of the error bars are a measure of the particle size distribution.

To understand the torque and the temperature profiles better, Differential Scanning Calorimetry (DSC) was performed on the homopolymers and the PS-PMMA diblocks. A differential scanning calorimeter (DSC 2200) was used for the purpose. The values of the transition temperatures are given in Table 3.1. PS has a transition at 100°C and PMMA has a transition at 117°C. A part of the diblock has some crystallinity due to the presence of some syndiotactic PMMA. Hence, the diblocks show a dual transition: one for the purely amorphous PS-PMMA chains (105°C) and the other for the ordered PMMA chains (at around 140°C).

3.3. Results

Fig. 3.1 shows the “emulsification curve” (Favis, 1994) obtained for the diblock having $M_w = 80K-80K$ using the order of addition #1. Once the diblock concentration exceeded 4 weight % of the dispersed weight fraction for 90:10 PS/PMMA blend ratio, there was no change in the dispersed phase size. Therefore, for all experiments, a diblock concentration of 10 % of the dispersed phase concentration was chosen. That means, if the dispersed phase concentration was 5 wt%, the diblock concentration was 0.5 wt% of the total blend.

The effect of order of addition of the components was studied for the PS/PMMA and the PS/LLDPE systems. Fig. 3.2 and Fig. 3.6 show the graphs of average dispersed phase drop diameter versus the molecular weight of the diblock for different orders of addition. The values of average dispersed phase diameter have been summarized in Table 3.3 (for the PS/PMMA system) and Table 3.4 (for the PS/LLDPE system). The graphs show that adding a copolymer is effective in stabilizing the interface. For the PS/PMMA system, there is a decrease in drop diameter from 0.4 μm for the uncompatibilized blend to 0.2-0.3 μm for the compatibilized blends (see Fig. 3.2). There is also a decrease in the standard deviation for the compatibilized blends which implies that in these blends there is a more uniform distribution of particle size compared to that found in the uncompatibilized case.

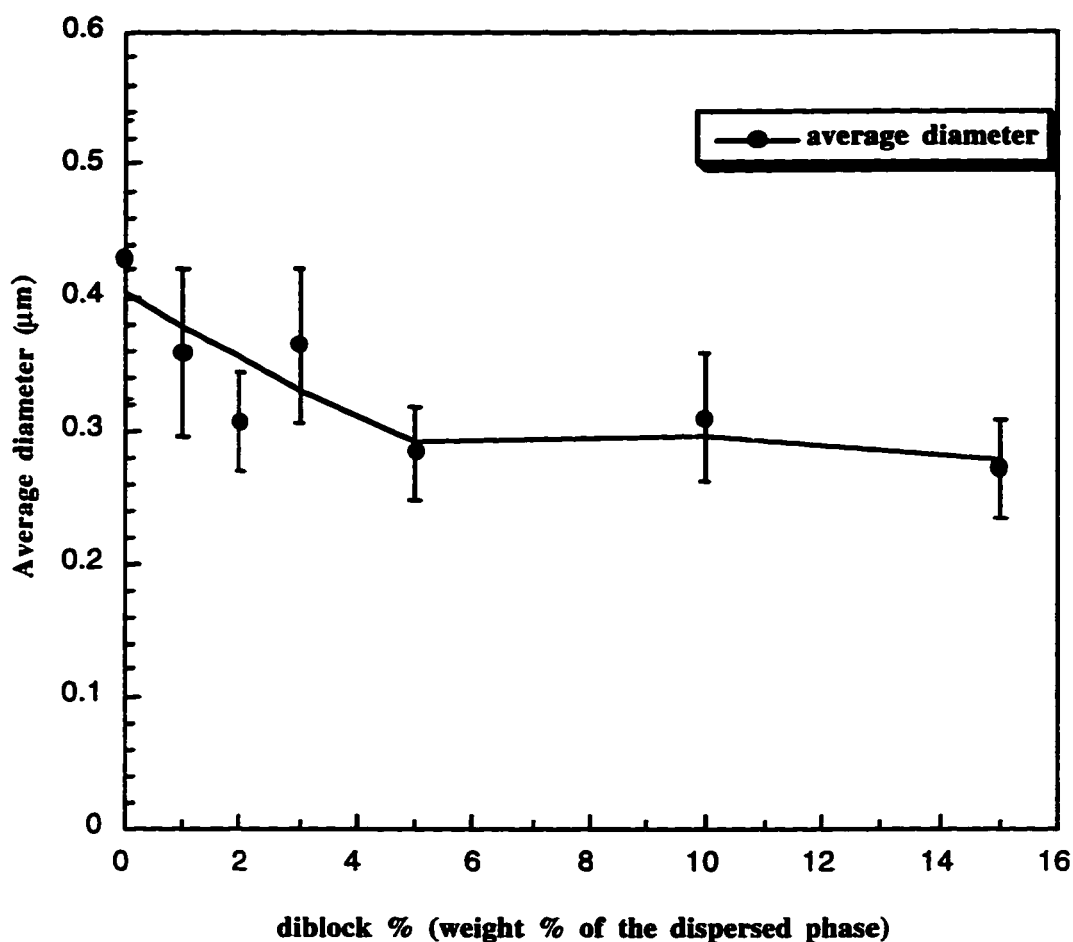


Fig 3.1
Average diameter of the dispersed PMMA phase (for a blend of 10 wt% PMMA in PS666D) versus PS-PMMA diblock concentration ($M_w=80K-80K$) (weight % of the dispersed phase). The temperature was 200°C and the rotation rate was 50 rpm. The critical diblock concentration to reach equilibrium was 4% of the dispersed phase (0.4% of the total blend).

It was mentioned earlier that for solution blends, the diblock molecular weight has to be greater than that of the homopolymers for compatibilization to be effective (Paul and Newman, 1978). This rule may not be applicable for melt blending operations, since in our experiments, short PS/PMMA diblocks ($M_w = 25K-25K$ and $50K-50K$) stabilized blends of long homopolymers ($M_{w,PS} = 200K$; $M_{w,PMMA} = 110K$).

Table 3.3. Results for the PS/PMMA system (with symmetrical PS/PMMA diblock copolymers).

Diameter for the uncompatibilized case = $0.43 \pm 0.11 \mu\text{m}$.

Diblock M_w	Diameter (order 1) (μm)	Diameter (order 2) (μm)	Diameter (order 3) (μm)	Diameter (order 4) (μm)
50,000	0.26 ± 0.04	0.32 ± 0.06	0.30 ± 0.03	0.22 ± 0.03
100,000	0.23 ± 0.04	0.21 ± 0.03	0.27 ± 0.05	0.20 ± 0.03
160,000	0.24 ± 0.04	0.23 ± 0.03	0.21 ± 0.02	0.19 ± 0.04

Fig. 3.2 shows how the average diameter changes with order of addition for the PS/PMMA system. The particle size depends greatly on the order of addition for the 25K-25K diblock. There is less variation in the diameter for the higher molecular weight diblocks when the order of addition is changed. Longer chain length diblocks have a higher penetration into the homopolymers. Therefore, a small amount of high molecular weight diblock is sufficient to stabilize the interface and order of addition may not play a large role.

Fig. 3.3(a), 3.4(a) and 3.5(a) show the effect of order of addition for the diblocks having $M_w = 25\text{K}-25\text{K}$; $50\text{K}-50\text{K}$ and $80\text{K}-80\text{K}$ respectively. The uncompatibilized blend has an average dispersed diameter of $0.43 \mu\text{m}$. Fig. 3.3a gives the results for the diblock having $M_w = 25\text{K}-25\text{K}$. The low molecular weight diblock is expected to be the most mobile; therefore, it was thought that this diblock should give the best dispersion. However, the diameters obtained for the 25K-25K diblock are larger than those obtained for the other diblocks. The diblock has a small chain length and therefore, its penetration into either phase will be limited. This leads to poor compatibilization of the blend and results in a higher particle diameter.

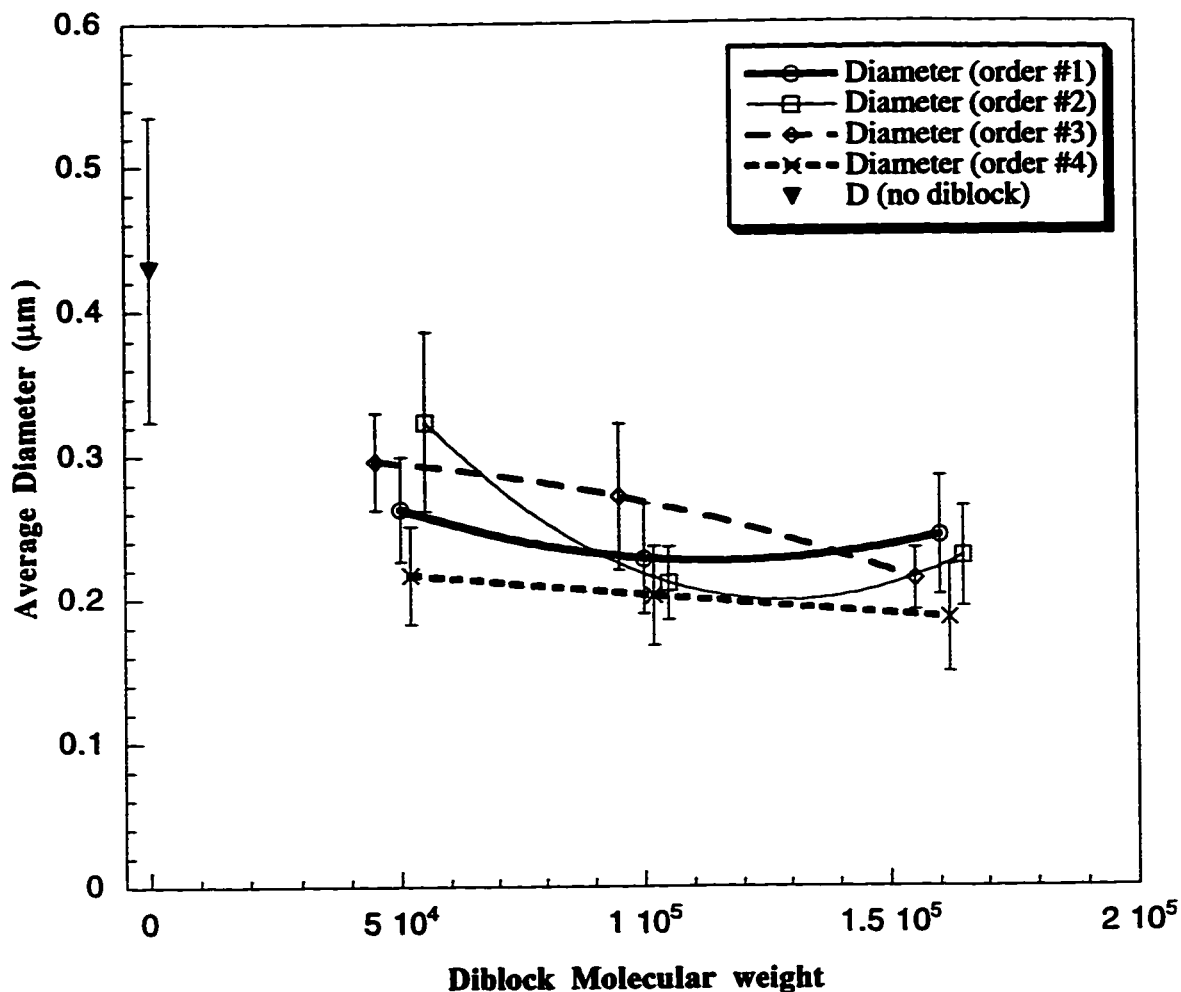


Fig 3.2
Average diameter of the dispersed PMMA phase (for the 90:10 PS/PMMA system) versus PS-PMMA diblock molecular weight. The temperature for all blends was 200°C and the rotation speed was 50 rpm. The graph is plotted for the several different orders of addition. The molecular weights are staggered to enable proper observation of the graph.

Torque profiles were studied to interpret the blending process. Fig. 3.3(b) gives the torque profile for all the orders of addition for the diblock with $M_w = 25K-25K$. When the diblock is added with either the dispersed phase or the matrix phase, two peaks are observed, each representing the melting of one phase. For the order of addition when the diblock is mixed with the matrix phase first, the small shoulder next to the main peak represents the melting of the dispersed phase (Fig. 3.3(b)). The peaks represent the relative amount of power input needed to completely melt a particular phase. Only one

peak is observed when all the components are added at the same time. The case where the components are premelted before mixing does not show a torque peak. Since the components are already melted when the mixing begins, only a small amount of power input is required.

Fig. 3.4(a) shows the average diameters for the different orders of addition of the diblock having $M_w = 50K-50K$. This diblock has less mobility than the 25K-25K diblock. However, because of the higher molecular weight, these blends require less copolymer to cover the interface and result in better stabilization of the interface. This leads to particle size smaller than the 25K-25K diblock. The torque profiles for the different orders of addition using this diblock are shown in Fig. 3.4(b) and the interpretation of the torques are similar to that of Fig. 3.3b.

Fig. 3.5(a) gives the profile for the diblock with $M_w = 80K-80K$. This was the largest molecular weight diblock studied for this system. Again, the best dispersion is achieved when all the components are premelted before mixing. When all the components are added together (order of addition 1), the diameter is large compared to the other orders of addition. The torque profile for this case (Fig. 3.5(b)) shows a much smaller relative to the other orders of addition.

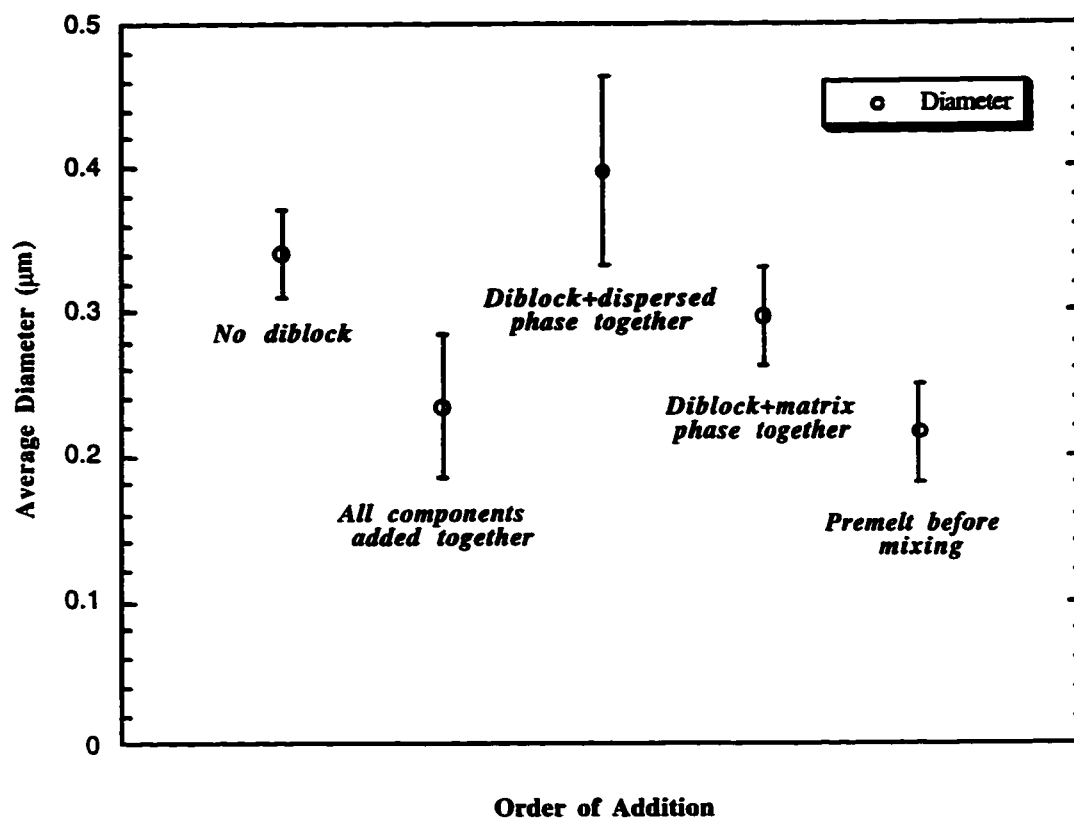


Fig 3.3 (a)
Effect of order of addition of the components on the average dispersed phase particle diameter for the PS/PMMA system (compatibilizer is PS-PMMA diblock having $M_w=25K-25K$).

Fig. 3.6 shows the average diameter of LLDPE versus the compatibilizer molecular weight for different orders of addition. Like the PS/PMMA system, the case where all the components are premelted before mixing gives the best dispersion for the PS/LLDPE system. This effect is independent of the molecular weight of the compatibilizer. For PS/LLDPE, the diameter increases with the molecular weight of the compatibilizer. One should note, however, that one of the compatibilizers, P(S-E/P), is a diblock (total $M_w=207$ K), whereas the other two are triblocks (total $M_w=75$ K and 275 K respectively). The diameter measured for the $M_w=275$ K compatibilizer is similar to that for the

uncompatibilized case. The molecular weights of the triblock (WRC 0023-89) and the diblock (WRC 0019-89) are greater than that of the homopolymers. These results indicate that compatibilization is better if the compatibilizer molecular weight is the same or lower than that of the homopolymers.

Table 3.4. Results for the PS/LLDPE system.

Diameter for the uncompatibilized case = $0.90 \pm 0.11 \mu\text{m}$.

Diblock M_w	Diameter (order 1) (μm)	Diameter (order 2) (μm)	Diameter (order 3) (μm)	Diameter (order 4) (μm)
75,000 ^a	0.62 ± 0.11	0.64 ± 0.11	0.67 ± 0.10	0.52 ± 0.07
207,000 ^b	0.59 ± 0.08	0.60 ± 0.07	0.79 ± 0.14	0.58 ± 0.08
275,000 ^c	0.69 ± 0.14	0.88 ± 0.19	0.87 ± 0.16	0.66 ± 0.09

^a S-(E/B)-S triblock (Styrene content = 30%)

^b S-(E/P) diblock (Styrene content = 27.6%)

^c S-(E/B)-S triblock (Styrene content = 32.9%)

The effect of order of addition of the 75K triblock on the dispersed phase diameter is shown in Fig. 3.7. The triblock is an S-EB-S, where the styrene blocks are thought to be compatible with the PS matrix and the ethylene-butylene blocks are thought to be compatible with the LLDPE phase. The diameter of the dispersed phase is similar for all the orders of addition except the case where all the components are premelted before mixing.

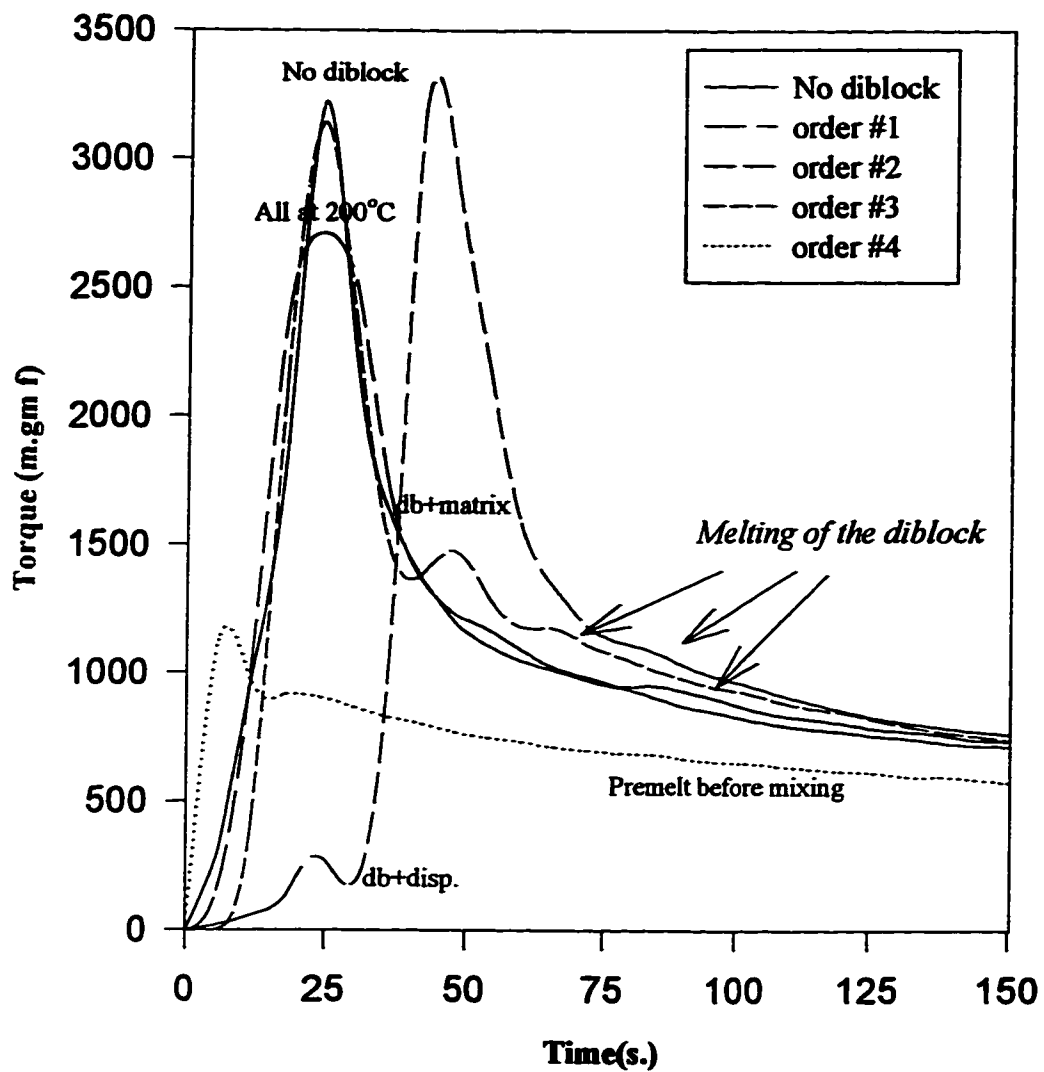


Fig 3.3 (b)
 Torque profiles for the different orders of addition for the PS/PMMA system (PS-PMMA diblock $M_w = 25K - 25K$).

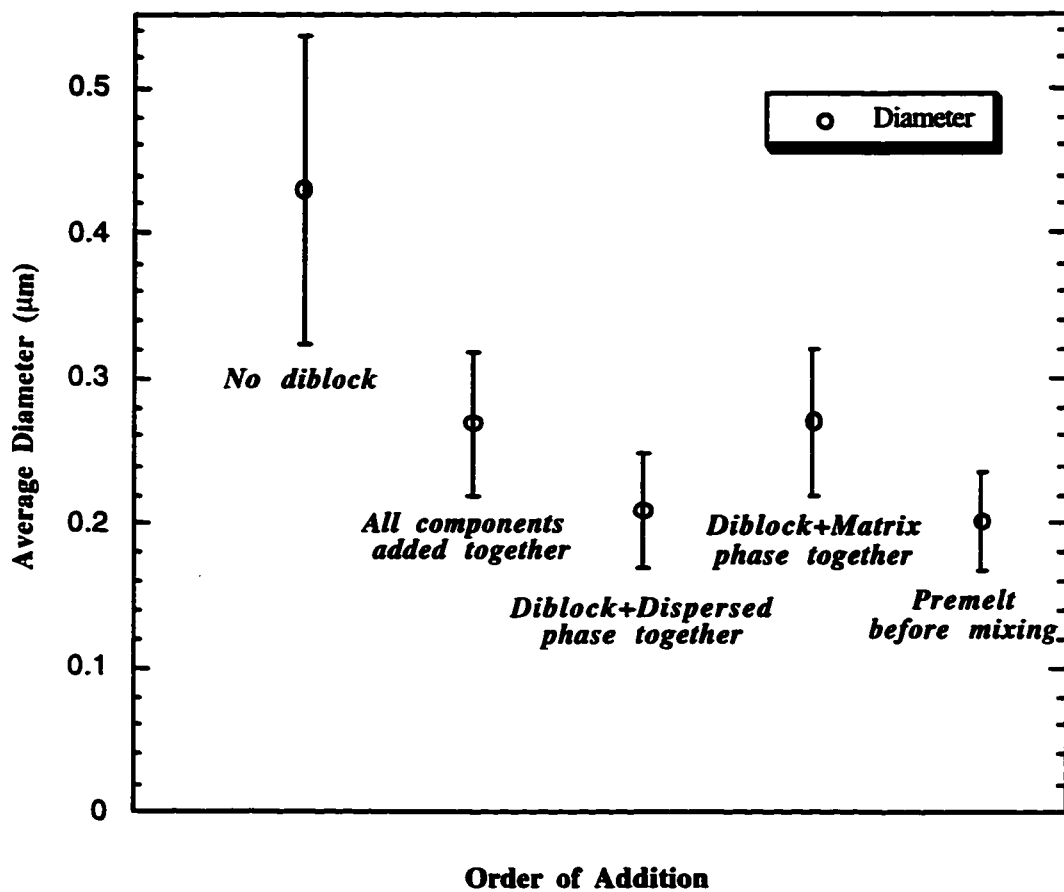


Fig 3.4 (a)
 Effect of order of addition of the components on the average dispersed phase particle diameter for the PS/PMMA system (compatibilizer is PS-PMMA diblock having $M_w=50\text{K}-50\text{K}$).

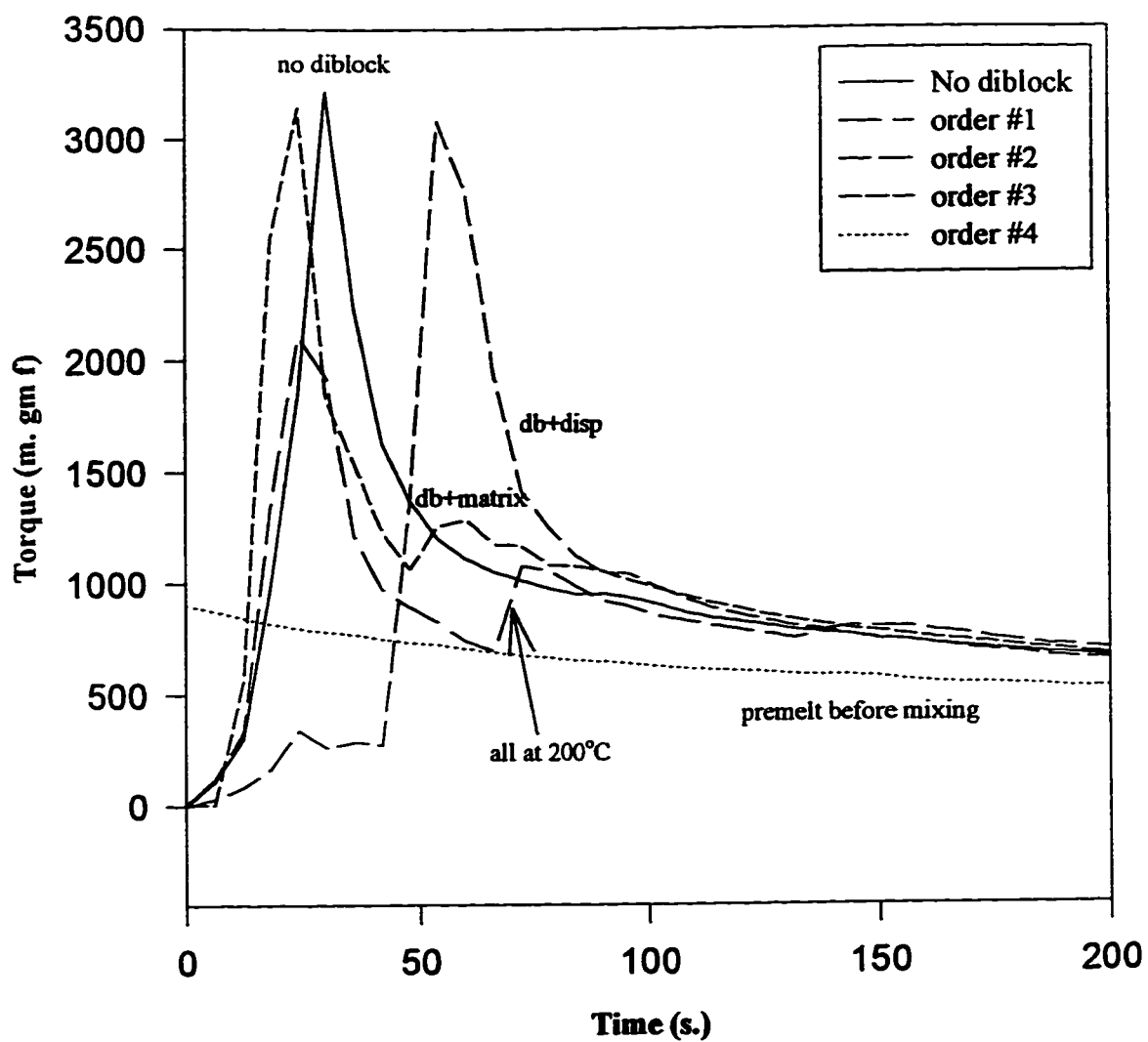


Fig 3.4 (b)
Torque profiles for the different orders of addition for the PS/PMMA system (PS-PMMA diblock $M_w = 50K - 50K$).

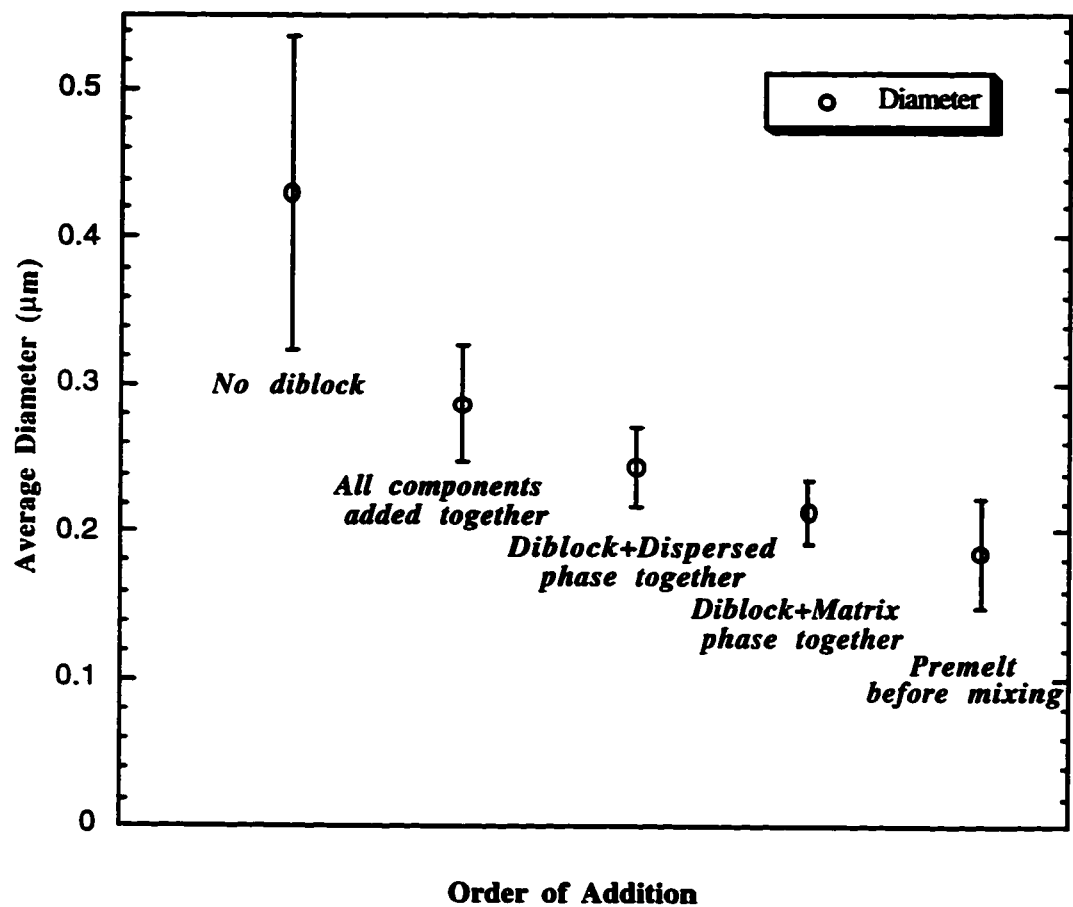


Fig 3.5 (a)
 Effect of order of addition of the components on the average dispersed phase particle diameter for the PS/PMMA system (compatibilizer is PS-PMMA diblock having $M_w=80\text{K}$ - 80K).

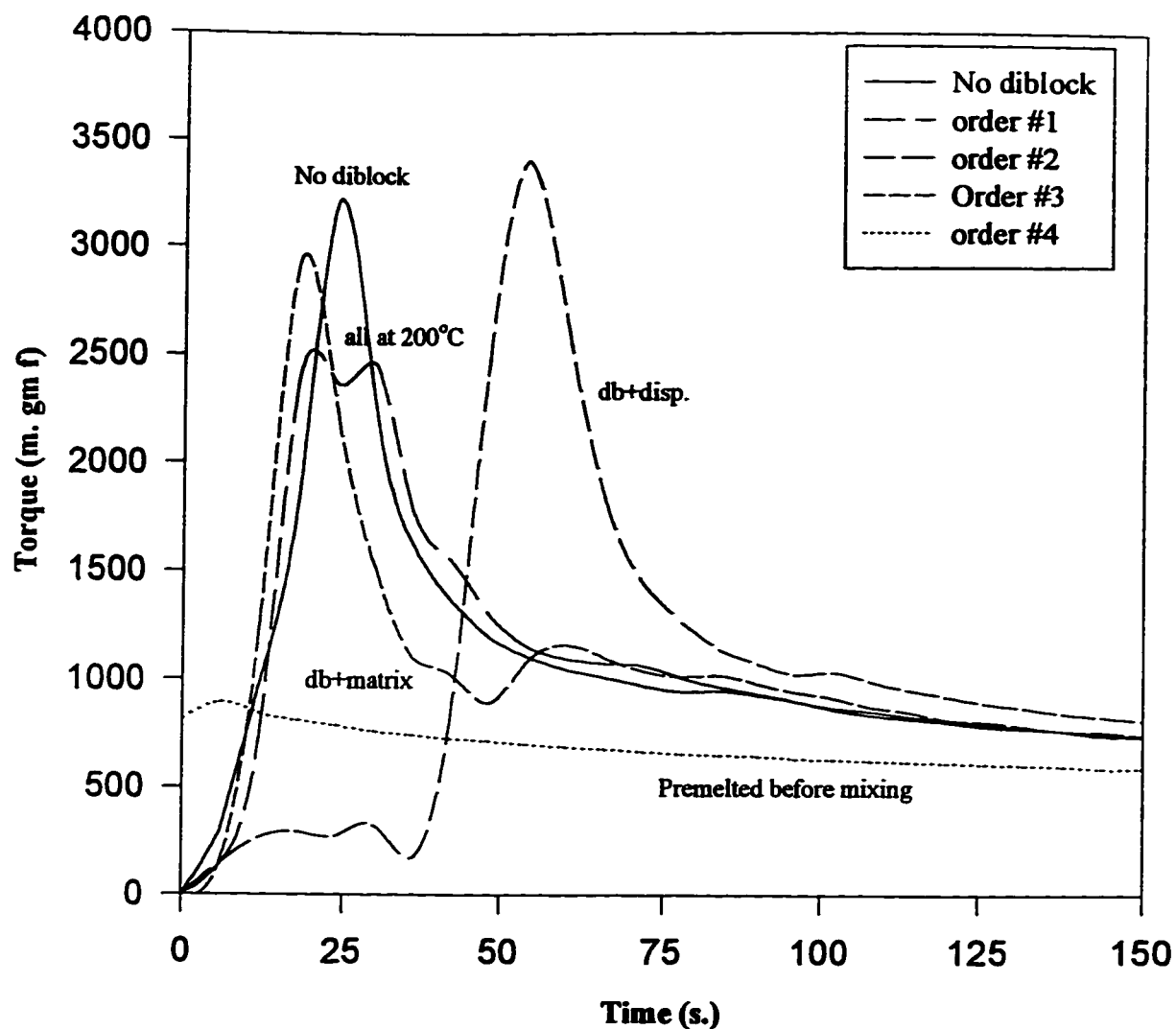


Fig 3.5 (b)
Torque profiles for the different orders of addition for the PS/PMMA system (PS-PMMA diblock $M_w = 80K - 80K$).

Fig. 3.8 shows the results for the diblock S-EP having $M_w=207 K$. Among all the addition orders, addition order 3 (in which the compatibilizer is added with the matrix phase) shows the largest dispersed phase diameter. Again, the best dispersion is achieved when all the components are premelted before mixing presumably because the diblock was at the interface at the start of the mixing process. Fig. 3.9 shows the effect of order of addition for the triblock S-EB-S with $M_w=275,000$. The dispersed phase diameter is large when the compatibilizer is added with either the dispersed phase or the matrix phase. The high molecular weight of the triblock hinders its diffusion to the interface. The diameter of

the LLDPE phase is small when all components are added simultaneously at 200°C and also when the components are premelted before mixing.

3.4. Discussion

Assuming that all of the copolymer reaches the interface, the amount of block copolymer required to saturate the interface in a polymer blend was estimated using the radius of gyration of one block and the total interfacial area in the blend. Since some copolymer may be in micelles, the value predicted may not be accurate. For a 90:10 blend, the amount of copolymer required for a 25K-25K diblock having a radius of 0.3 μm is 1.6 wt% of the dispersed phase (i.e. 0.16 wt% of the total blend). Experimentally, it was observed that beyond 4 wt% of the dispersed phase (i.e. 0.4 wt% of the total blend), there is no reduction in dispersed phase particle size. However, the prediction from the simple calculation assumed that all the copolymer reaches the interface.

Fig. 3.10 shows the SEM micrographs for the blends prepared for the “emulsification” curve (Fig. 3.1). The micrographs show the blend morphology for a PS/PMMA blend compatibilized using an 80K - 80K diblock. The weight fraction of the compatibilizer was increased and the average particle diameter measured. From the micrographs, it can be seen that the average particle size decreased with increase in the compatibilizer weight percent. There is a sharp decrease initially and after critical diblock concentration, the diameter levels off.

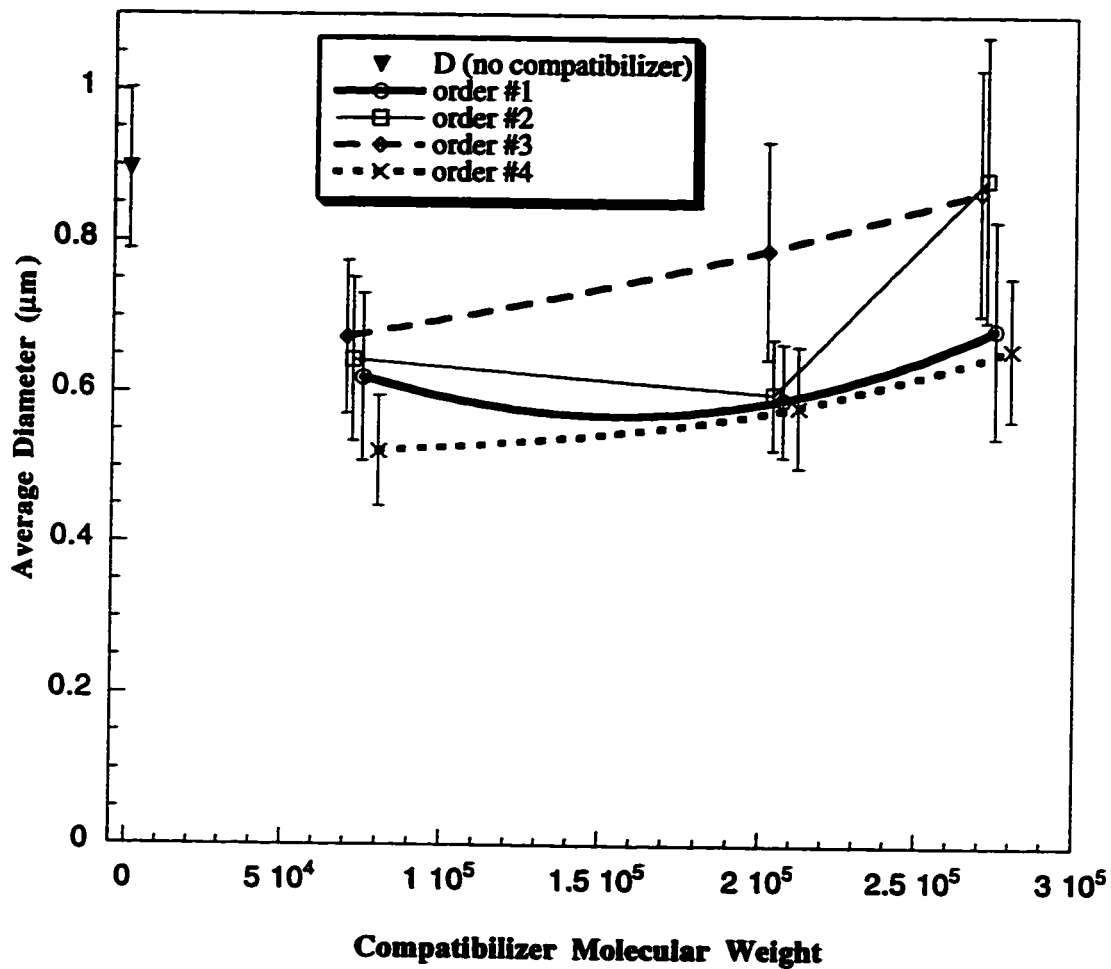


Fig 3.6
 Average diameter of the dispersed LLDPE phase (for the 90:10 PS/LLDPE system) versus total compatibilizer molecular weight. The temperature for all blends was 200°C and the rotation speed was 50 rpm. The graph is plotted for the several different orders of addition. The diameters for each diblock are staggered to enable proper observation of the graph.

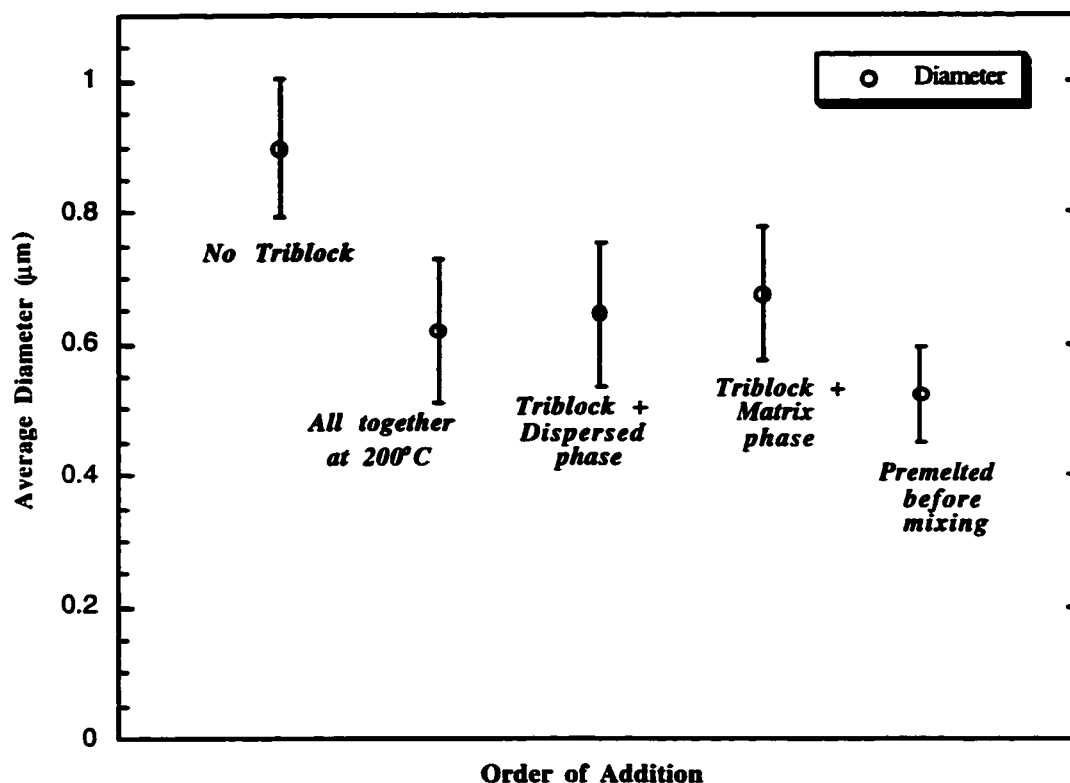


Fig 3.7
Effect of order of addition of the components on the average dispersed phase particle diameter for the PS/LLDPE system (compatibilization done by triblock having $M_w = 75$ K).

The order of addition played a role in diblock morphology generation. From Fig. 3.2, it is observed that regardless of the diblock molecular weight, the best dispersion is obtained when the components were premelted before mixing (order of addition 4). In this method of addition, the diblock was forced to be at the interface before mixing began. No melting occurred during the addition of pellets or powder to a stationary mixer at room temperature. Since the pellets of PMMA, the pellets of PS and the copolymer powder were fed to a cold mixer, the copolymer powder coated the pellets before melting. When the mixer temperature increased to 200°C, the components melted. Then the roller blades were

rotated and the pellets broke up into small drops. From the very start of the mixing operation, the compatibilizer was at the interface. Therefore, as the drops broke up, the compatibilizer stabilized the interface and prevented coalescence. As a result, the smallest particle diameter was obtained when all the components were premelted before mixing. The stabilization for this order of addition (premelted case) was not greatly dependent on the molecular weight of the diblock (see Fig. 3.2). The diblock saturated the interface from the start of the mixing operation and its relative mobility was not important for this addition order.

For the 25K-25K PS-PMMA diblock (Fig. 3.3(a)), we observed the largest dispersed phase particle diameter when the diblock and the dispersed phase were added together (order of addition 2). Table 3.1 shows that the viscosity of PMMA at a shear rate of 65 s^{-1} is 11000 Pa.s, which is over 11 times that of PS at the same shear rate (950 Pa.s). When the 25K-25K diblock was added with the high viscosity dispersed phase PMMA (see Table 3.1), it may have been trapped in the dispersed phase. The diblock chains may not have been able to diffuse through the highly viscous PMMA. When the diblock was added with the low viscosity matrix phase PS (order of addition 3), the particle size was small since the diblock was able to diffuse to the interface resulting in better stabilization. The average diameter for the case when all components were added together at 200°C (order of addition 1) is comparable to that for the case where all components were premelted before mixing. The two orders of addition have comparable particle diameters because of the high mobility of the 25K-25K diblock. Among all the addition orders, the premelted case had the smallest particle diameter.

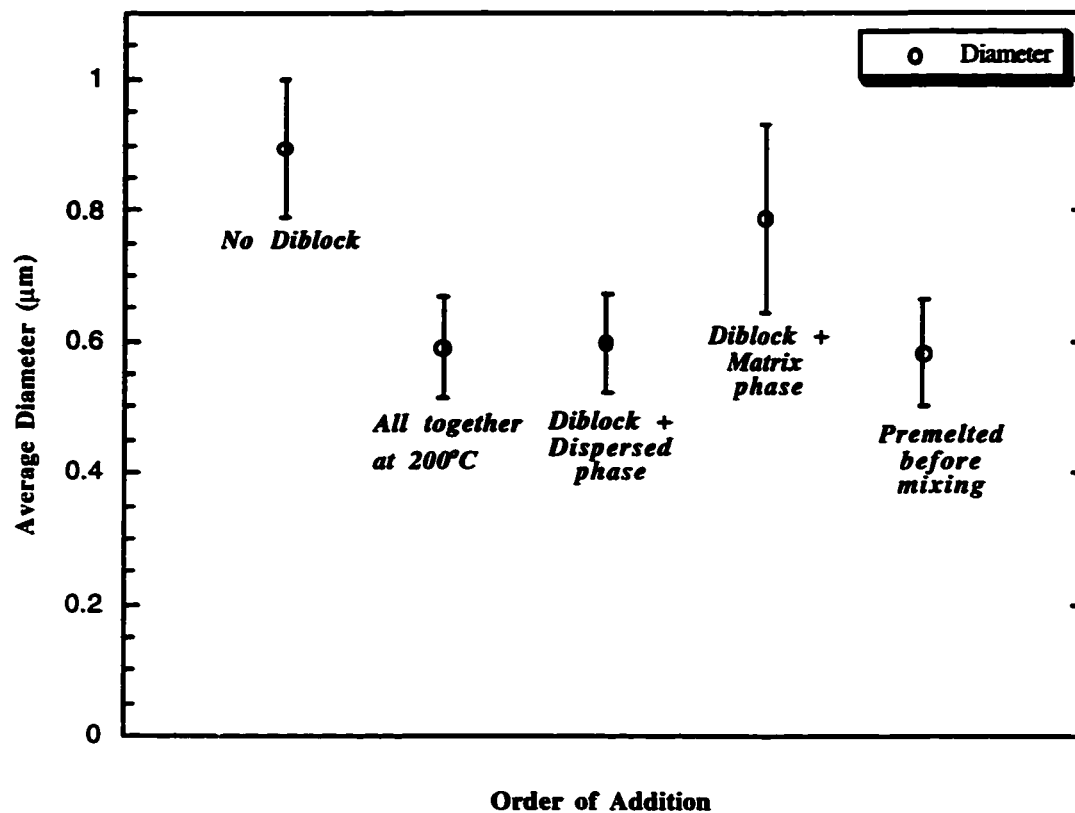


Fig 3.8
 Effect of order of addition of the components on the average dispersed phase particle diameter for the PS/LLDPE system (compatibilization done by triblock having $M_w = 207$ K).

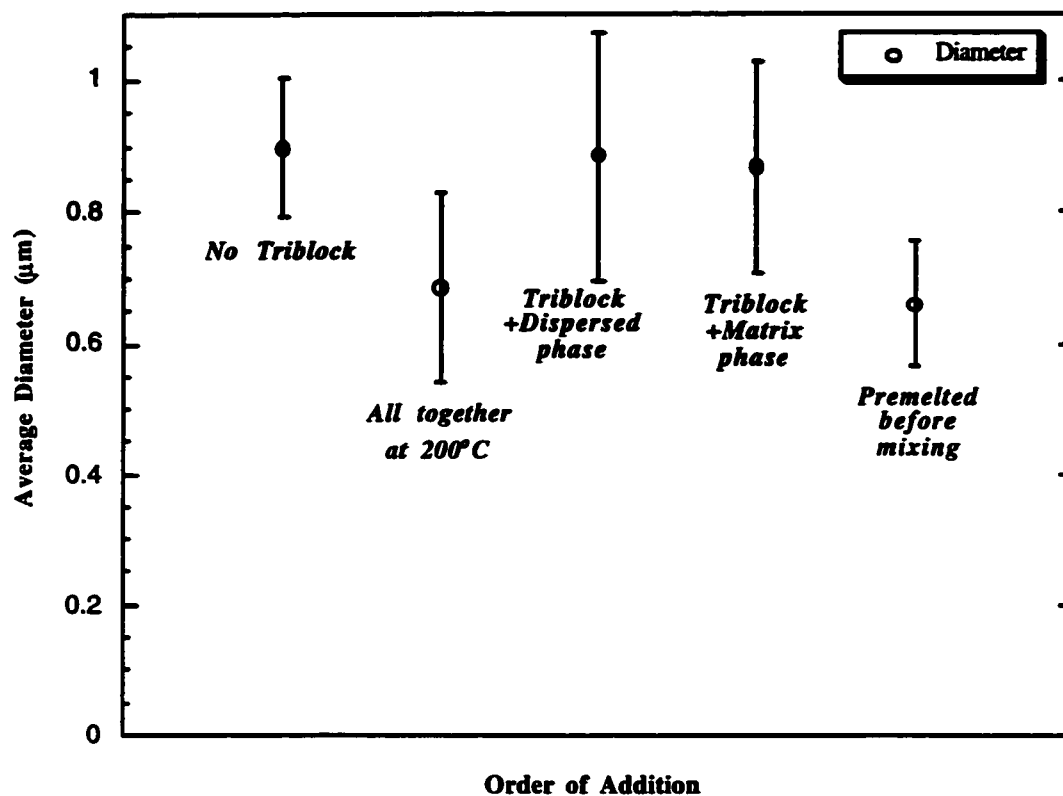
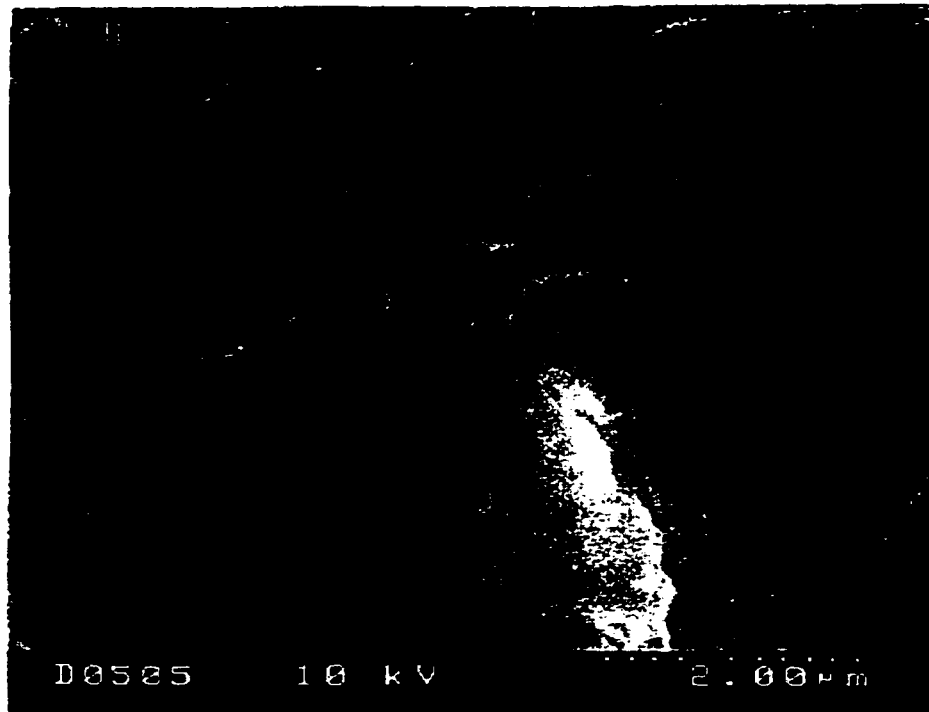
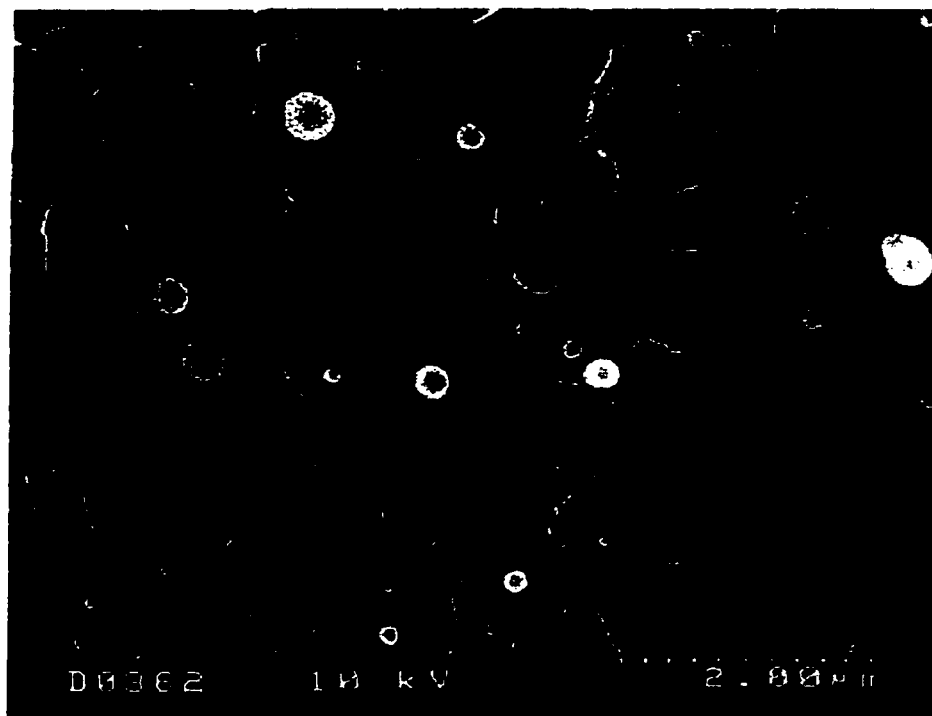


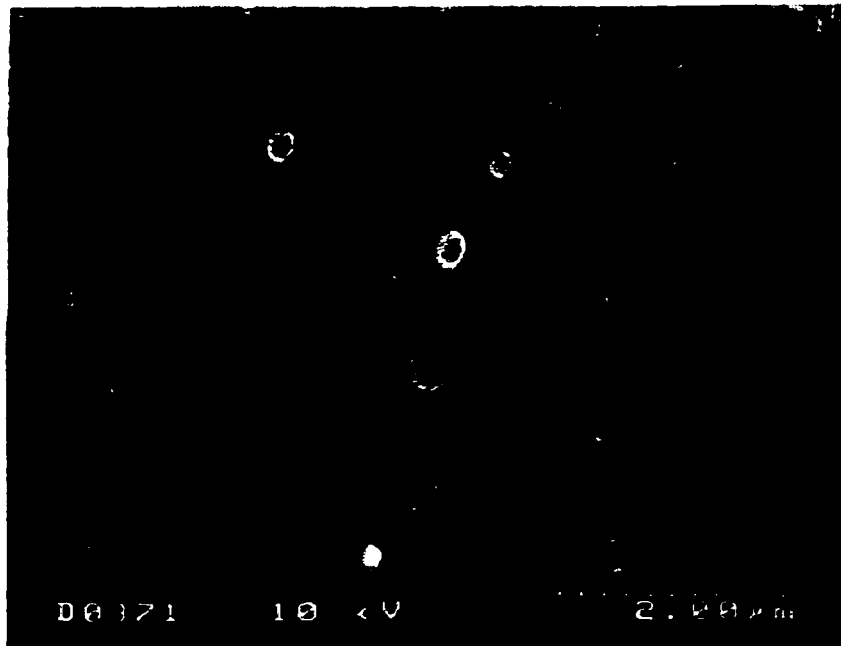
Fig 3.9
 Effect of order of addition of the components on the average dispersed phase particle diameter for the PS/LLDPE system (compatibilization done by triblock having $M_w = 275$ K).



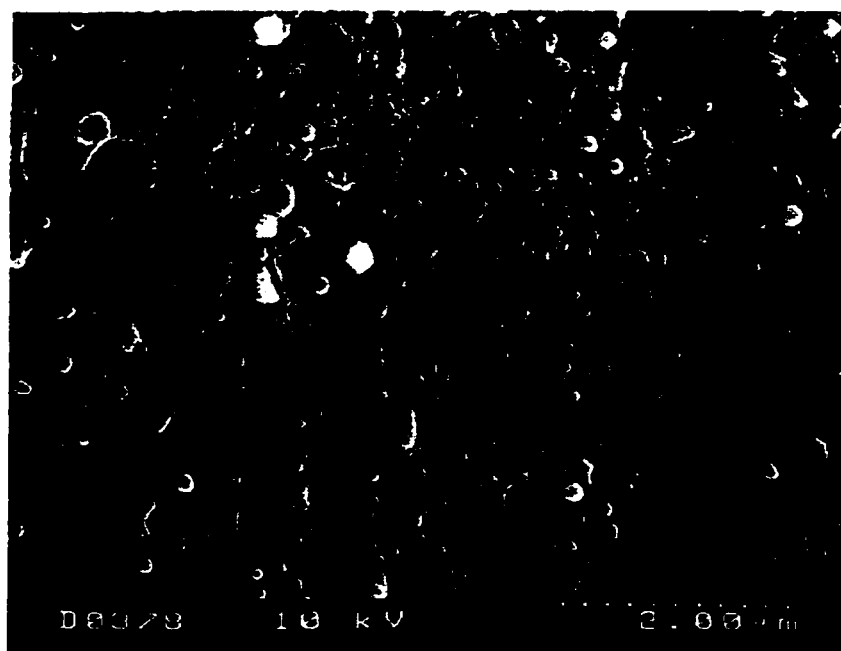
(a)



(b)



(c)



(d)

Fig 3.10
SEM micrographs showing the dispersed PMMA drops in a matrix of PS for the "emulsification" curve [Fig 3.1] of 90:10 PS:PMMA blend with the PS-PMMA 80K-80K diblock added at the following compositions: (a) 0.5 wt%, (b) 1 wt%, (c) 5 wt% and (d) 15 wt% of the dispersed phase concentration.

The torque traces are used to interpret the blending process. Fig. 3.3(b), 3.4(b) and 3.5(b) show the torque traces for the blends compatibilized with the diblocks having molecular weights 25K-25K, 50K-50K and 80K-80K respectively. The torque traces for nearly all the addition orders showed a small bump at a temperature higher than the melting points of the homopolymers. The “bumps” have been marked out in Fig. 3.3(b) and are thought to be due to melting of the diblock. Therefore, the diblock is thought to melt after the two main components. The PS-PMMA diblocks showed a dual transition in their melting curves during the differential scanning calorimetry (DSC) (see Table 3.1). Some of the PMMA had syndiotacticity. This resulted in a melting transition at 140°C. As a result, the copolymer melted at a later time as compared to the individual homopolymers. This hinders compatibilization since the diblock may have a tendency to get stuck in the phase which melts first.

For the PS/PMMA system compatibilized with the 80K-80K diblock, the minimum diameter was observed for the case when the components were premelted before mixing. The higher molecular weight diblock cannot diffuse easily to the interface. Hence, for the case where all the components were added together (addition order 1), the diffusion of the compatibilizer to the interface was relatively slow. However, because of the large chain length, only a small amount of compatibilizer was required to stabilize the dispersed phase and the compatibilization was more effective than the 25K-25K diblock (Fig. 3.2). When the diblock was added with the dispersed phase PMMA, the diblock could not diffuse through the high viscosity dispersed phase. Therefore, the diameter observed for order of addition 2 (diblock and dispersed phase together) was greater than the diameter observed for addition order 3 (diblock and matrix together).

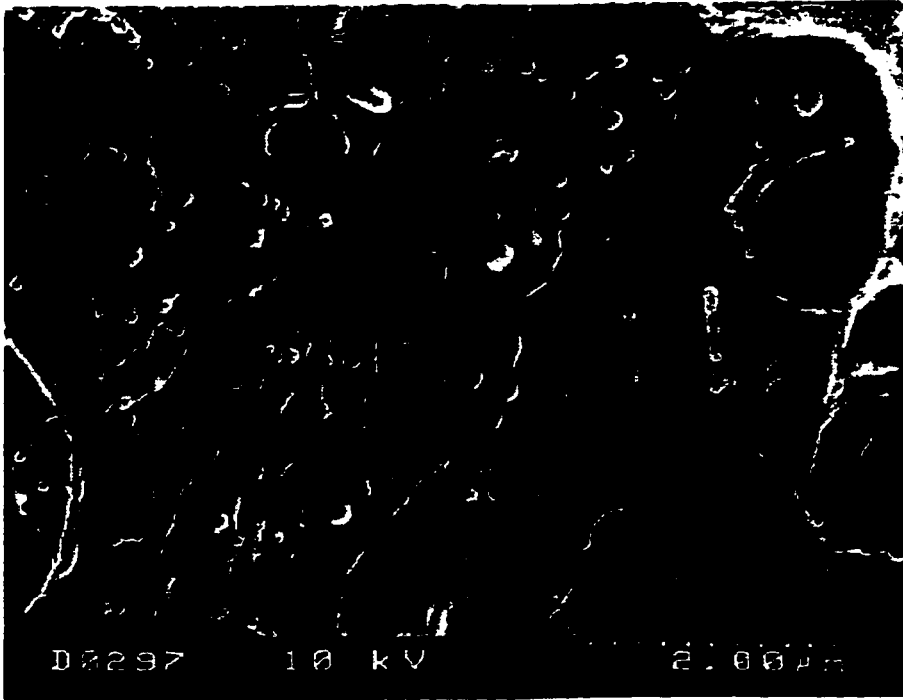
The torque profiles for all the compatibilized blends had one thing in common. The addition order in which all the components were added together at 200°C (order of addition #1) showed a smaller torque peak as compared to the other addition orders (Figs. 3.3(b), 3.4(b), and 3.5(b)). The presence of the compatibilizer reduced the torque peak from about

3250 to about 2600 m-gmf. The compatibilizer may have lubricated the mixer and decreased the resistance. However, the torque decrease was not evident for the other addition orders in which the compatibilizer was present.

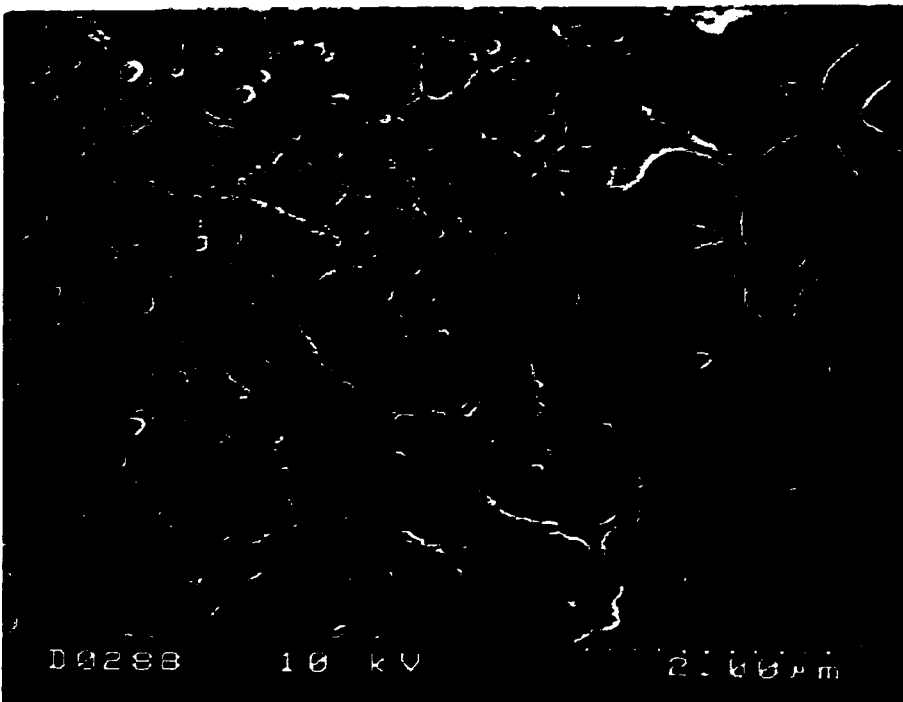
Fig. 3.11 shows the SEM micrographs of the 90/10 PS/PMMA blend compatibilized with the diblocks. For order of addition 4 (premelting before mixing), the particle diameters for different diblock molecular weight are comparable. However, the diameter decreases modestly as the molecular weight of the diblock increases.

The SEM micrographs showing the effect of order of addition for the 80K-80K PS-PMMA diblock are given in Fig. 3.12. The uncompatibilized system has a larger diameter than the compatibilized systems. Order of addition 4 (premelting before mixing) does show smaller particles than the other addition orders and this is again in agreement with the results shown (Fig. 3.2).

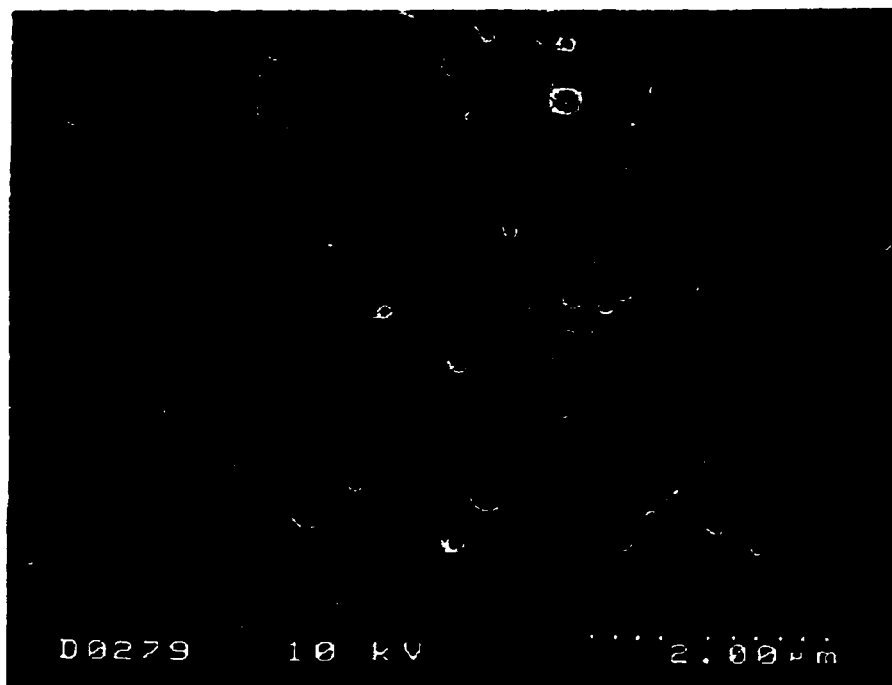
The PS/LLDPE system was also studied and the compatibilization performed using the different molecular weight diblocks and triblocks (Fig. 3.6). All the P(S/E-P) compatibilizers had styrene contents of around 30 wt%. Thus, these were different from the symmetric diblock copolymers used for the PS-PMMA system. The smallest diameter for the PS/LLDPE system was observed for the addition order where the components were premelted before mixing. The triblocks and the diblock was at the interface from the start of the mixing operation. The compatibilization occurred differently for the triblock and the diblock, but the end result could be generalized as a function of the addition order.



(a)



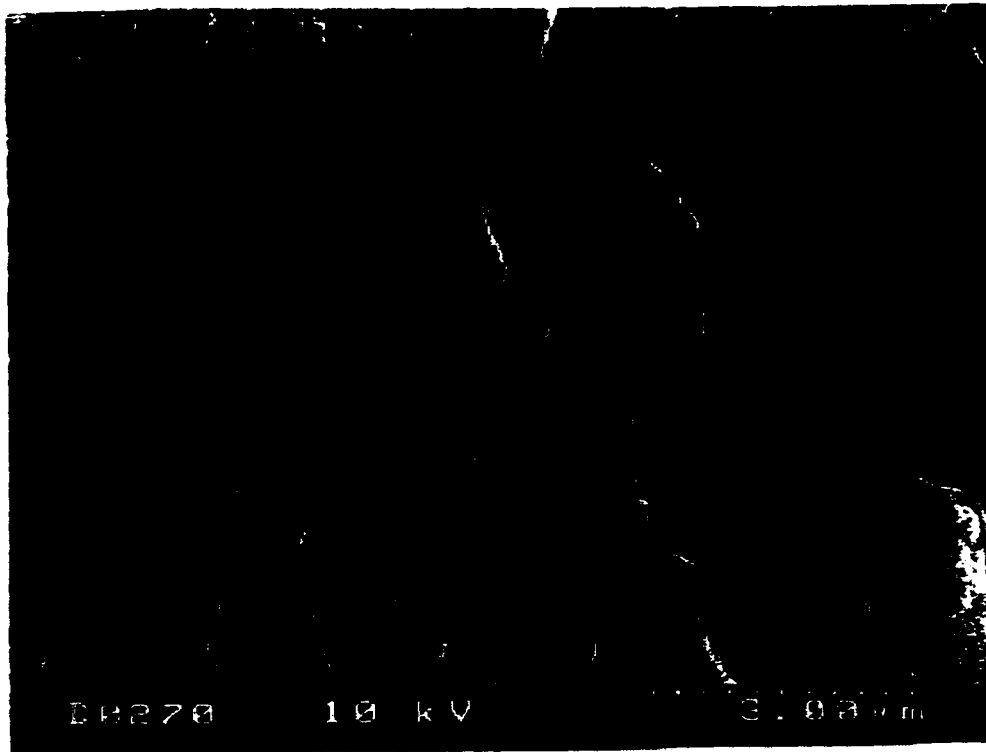
(b)



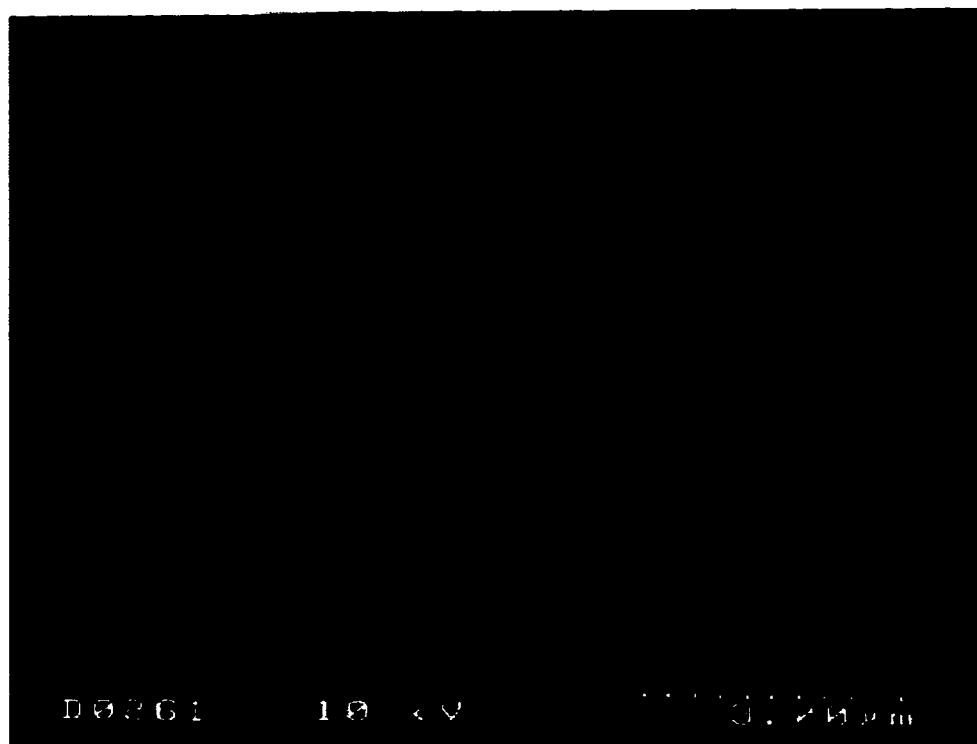
(c)

Fig 3.11
SEM micrographs showing the effect of molecular weight of the PS-PMMA diblock compatibilizer on the 90:10 PS/PMMA blend. All the micrographs are for the same order of addition (#4) using different diblock molecular weights (a) 25K-25K, (b) 50K-50K and (c) 80K-80K.

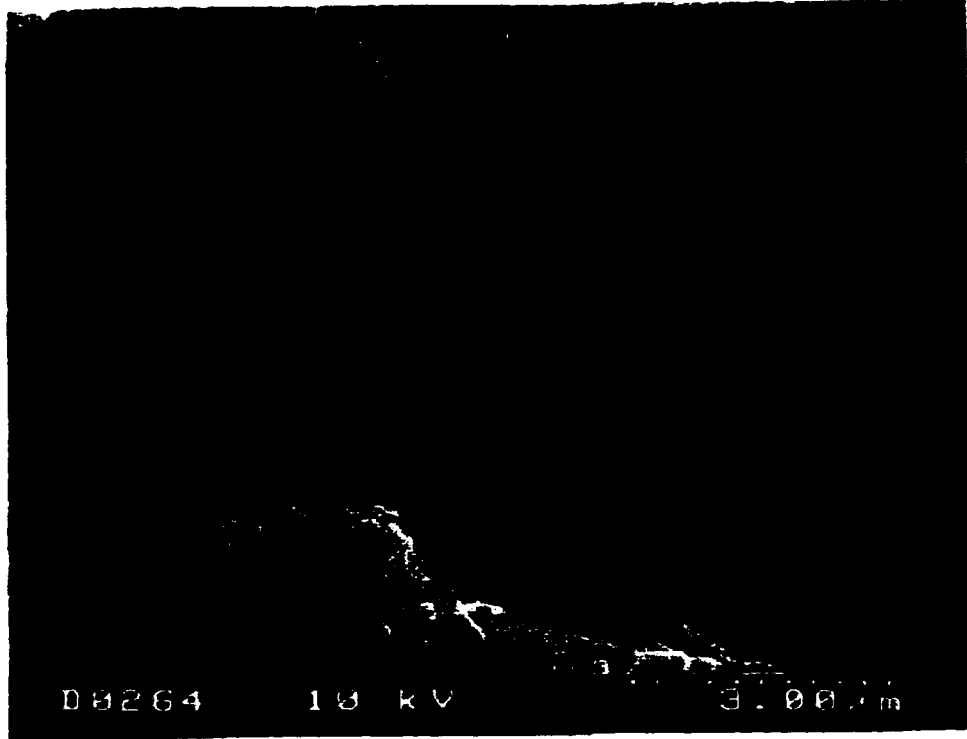
Fig. 3.13 shows the SEM micrographs for the PS/LLDPE blends compatibilized using the two triblocks and the diblock. The effect of molecular weight of the compatibilizer can be seen from Fig. 3.13. All the micrographs are for order of addition #4 where all the components were premelted before mixing.



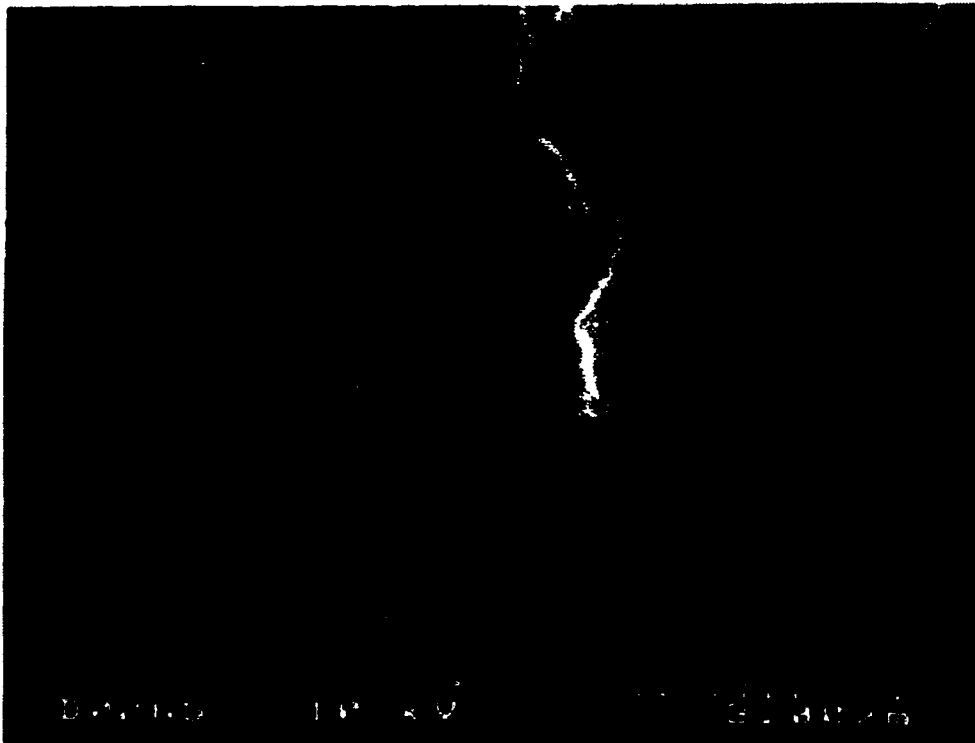
(a)



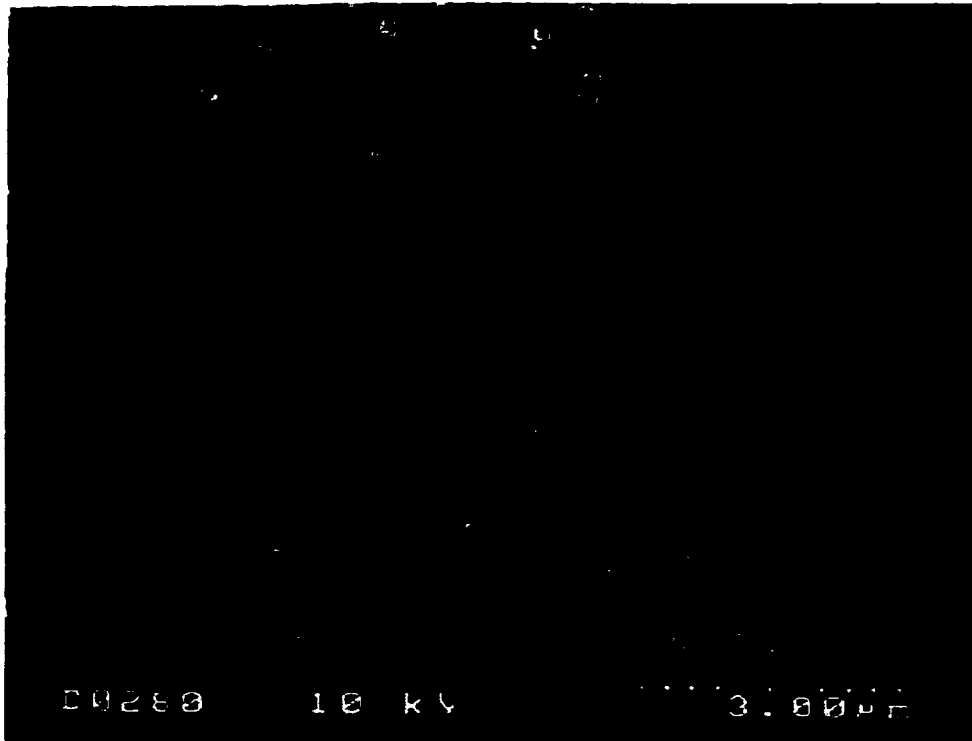
(b)



(c)

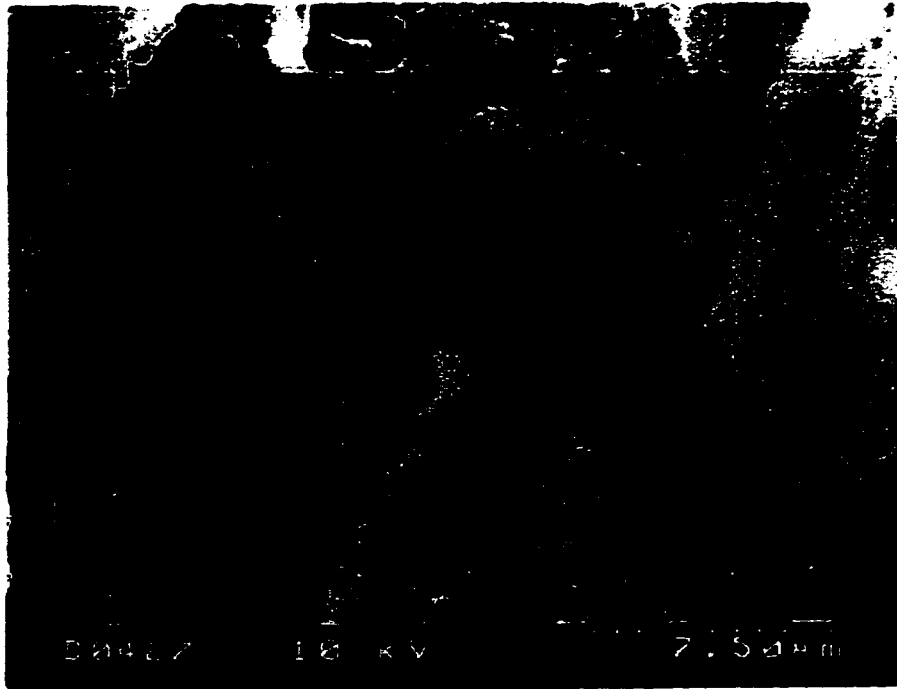


(d)

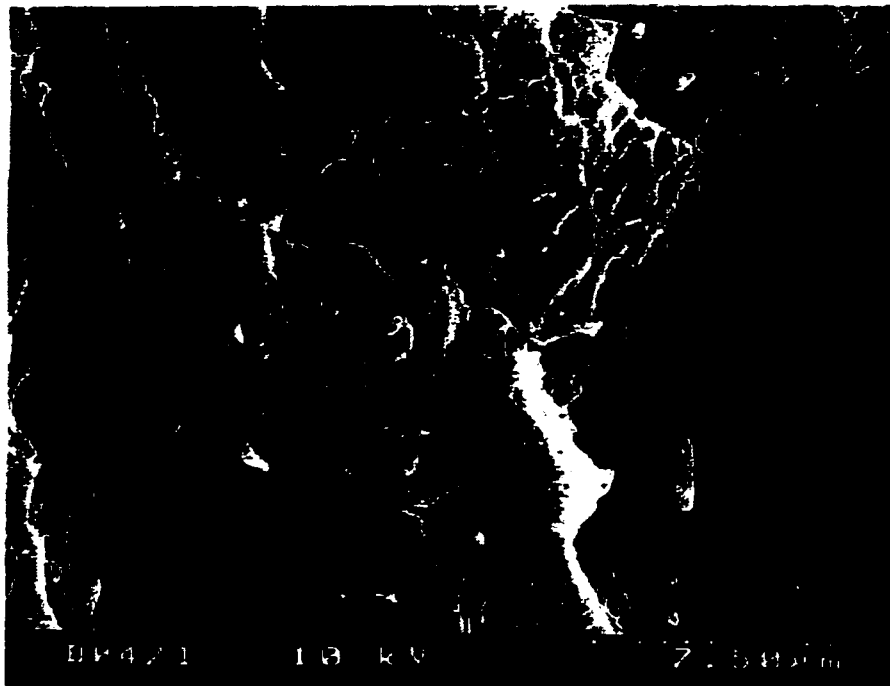


(e)

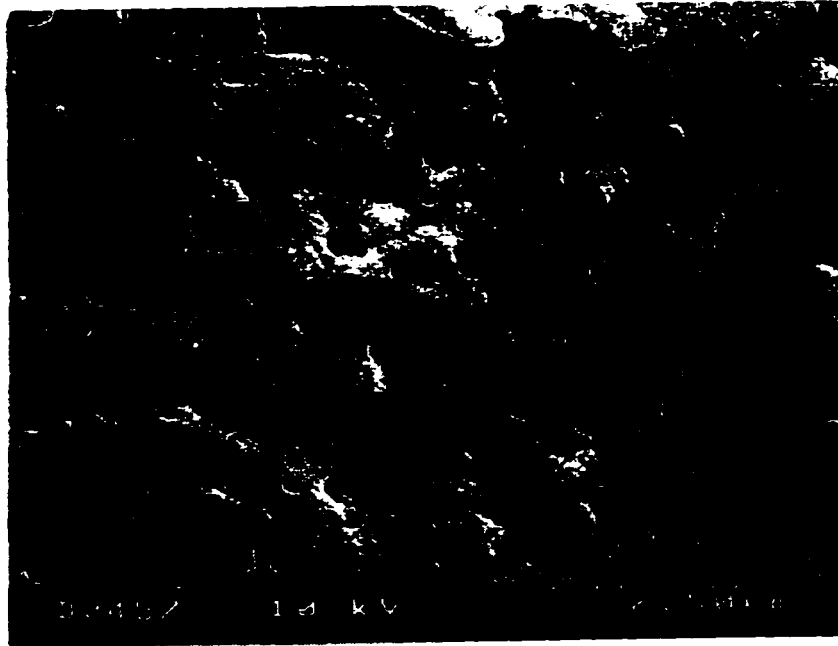
Fig 3.12
SEM micrographs showing the effect of order of addition of the PS-PMMA diblock compatibilizer ($M_w = 80K-80K$) on the dispersed phase drop diameter for the PS/PMMA system. All the pictures are for the same diblock but represent the following orders of addition (a) no diblock, (b) order #1, (c) order #2, (d) order #3 and (e) order #4.



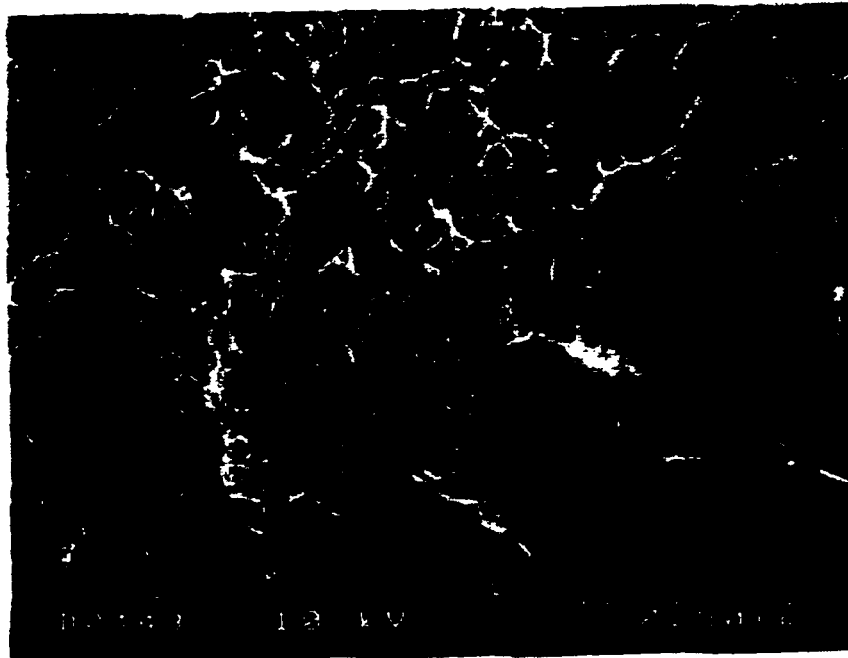
(a)



(b)



(c)



(d)

Fig 3.13
SEM micrographs showing the effect of molecular weight of the compatibilizer on the dispersed phase drop diameter for the 90:10 PS/LLDPE system. All the pictures are for the same order of addition [order #4] but the compatibilization is done using the following compatibilizers: (a) no compatibilizer, (b) $M_w = 75K$, (c) $M_w = 207K$ and (d) $M_w = 275K$.

Fig. 3.13 (a) shows the micrograph for the uncompatibilized system which clearly has the largest particles. The particles for the different compatibilized system are comparable to each other in sizes.

For the 75K triblock, the best dispersion was obtained when all the components were premelted before mixing (Fig. 3.7). However, there was little difference for the other orders of addition. The 75K compatibilizer was the most mobile among the P(S/E-P) compatibilizers chosen. When the other compatibilizers were used, the degree of stabilization was less and larger dispersed phase drop diameters were obtained.

Only one diblock was used for compatibilizing the PS/LLDPE phase. The molecular weight of the S/E-P diblock was 207K and the diblock had a styrene content of 27.6 weight%. When the diblock was added with the matrix phase (PS) (addition order 3), the large (E-P) fraction of the compatibilizer was not compatible with it. As a result, the diblock would have formed micelles. The E-P block would have formed the inner core of the micelle and the PS block would have been present outside, since the PS part of the diblock was compatible with the matrix phase. The inner core would be strong due to the large E-P fraction. Hence, it would have been difficult to break these micelles compared to the micelle produced when the styrene formed the inner core. When the LLDPE phase was added to the mixer (addition order 3), the stable micelles did not break and thus, could not migrate to the interface leading to a poor morphological stabilization.

However, when the compatibilizer was added with the dispersed phase (addition order 2), the large E-P fraction was compatible with the LLDPE phase. The small PS fraction formed the core and these micelles could be broken easily in the shear field when the matrix phase was added (PS). The formation of micelles was thus retarded and effective stabilization of the interface occurred. This led to a decrease in the diameter of the dispersed phase for order of addition #2.

The effect of order of addition on dispersed phase particle diameter compatibilized by the S-EB-S triblock ($M_w=275$ K) is shown in Fig. 3.9. Due to the high fraction of E-P

be less than or equal to that of homopolymers for effective compatibilization. When the molecular weight of the compatibilizer was larger than that of the homopolymers, effective stabilization of the interface was not achieved. As the molecular weight of the compatibilizer increases, diffusion becomes more important. From the torque peaks for the different orders of addition, the times when each of the blend components melted were determined. The peak corresponding to the melting of the compatibilizer in the PS/PMMA blends could be observed since the diblock had a higher melting transition.

3.6 References

- Borggreve, R. J.; Gaymans, R. J.; Eichenwald, H. M., *Polymer*, **30**, 78 (1989).
- Cruz-Orive, L. M., *J. Microsc.*, **107**, 235 (1976).
- Favis, B. D., *Polymer*, **35**, 1552 (1994).
- Fayt, R.; Jerome, R.; Teyssie, Ph., *J. Polym. Sci. Polym. Lett. Ed.*, **24**, 25 (1986).
- Fayt, R.; Teyssie, Ph., *Polym. Eng. Sci.*, **30**, 937 (1990).
- Liu, N. C.; Baker, W. E., *Polym. Eng. Sci.*, **32**, 1695 (1992).^a
- Liu, N. C.; Baker, W. E., *Adv. Polym. Tech.*, **11**, 249 (1992).^b
- Locke, C. E.; Paul, D. R., *J. Appl. Polym. Sci.*, **17**, 2791 (1973).
- Nakayama, A.; Inoue, T.; Guegan, P.; Macosko, C. W., *ACS Polymer Preprints*, American Chemical Society, (1993), 840. Also submitted to *Macromolecules*.
- Nakayama, A., Masters Thesis, Department of Organic and Polymeric Materials, Tokyo Institute of Technology, Tokyo, 1994.
- Paul, D. R., in "Polymer Blends", Vol. 2, D. R. Paul and S. Newman, Eds., Academic Press, New York, 1978.
- Russ, J. C., in "Practical Stereology", chap. 4, Plenum Press, New York, 1986.
- Schwarz, M. C.; Barlow, J. W.; Paul, D. R., *J. Appl. Polym. Sci.*, **37**, 403 (1989).
- Scott, C. E., PhD thesis, University of Minnesota, 1990.
- Scott, C. E.; Macosko, C. W., *Polym. Bull.*, **26**, 341 (1991).
- Subramanian, P.M., *Polym. Eng. Sci.*, **25**, 483 (1985).
- Sundararaj, U.; Macosko, C. W.; Rolando, R. J.; Chan, H. T., *Polym. Eng. Sci.*, **32**, 1814 (1992).^a

Sundararaj, U.; Macosko, C. W.; Shih, C. K., *Soc. Plast. Eng. Tech. Papers*, **50**, 1802 (1992).^b

Sundararaj, U.; Macosko, C. W., *Macromolecules*, **28**, 2647 (1995).

Tremblay, A.; Tremblay, S.; Favis, B. D.; Selmani, A.; L'Esperance, G., *Macromolecules*, **28**, 4771 (1995).

van Krevelen, D. W., in "Properties of Polymers", chap. 3, Elsevier, Amsterdam, 1976.

Wu, S, *Polymer*, **26**, 1855 (1985).

Yang, L.; Smith, T. G.; Bigio, D., *J. Appl. Polym. Sci.*, **58**, 117 (1995).

Chapter 4

VISUALIZATION OF POLYMER MIXING

4.1 Introduction

Polymer blending is the primary method used in industry to obtain products having better mechanical properties and higher performance than existing homopolymers. Blends prolong product life and reduce cost. The cost and technology required to synthesize new polymers is exorbitant compared to that required to develop a new blend. When two polymers are blended, one phase is usually dispersed inside the other. Visualization can yield key information about deformation mechanisms and blend texture during processing. Visualization can help us in understanding the development of morphology during blending by capturing the breaking mechanism. The pellets are stretched into sheets and these sheets break up to form drops (Sundararaj *et al.*, 1992a). During melt blending, an interesting phenomenon can take place - the two phases can switch during mixing. If the minor phase (the phase with lower concentration) has a softening temperature which is lower than that of the major phase (the phase with higher concentration), then the minor phase will melt first and become the continuous phase. When the major phase melts, there is an inversion of phases. This phenomenon was termed as “phase inversion” (Shih; 1992, 1995). The same phenomenon has also been referred to as “inversion of phase continuity” by Sundararaj *et al.* (1996).

4.2 Background

For systems exhibiting phase inversion, Shih has described four different rheological regimes:

1. Elastic solid pellets
2. Deformable solid pellets
3. Transition material

A. Solid particles in a suspension of fluid

B. Semi-fluid material

C. Dough-like material

4. Viscoelastic fluid

The inversion of phases occurs in Regime 3 and it is accompanied by a sharp peak in the magnitude of torque. According to Shih (1991), the torque is caused by the opposition of pellets to the rotor motion. As the material melts, the resistance offered increases and this leads to an increase in torque. The frictional heating taking place causes energy dissipation which consequently leads to a temperature rise in the mixer. Complex changes in the rheological properties take place during the mixing process. These can be followed by observing the torque. All the runs were observed visually through a glass front plate built into the front heating plate of the mixer.

There are many models for phase inversion achieved by slowly increasing one component in the blend mixture (Metelkin and Blekht, 1984; Jordhamo, *et al.*, 1986; Miles and Zurek, 1988; Favis and Chalifoux, 1988; Utracki 1991; Fortelny and Kovar, 1992; Favis *et al.*, 1995). This kind of phase inversion pertains to the structure observed at the end of blending. Other work has involved the use of phase inversion in the synthesis of high impact polystyrene (HIPS) (Molau, 1965). The HIPS involves the dispersion of rubber in a matrix of polystyrene (PS) which increases the impact strength of pure PS. The process involves the addition of rubber to the styrene monomer. As the styrene polymerizes, there is an inversion of phase continuity as the PS coats the rubber phase. Our work, however, studies phase inversion during the mixing of two polymers.

It has been reported that the inversion of phases causes the formation of a unique morphology. The matrix phase particles are occluded inside the dispersed phase (Favis, 1992; Sundararaj, 1994). In some blending protocols, polymer A is dispersed inside polymer B and then a large quantity of polymer A is added to provoke phase inversion. Small particles of the major phase are trapped inside the minor phase melt. For a reactive

system, these major phase particles are stabilized due to the formation of an *in-situ* copolymer at the interface and cannot coalesce with the matrix (Sundararaj, 1994).

Sundararaj *et al.* (1996) have studied the effect of adding a diblock copolymer on the inversion of phase continuity. They observed that a diblock copolymer increases the torque marginally but a reactive system exhibits a much larger rise in torque. The size of the major component pellets was also shown to have an effect on the torque magnitude.

The visual glass plate was used to observe the blending mechanism in some normal (non phase inverting) systems too. Experiments have been done in a twin - screw extruder (Sundararaj *et al.*, 1992a) which showed that the vital morphology change took place during the initial stages of mixing. Sundararaj *et al.* (1995) have reported that sheets of the dispersed phase are formed which break up into cylinders depending on the mechanism involved. However, the visualization of a batch mixer has not been reported in much detail. To observe the dispersion behavior inside the Haake mixer, it is important to ramp the temperature very slowly so that the melting of each phase can be separate. Also, the run has to be performed at a slow rotation rate so that the morphology development is clearly visible.

4.3 Experimental

4.3.1 Design of the Glass Plate

To visually observe the mixing operation, the front part of the mixer had a glass plate built into it. The design of the glass front plate is shown in Fig. 4.1. The front view and the side view have been shown. The front plate was made of 316 stainless steel. The equipment dimensions are shown in the Fig. 4.1.

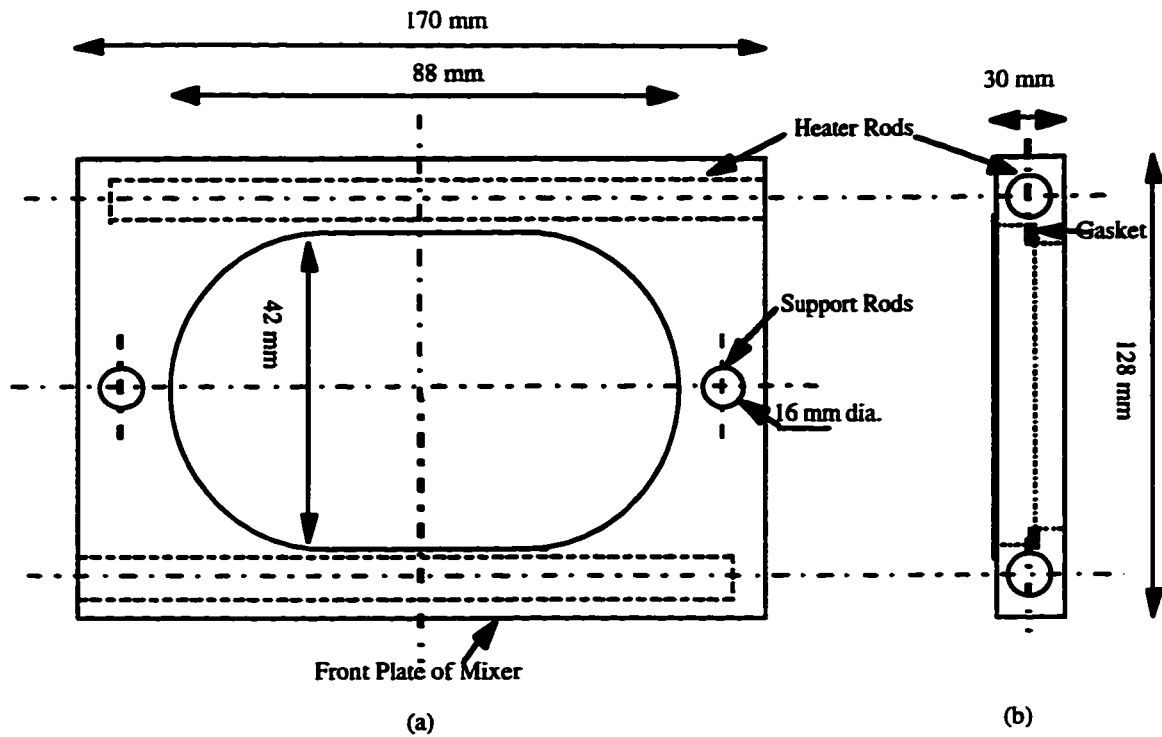


Fig 4.1 (a)
 Design of the metal front plate used for the visualization purposes. The figure shows the orthographic views (not drawn to scale) of the front plate of the mixer, (a) Front view and (b) Side view. The glass slab had the dimensions of the oval hole in the metal plate.

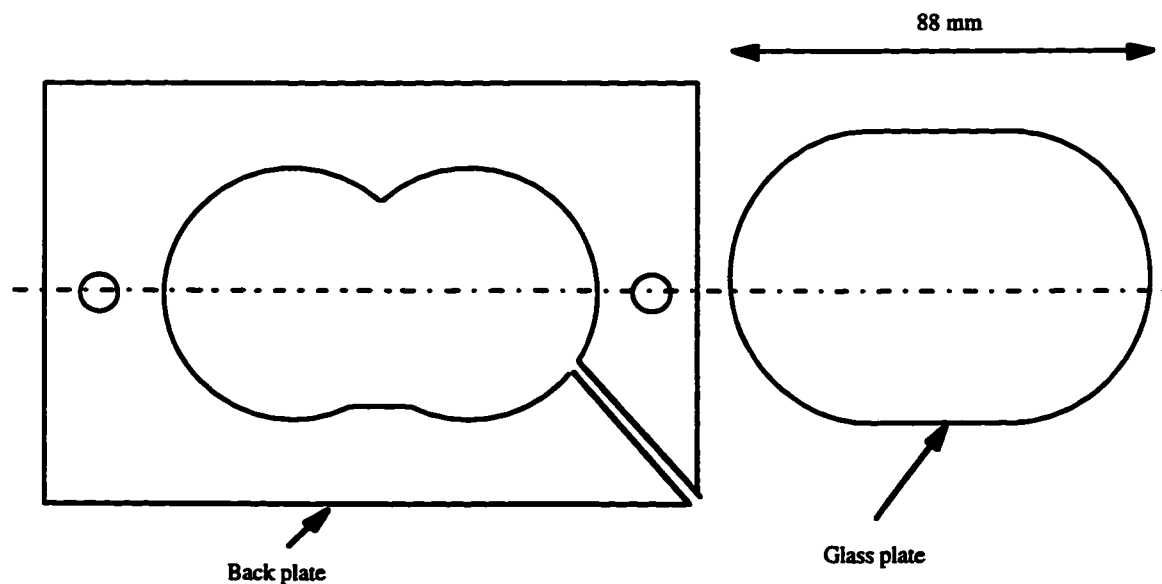


Fig. 4.1 (b)
 The back plate (used to protect the glass plate) and the glass plate (not drawn to scale).

The glass slab was made of Pyrex. A graphite gasket was used to protect the glass slab from cracking due to vibrations and differences in thermal expansion between the metal and the glass. The two heater rods were acquired from Tru-Temp Electric Heat Limited. The heater rods were type EG and each had 500 W power. The presence of a block of glass should not hinder the heating process greatly.

4.3.2. Material and Description of Runs

Table 4.1 gives a list of the materials, abbreviations, transition temperatures and viscosities at a frequency of 65 s^{-1} . The dynamic viscosities were measured using a Rheometrics Mechanical Spectrometer (RMS 800) with 25 mm parallel plate fixtures at 10% strain. It was confirmed that the polymer exhibited linear viscoelastic behavior at this strain. The measurement of the rheological properties has been described in detail in appendix D.

The first system studied was a non-reactive blend of polyamide (PA) and polystyrene (PS). The polyamide used was Zytel 330 (PA 330) which was obtained from Dupont. It is a partially aromatic, amorphous Nylon. The polystyrene used was Dow Styron 666D (PS 666D) which is reported to have a melt index of 7.5 and has a molecular weight of $M_w = 200,000$. For the reactive system of PA and PS, a polystyrene-maleic anhydride (PSMA) was used. The polymer is an Arco Dylark with 17 wt% MA having a molecular weight of $M_w = 225,000$. The maleic anhydride chains grafted onto the PS backbone react with the amine groups on the polyamide. Another system was a reactive system of polyamide (PA 330) and ethylene propylene maleic anhydride (EPMA). The EPMA was obtained from Exxon and it had a MA graft of 0.7% and $M_w = 84,000$. Another system was polyarylate (PAR) blended with PS666D. PAR was obtained from Dupont.

Table 4.1 Properties of Polymers

Polymer (Abbreviation)	Softening Temperature * (°C)	Average Pellet Size (mm)	Viscosity at 65 s ⁻¹ and 200°C (kPa.s)
Polystyrene (PS666D)	95	2.4	0.95
Polyarylate (PAR)	240	2.5	4.20 ⁺
Polystyrene- maleic anhydride (PSMA5%)	125	2.6	0.85
Polyamide (PA330)	130	2.3	10.00
Ethylene- Propylene Maleic-Anhydride (EP-MA)	105	2.6	2.40
Polycarbonate (PC)	190	2.1	2.20 ^a
Polyetherimide (PEI)	230	2.5	1.06 ³

+ At 260°C.

^a At 250°C.

³ At 340°C.

* Softening temperature corresponds to the temperature when the torque changes in the Haake mixer.

For the non-phase inverting system, blends of polycarbonate (PC) and polyetherimide (PEI) were studied. The polycarbonate used was Lexan 130 obtained from GE Plastics. The polyetherimide was Ultem 1010 and was also obtained from GE Plastics. These were obtained in different colors to enhance contrast with the transparent PC. For all the blends studied, the temperature was ramped from 200 - 300°C at a rate of 2 °C/minute. The rotation rate for these non-phase inverting systems was 10 rpm. A slow rotation rate and temperature ramp was deliberately chosen in order to clearly capture the blending

process. The mixer was preheated to 200°C and the materials were added to it. The mixer was maintained at this temperature for 1.0 minute to allow the material to heat up to the wall temperature. After 1.0 minute, the temperature was ramped at a specific rate and the mixing was photographed using a camera and was recorded onto a VCR. The image was magnified (~20 X) using a zoom lens.

For the PA/PS blends, the temperature was ramped from 80-180°C. For most of the runs, the temperature was ramped at a rate of 5 °C/minute. This rate was sufficient to distinguish the melting peaks of the two phases. The effect of different ramping rates was studied. At the start of each run, the mixer was preheated to the starting temperature of 80°C. The pellets of the two phases were then added to the mixer. The mixer was kept at 80°C for one minute and then the temperature was ramped at the defined rate. The effect of shear rate on the onset of phase inversion was also studied. Blends having 20% dispersed weight fraction were prepared at the same ramping rate but at different shear rates.

The effect of reaction was studied by comparing the inversion for the reactive and non-reactive PA/PS(MA) systems. The reaction occurred between the amine groups of the polyamide and the maleic anhydride grafted onto the polystyrene. All the runs are summarized in Tables 4.2, 4.3 and 4.4.

4.3.3. Procedure

Sundararaj *et al.* (1992b) indicated that optimum mixing is obtained when the melt volume occupies 78% of the mixer volume. If the volume is less than optimum, there are a lot of vacant sites and there is insufficient exchange of material. On the other hand, a melt volume higher than 78% causes stagnant pockets in the mixer. Thus, it is essential to have an optimum filling of the mixer for efficient mixing.

The polymers used for the visualization experiments were obtained in pellet form. Before blending, the pellets were dried overnight at a temperature of 80°C to remove any traces of volatile material. This temperature was below the softening transition temperatures of the polymers chosen. The torque rheometer (Haake Rheocord 90) with a

batch mixer (600 series) and roller blades was used for all the experiments. The weight of each component was calculated using molar volume correlations given by van Krevelen (1976).

The mixer was preheated to the required temperature before adding the pellets through a feed chute and pushing them into the mixer using a ram with a 5 kg mass. Once the mixer attained a steady starting temperature, the material was added and at the same time the temperature was ramped at a certain rate. The effect of different ramping rates on phase inversion were studied. The ramping was done over a temperature range centered at the transition temperature of the major phase. The temperature ramping expanded the torque profile and more closely approximated the extrusion process where the temperature increases as the matrix flows down the extruder. Since the temperature was increased slowly in this case, the melting of the two phases could be distinguished.

The runs are summarized in Tables 4.2, 4.3 and 4.4. During the run, the rheocord program measured the torque and the melt temperature on-line. For all blends, a glass front plate was attached to the mixer and the mixing was recorded using a TMC-7 PULNiX camera connected to a JVC SR-S360U VCR. After the run was completed, the motor was stopped and the front and the middle section of the mixer barrel were removed to expose the roller blades. Some of the polymer was attached to the rotor blades and a sample was removed from the indents between the blades and immediately quenched in liquid nitrogen. The sample was withdrawn within 30 seconds of stopping the motor.

Table 4.2 PA/PS Runs (Reactive and Non-reactive)

Temperature range for all runs : 80-180°C

Weight % (Minor phase)	Ramping rate (°C/min.)	Rotation Rate (rpm)	Inversion Temperature (°C)	Inversion Torque Peak (m g-f)
20	1	50	140	4600
20	2	50	145	4600
20	5	20	162	2500
20	5	50	150	3800
20	5	75	164	3300
20	5	125	145	3950
20	5	150	145	4300
20*	5	125	160	4700

* Reactive system (PA/PSMA).

Table 4.3 PA330/EPMA runs

Temperature range for all runs : 90-160°C

Weight % (Minor phase)	Ramping rate (°C/min.)	Rotation Rate (rpm)	Inversion Temperature (°C)	Inversion Torque Peak (m g-f)
2	2	50	180	6200
5	2	50	191	5950
8	2	50	195	6250
20	2	50	200	6600

In most cases, a fracture surface was created when the hot sample imploded by rapid quenching in liquid nitrogen. When the sample did not implode by quenching, the

fracture surface was obtained by cooling in liquid nitrogen and then breaking the sample using a hammer. The sample was then prepared for scanning electron microscopy (SEM) by sticking it onto a SEM stub and applying a coating of carbon.

Table 4.4 PC/PEI run (Non - Phase Inverting)

Temperature range for all runs : 200-300°C

Weight % (Minor phase)	Ramping rate (°C/min.)	Rotation Rate (rpm)	Torque Peak (m g-f)
20	2	10	4750

In some cases, one of the phases was selectively extracted to see the morphology development of the other phase during the course of mixing. From the original run, we selected some critical times when the torque changed (i.e. some change in morphology was occurring). The run was then repeated but the mixing was stopped at one of the pre-determined points. A small piece of the sample was placed in a vial containing the solvent of a particular phase and the solution was mixed for 24 hours with a magnetic stirrer and a stir plate. The PS phase was dissolved using methylene chloride and the PA phase was dissolved using formic acid. The SEM was performed using a HITACHI S-2700 instrument.

The diameter of the dispersed phase was measured using the image analysis software NIH Image 1.58b33, developed by the National Institute of Health (NIH). The particles in the SEM micrographs were outlined. This traced image was scanned into the computer and the diameter of each particle was calculated using the measured area and assuming that the particle was spherical.

4.4 Results

To observe the phase inversion process clearly, polyarylate (PAR) and polystyrene (PS) were blended. The PAR pellets were dark brown in color while the PS pellets were transparent, and hence, visualization was enhanced. The initial temperature was 220°C,

and as a result, the PS melted immediately upon addition into the mixer. Fig. 4.2 shows

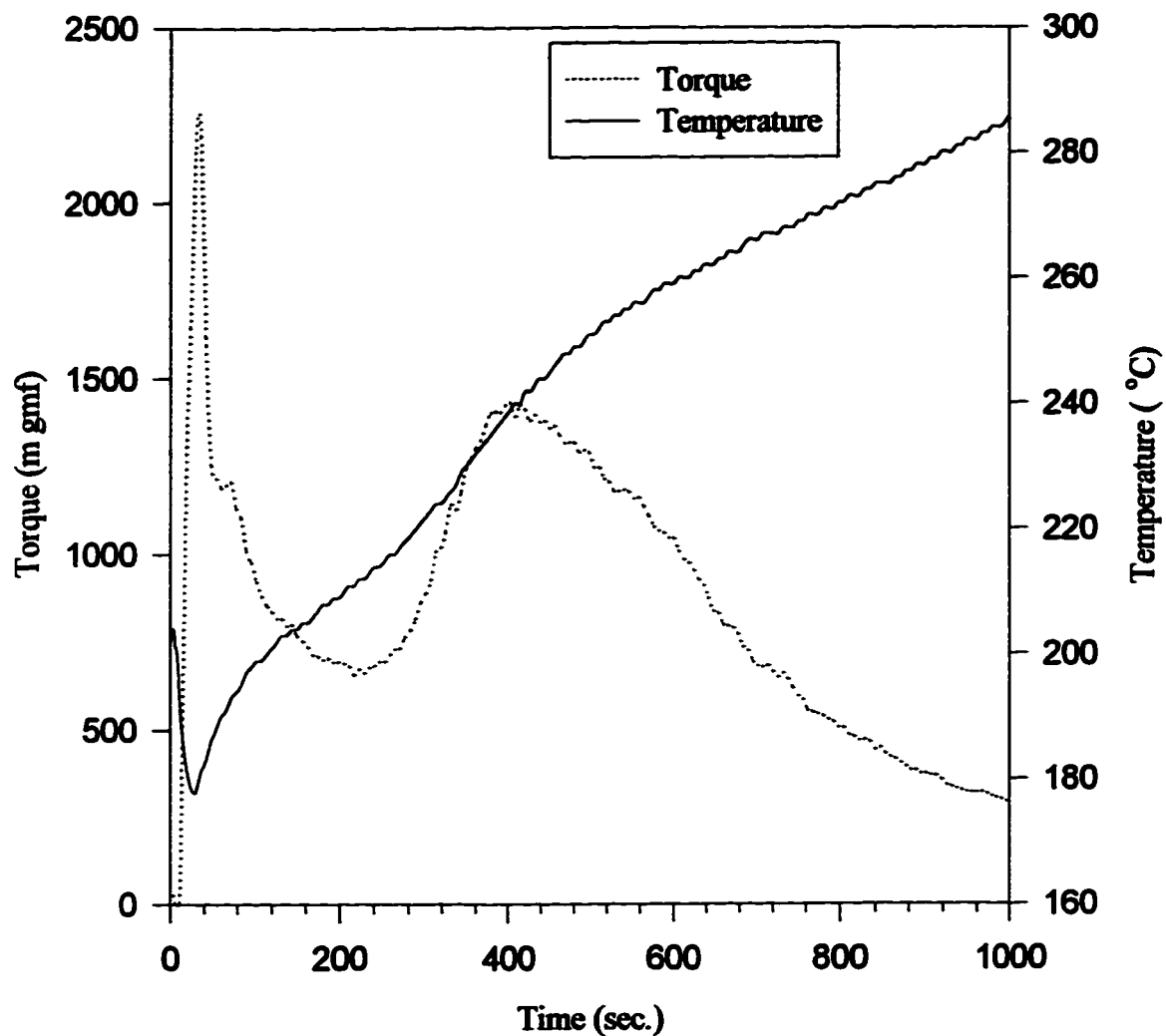


Fig 4.2
Torque and temperature profiles for the PAR/PS blend (80/20). The mixing was done at 50 rpm and with a ramp from 220 - 300°C at a rate of 5°C/min.

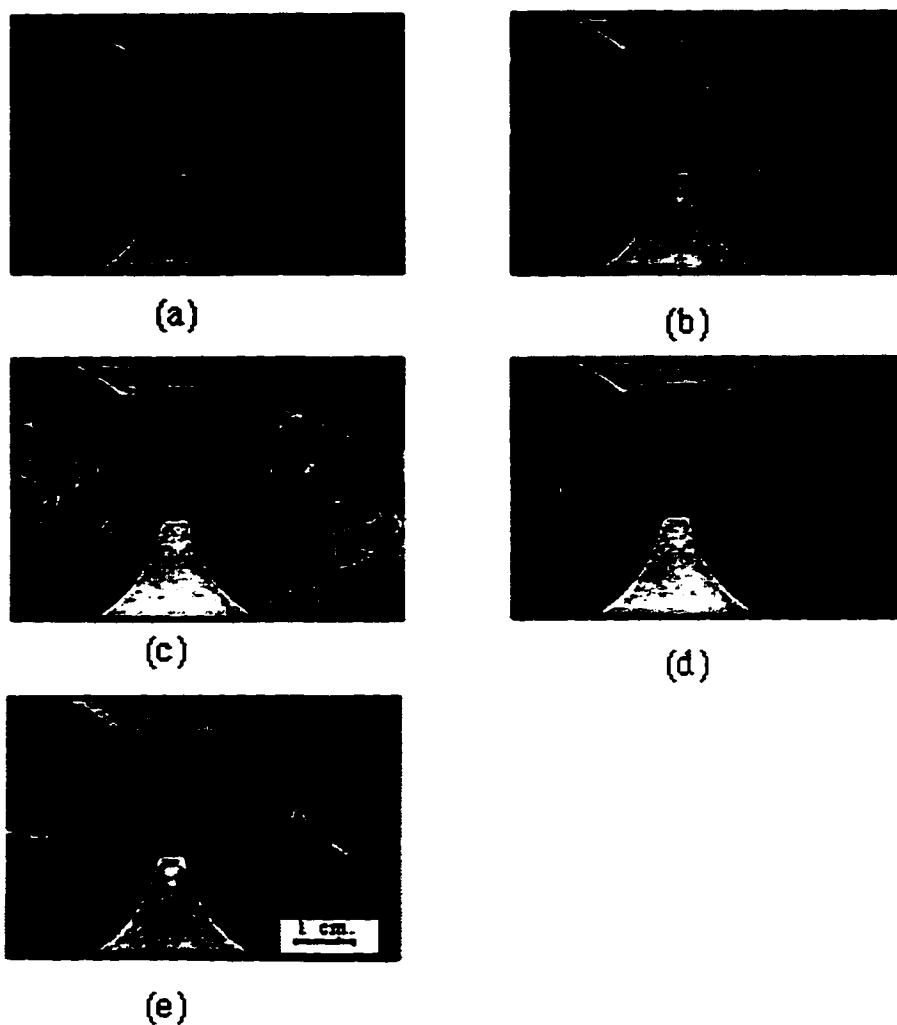


Fig 4.3.

Snapshots of the mixer window showing the different physical regimes as written below. The system is PAR/PS (80/20 blend) mixed at 50 rpm with a temperature ramp from 220-300°C at a rate of 5°C/min. (a) The PS has melted and covered the PAR pellets ($T=190^{\circ}\text{C}/\text{min.}$) (Refer to Fig. 4.2). (b) same as in (a) but the PS has now completely covered the PAR. (c) The PAR is softening at this point ($T=240^{\circ}\text{C}/\text{min.}$). (d) The PAR phase is starting to invert. The dark PAR phase is slowly blending into the matrix. (e) A uniform viscoelastic fluid is observed. All pictures are at the same magnification.

The temperature initially decreased when the cold pellets were added to the heated mixer as some energy was used to heat up the pellets to the mixer temperature. The curve has a sharp peak when the PS pellets soften and are deformed at a high shear rate. The

snapshots of the glass front plate at different times showing the development of the regimes are depicted in Fig. 4.3. The middle of the mixer between the blades is the most representative part of the entire blend sample. It is important to disregard the surface of the blades since often solid pellets are trapped between the blades and the glass plate. The initial morphology was PAR pellets dispersed inside a PS matrix (Fig. 4.3(a)). Fig. 4.3(b) shows the snapshot just before the PAR pellets begin to soften. The refractive index of the pellets changed and they appeared shiny. The temperature at this point was approximately 220°C. The torque shows a minima (Fig. 4.2) just before the PAR started to soften. After 3 minutes of mixing, the PAR pellets slowly deformed. The dark PAR lost its pellet shape and extended into a long sausage-type structure (Fig. 4.3(c)). The torque curve rose during this period. The torque peak occurred at a temperature around 240°C (Fig. 4.2). The snapshot in Fig. 4.3(d) shows the phase inversion which occurred just after the torque peak. A uniform viscoelastic fluid is observed in Fig. 4.3(e). The torque at this point was decreasing and continued to decrease. SEM was performed on the blend at the end of the run. The diameter of the dispersed PS drops at the end of blending was 1.9 μm . Fig. 4.4 shows an SEM micrograph of the PAR/PS blend at the completion of the run.

The inversion was visualized for the non-reactive and the reactive PA/PS(MA) blends. In both cases, Shih's (1995) four different physical states were observed. The pellets were added to the mixer which had been pre-heated to 80°C. This was lower than the softening temperature of the polymers. Fig. 4.5 compares torque versus time profiles between the reactive and non-reactive PA/PS blends. The comparison of torque versus temperature profiles for the same two blends is shown in Fig. 4.6. Fig. 4.7 compares the final morphology of the reactive and non-reactive PA/PS blend. There is a considerable decrease in particle size of the dispersed phase. The PS phase drop diameter for the uncompatibilized blend was calculated as 1.9 μm whereas the diameter for the compatibilized blend was 0.3 μm . Hence, reaction causes a six-fold decrease in dispersed

phase particle diameter. Reaction also leads to stabilization of the dispersed drops and prevents coalescence.

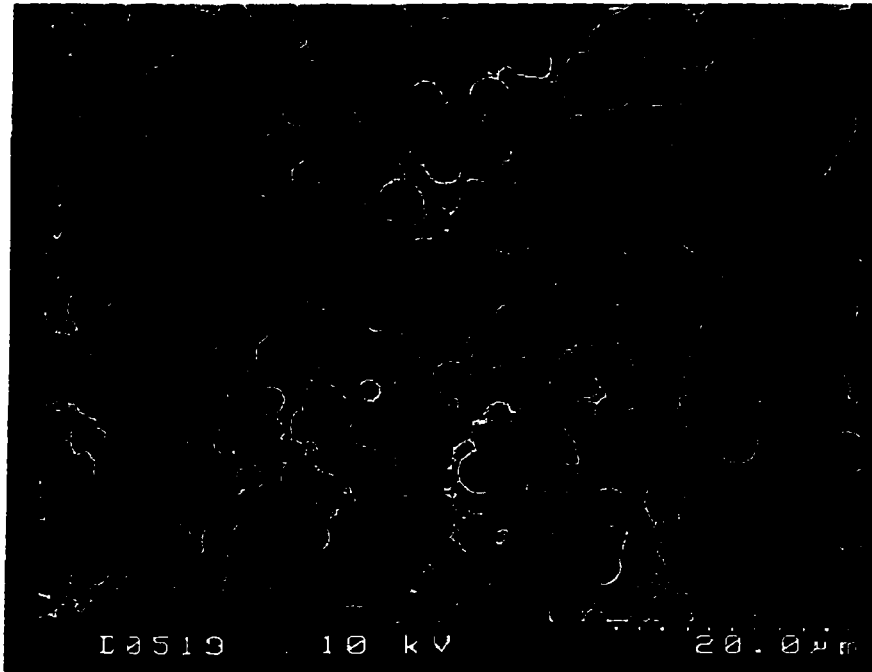


Fig 4.4
Morphology of the PAR/PS blend (80/20). The mixing was done at 50 rpm and with a ramp from 220 - 300°C at a rate of 5°C/minute. The final structure consists of PS drops dispersed in a matrix of PAR.

The non-reactive blend was studied in detail by observing the changes in blend texture and stopping the mixer at different times to examine the morphology. The different regimes that were observed are described below:

**Elastic solid pellets*

The PS has a glass transition temperature of 100°C. As the temperature rises from 80°C, the PS softens first. The PS forms the continuous phase and covers the pellets of PA. Hence, the PA phase is present as elastic solids in the matrix of PS. The torque shows a small shoulder due to the melting of the polystyrene (Fig. 4.5). The value of the torque peak is usually around 1500 m.gm-f. The torque peak is due to the increased resistance to rotor rotation due to the melting of polymer.

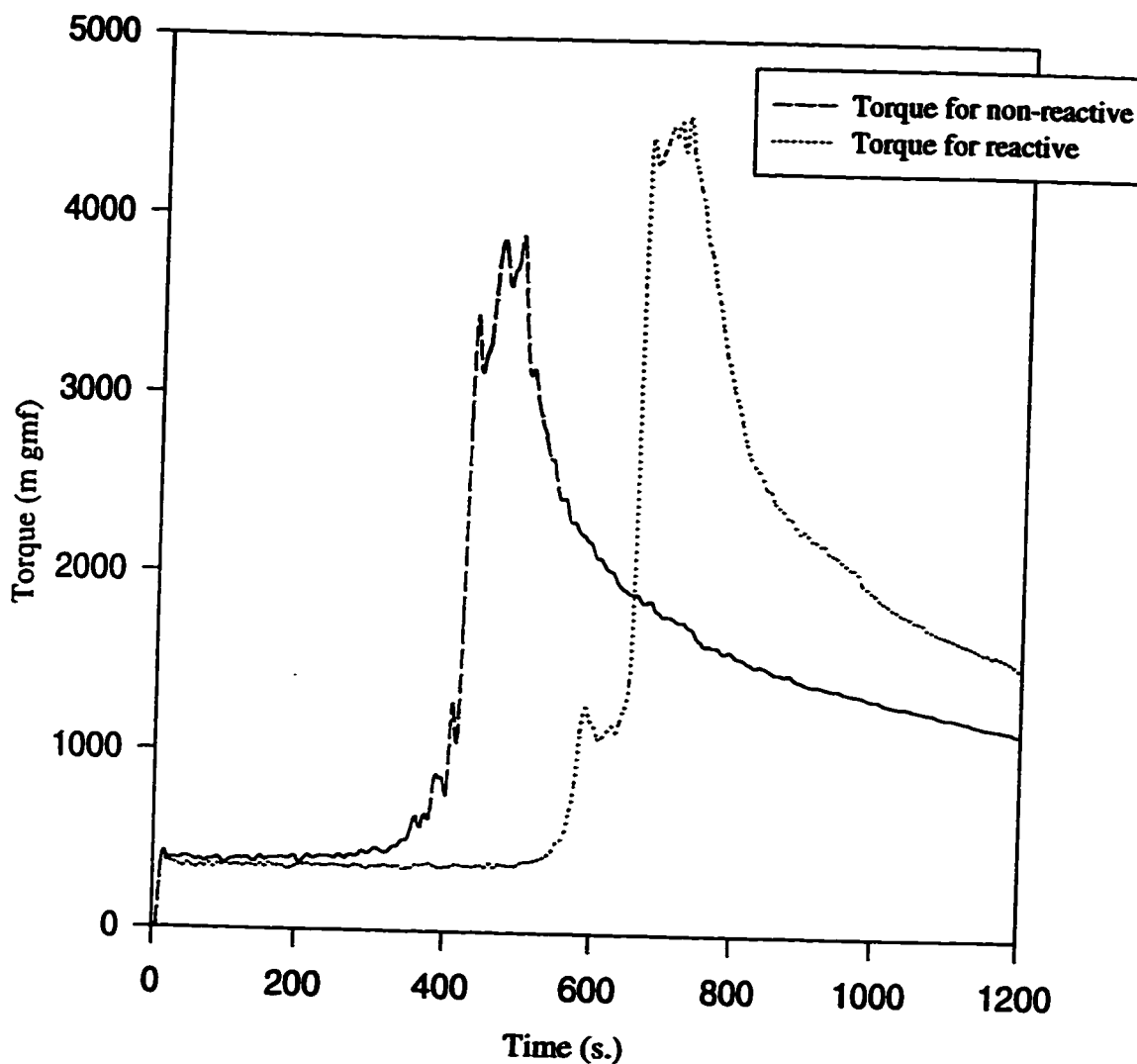


Fig 4.5
Effect of reaction. The torque is plotted versus the time for the 80:20 PA330/PS666D and the PA330/PSMA5% blends. The mixing was done at 125 rpm and the temperature was ramped from 80 to 180°C at 5°C/min. The reactive system shows a higher torque peak which occurs at a later time.

The morphology of each phase at the four different physical regimes of the torque profile was studied. At Stage 1, the polyamide is still present as pellets. The polystyrene pellets soften and deform. An attempt was made to capture the morphology of the regime by stopping the mixer at 125°C. The phases were selectively dissolved. The PS was dissolved in methylene chloride (CH_2Cl_2) to leave the PA phase. The PA was dissolved in

formic acid to leave the PS phase. Fig. 4.8 (a) shows the PS morphology when the PS just begins to melt.

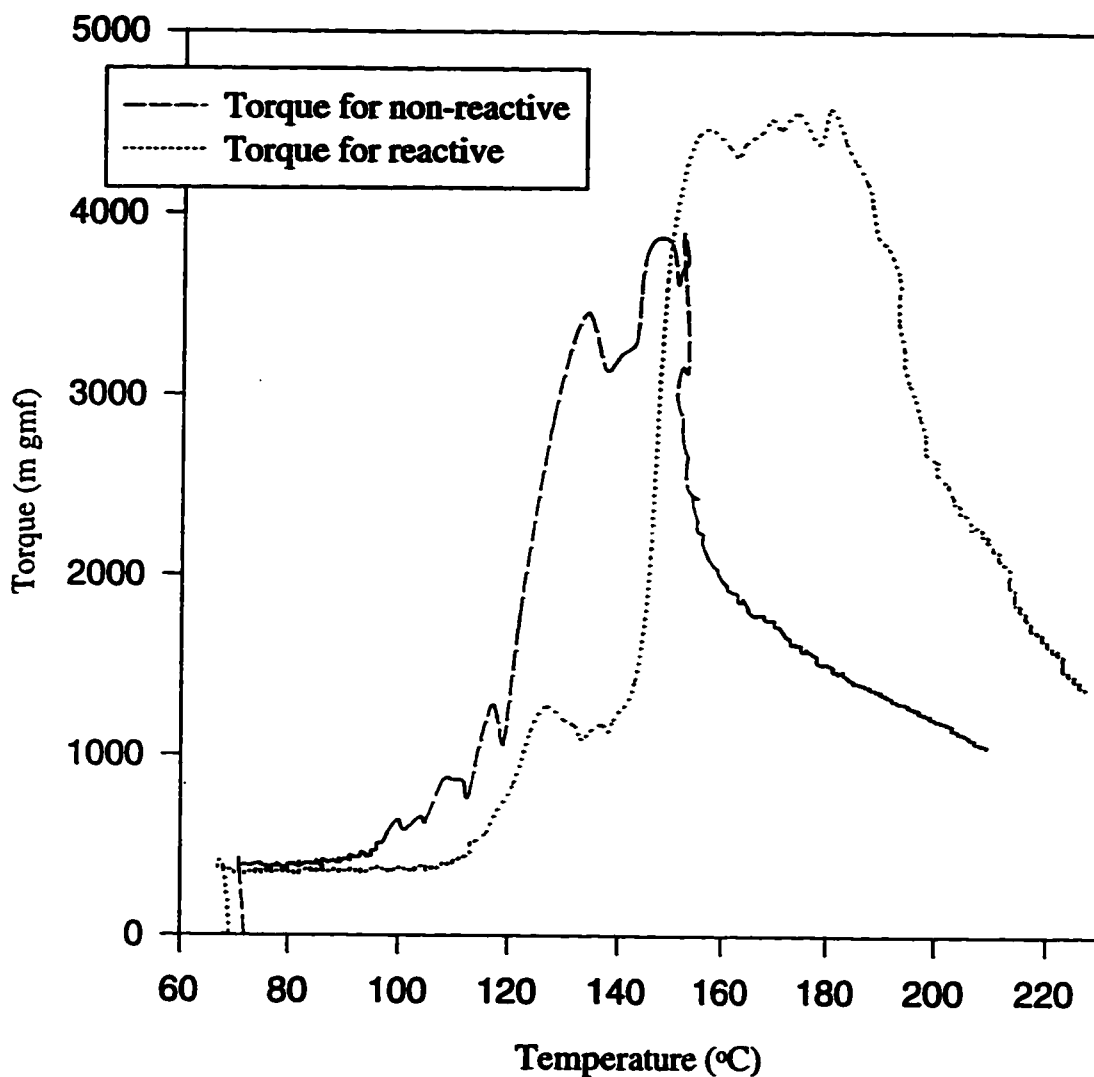


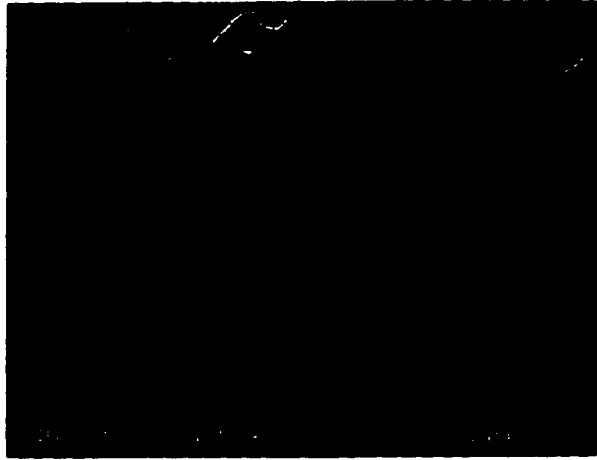
Fig 4.6
Effect of reaction. The torque is plotted versus the temperature for the 80:20 PA330/PS666D and the PA330/PSMA5% blends. The mixing was done at 125 rpm with a ramp from 80 - 180°C at 5°C/minute.

**Deformable pellets*

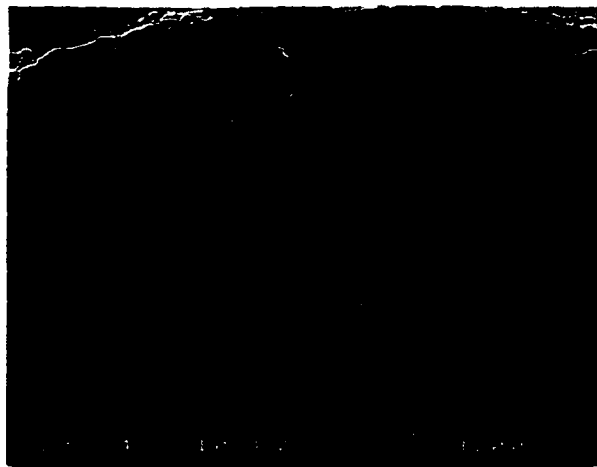
Near the softening point of the PA, the torque increases rapidly (Fig. 4.6). There is more resistance to the rotor blades as the PA pellets melt. The material melts and sheets of PA are peeled off from the surface (Scott, 1991; Sundararaj *et al.*, 1992; Sundararaj *et al.*, 1995). The morphology is shown in Fig. 4.8 (b) and Fig. 4.9 (a). The PS is still the

continuous phase when the PA phase starts to melt around 120°C. Once the pellets melt, the large PA viscosity causes an increased resistance to rotor movement leading to an increased torque.

For the non-reactive system, there is an increase in torque by about 4 times. The reactive system shows a higher torque peak as compared to the non-reactive system (Fig. 4.5). The increase is now also due to the reaction taking place between the PA and the maleic anhydride grafted onto the PS. The reaction creates large copolymer molecules and cross-linked interfaces. This increases the resistance to the torque.



(a)



(b)

Fig 4.7

A non-reactive and reactive blend of PA330 and PS666D. The weight fraction of PS is 20% and the mixer was rotating at 125 rpm. (a) non-reactive and (b) reactive PA/PS. The SEM scans were taken at the end of the run, i.e. when the torque attained a constant value. Reaction causes a sharp decrease in the dispersed phase particle diameter. Both pictures have the same magnification. There is also a change in the final morphology. We obtain a much finer morphology for the reactive system as compared to the non-reactive system.

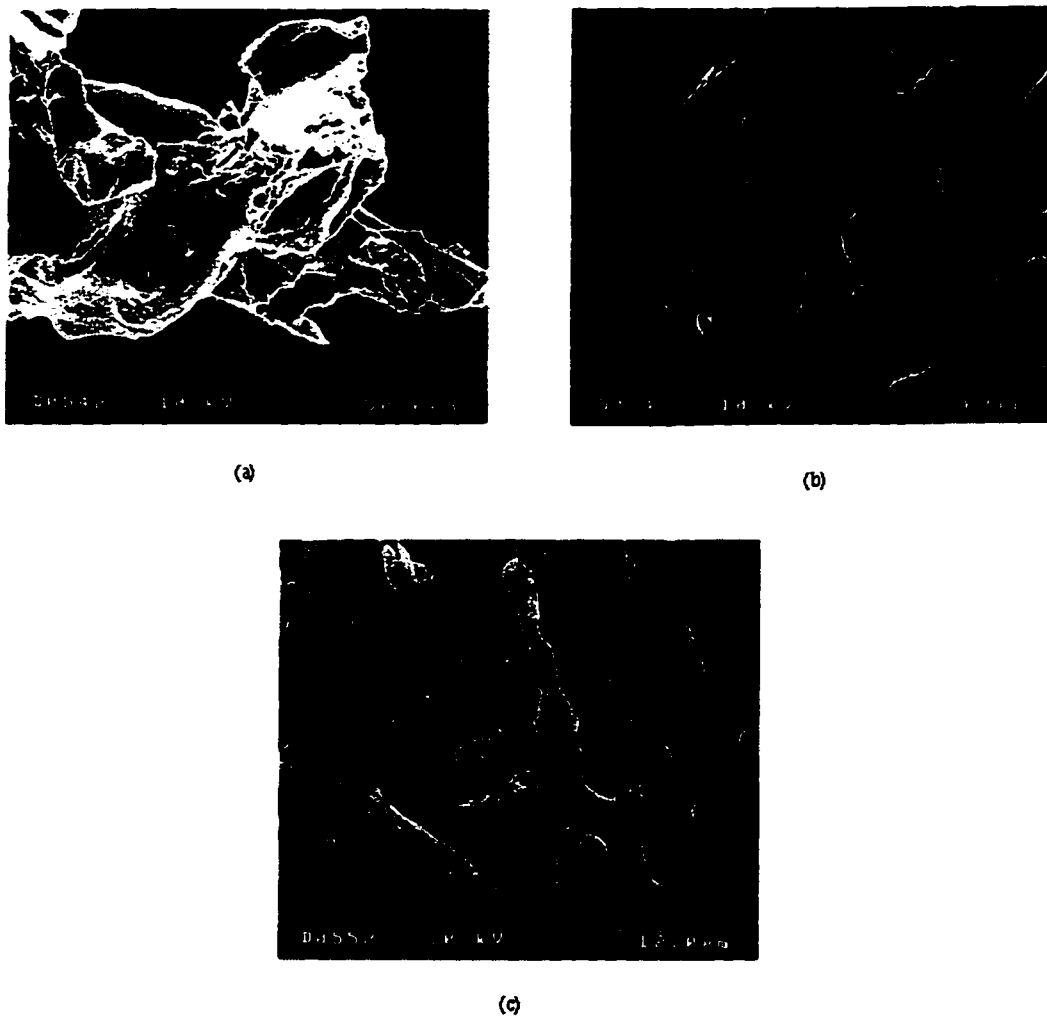


Fig 4.8.
PS morphology at different times after dissolving out the PA330 from the blend sample. The blend studied was PA330/PS=80:20 mixed at 125 rpm. The PA was dissolved using 95% formic acid (HCOOH). (a) After 7 minutes of mixing, a PS sheet is shown. (b) After 7.5 minutes of mixing, the PA pellets are starting to deform and the holes represent the dissolved PA. The PS is still the continuous phase. (c) After 9.25 minutes of mixing, the PS is now the dispersed phase. However, the PS has not yet reached a final dispersed particle morphology.

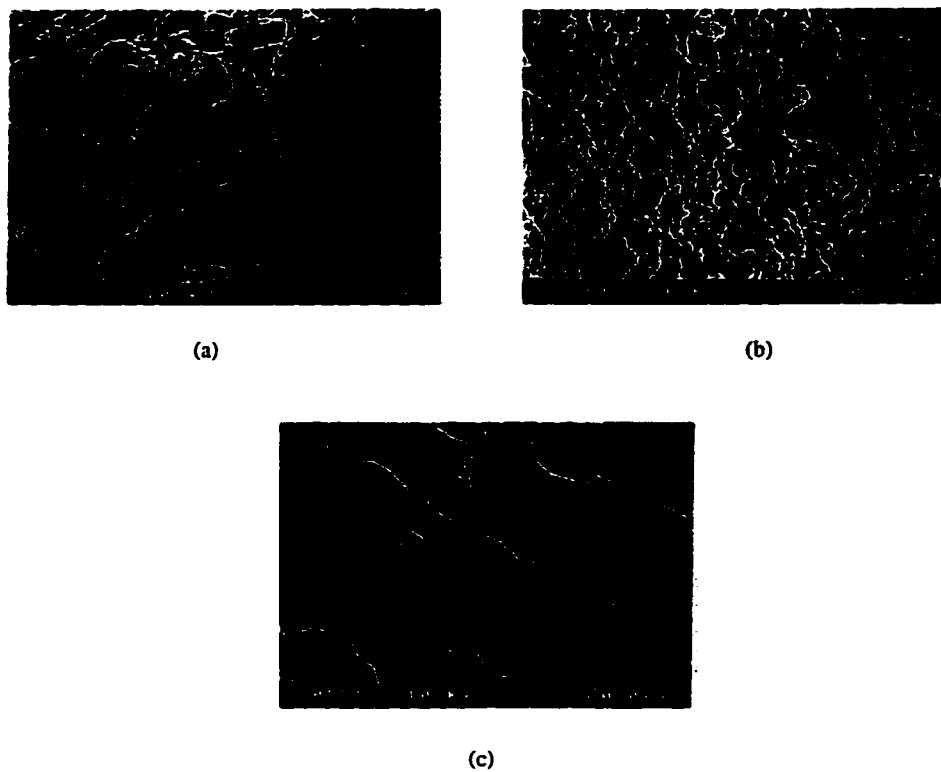


Fig 4.9.
PA morphology at different times after dissolving out PS from the blend sample. The blend is PA330:PS=80:20. The PS is dissolved using methylene chloride (CH_2Cl_2). (a) After 7.5 minutes of mixing, the PA pellets were broken up by sheet formation. The temperature at this point is around 135°C . The PA starts deforming and sheets are peeled from the surface. (b) After 9.25 minutes of mixing, phase inversion has occurred and the PA is the continuous phase. But the PS is still not completely dispersed (Fig. 4.5.a). (c) After 10.5 minutes of mixing, the torque becomes steady as a final morphology is attained.

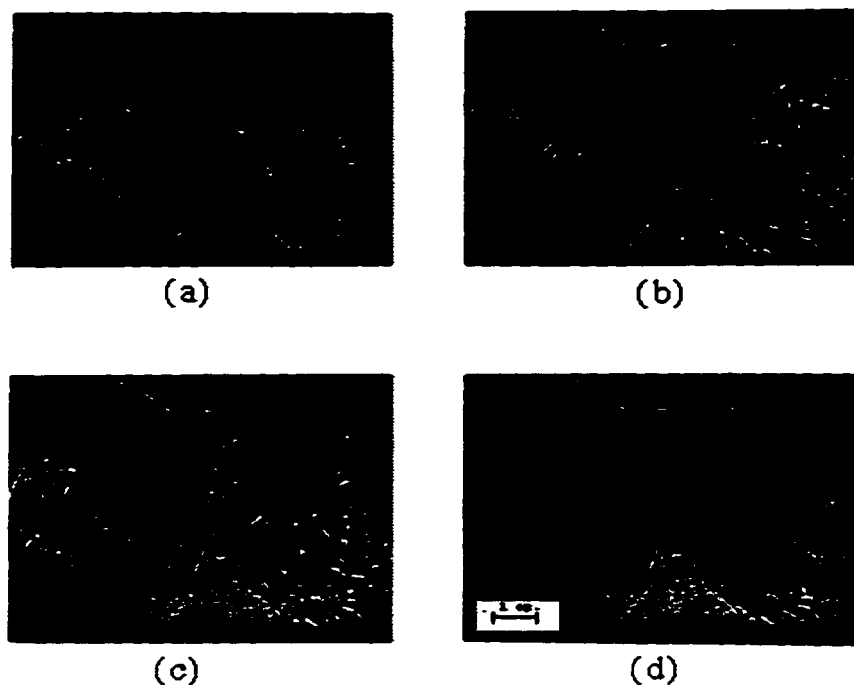


Fig. 4. 10

Snapshots of the mixer glass window showing the different physical regimes of the phase inversion process. The system shown is PA/PS (80/20 blend) mixed at 125 rpm with the temperature ramped from 80 - 180°C at a rate of 5°C/min. (a) The PS has melted and covered the PA pellets (T=118°C). The torque shows a small peak (Fig. 4.6). (b) The PA pellets soften and start deforming (T=125°C). (c) The phase inversion has occurred at this point. PA coalesces to form the major phase (T=145°C). The torque passes through a maxima. (d) A viscoelastic fluid phase is observed (T=160°C) and the torque reaches a steady value. All pictures are at the same magnification.

**Transition material*

The phase inversion occurs during this regime as the torque peaks. During this regime, the PA coalesces together to form the continuous phase. The morphologies of each of the two phases are shown in Fig. 4.8 (c) and Fig. 4.9 (b). The PS still was not completely dispersed and a fibrous PS structure criss-crosses the entire sample. However, at the same stage, the PA sample shows a matrix with hole-like structures. These holes are the sites where the fibrous structure of PS was present. The torque for the non-reactive case showed a peak of 4000 m gm-f whereas the reactive system had a peak of 4500

m.gm-f. The reactive system had a broader peak since reaction delays inversion (Sundararaj *et al.*, 1996).

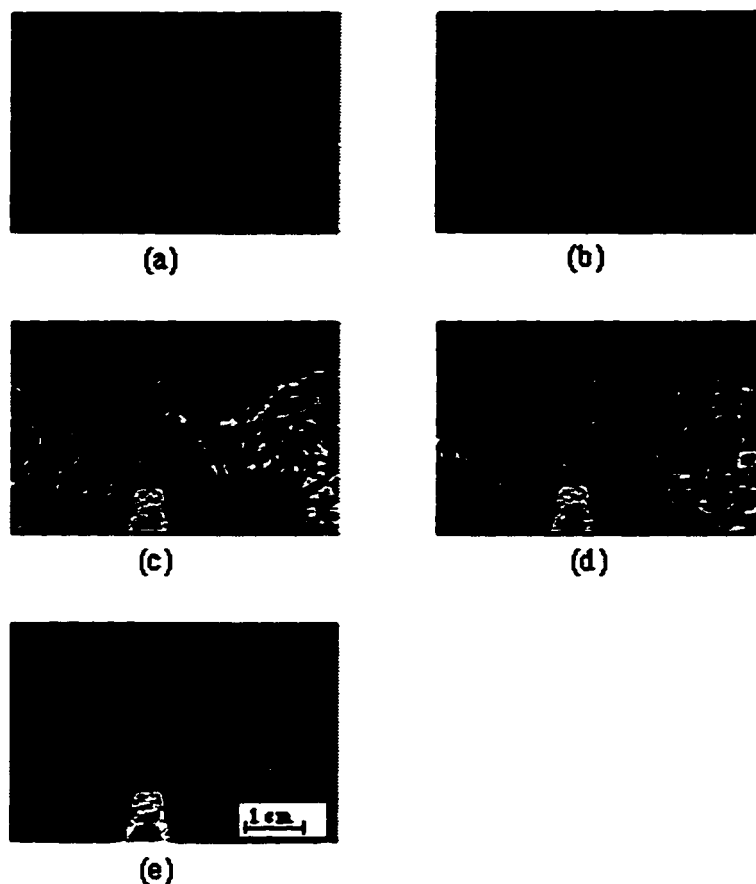


Fig. 4.11
Snapshots of the mixer glass window showing the different physical regimes of the phase inversion process. The system shown is PA/PSMA (80/20 blend) mixed at 125 rpm with the temperature ramped from 80 - 180°C at a rate of 5°C/min. (a) The PS has melted and covered the PA pellets (T=125°C). (b) Same as (a) but the PS has now completely covered the PA. (c) The PA is softening at this point and the pellets become more transparent (T=150°C). (d) The inversion and reaction proceed within the mixer (T=165°C). The torque has reached a maximum. The torque range during this maxima is a lot more than that for the non-reactive system (Fig 4.6). (e) A uniform viscoelastic fluid is observed (T=200°C). All pictures are at the same magnification.

**Viscoelastic fluid*

After phase inversion, the mixture is like a viscoelastic fluid with no solid characteristics. The viscosity of the matrix phase decreases with time (since the temperature is being ramped) and this decreases the resistance on the roller blades and the torque decreases. However, it still takes some time for the PS to attain its final steady drop size. These observations are consistent with those reported by Shih (1992). The development of morphology was captured using the glass plate for the reactive and the non-reactive systems (PA/PS and PA/PS-MA). Fig. 4. 10 and Fig. 4.11 show the different physical regimes seen for the non-reactive and the reactive systems respectively.

The effect of ramping rates on the torque profile was studied. Three different ramping rates were chosen for a 80:20 PA/PS blend mixed at 50 rpm. The ramping rates were 1, 2, and 5 °C per minute. Fig. 4.12 (a) and (b) give the torque versus time and torque versus temperature profiles of all the runs performed. The effect of shear rate on the torque profile was also studied. The same system of PA/PS was blended at different rotation rates. The torque and temperature plots are shown in Fig. 4.13 (a) and (b). The effect of changing the dispersed phase concentration on the phase inversion was studied for the PA330/EPMA system (Fig. 4.14). The weight percentage of the dispersed phase was varied and the resulting torque profiles were analyzed.

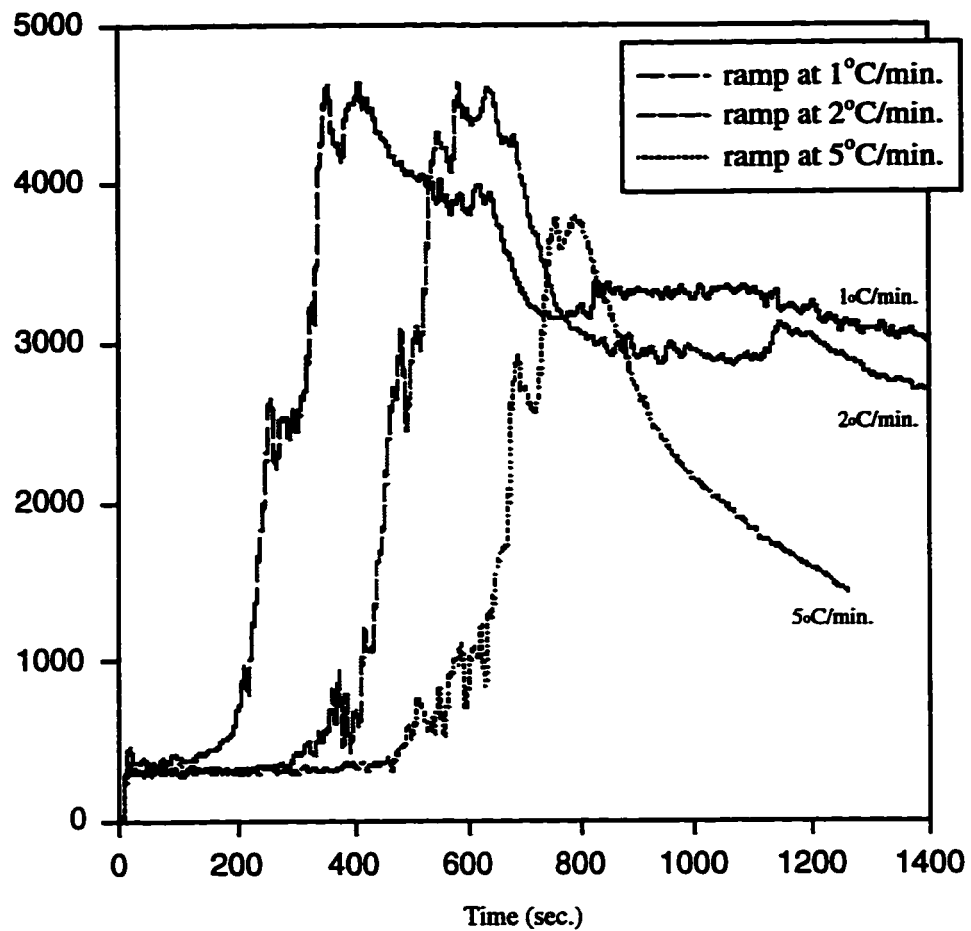


Fig 4.12 (a)
 Effect of ramping. The torque versus time curves for the 80:20 PA330/PS666D blends mixed at three different ramps. The temperature was ramped from 80-180°C at rates of 1, 2, and 5°C/min. and the rotor was kept at 50 rpm.

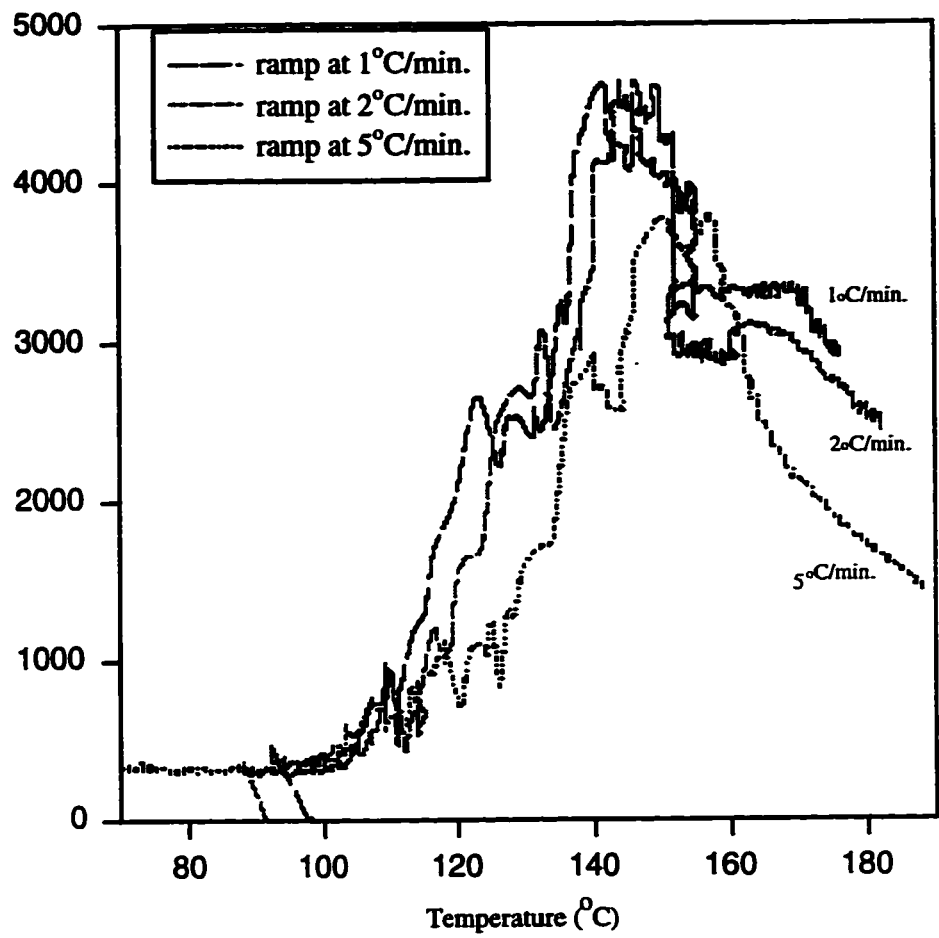


Fig 4.12 (b)
 Effect of ramping. The torque versus temperature curves for the 80:20 PA330/PS666D blends mixed at three different ramps. The temperature was ramped from 80-180°C at rates of 1, 2, and 5°C/min. and the rotor was kept at 50 rpm.

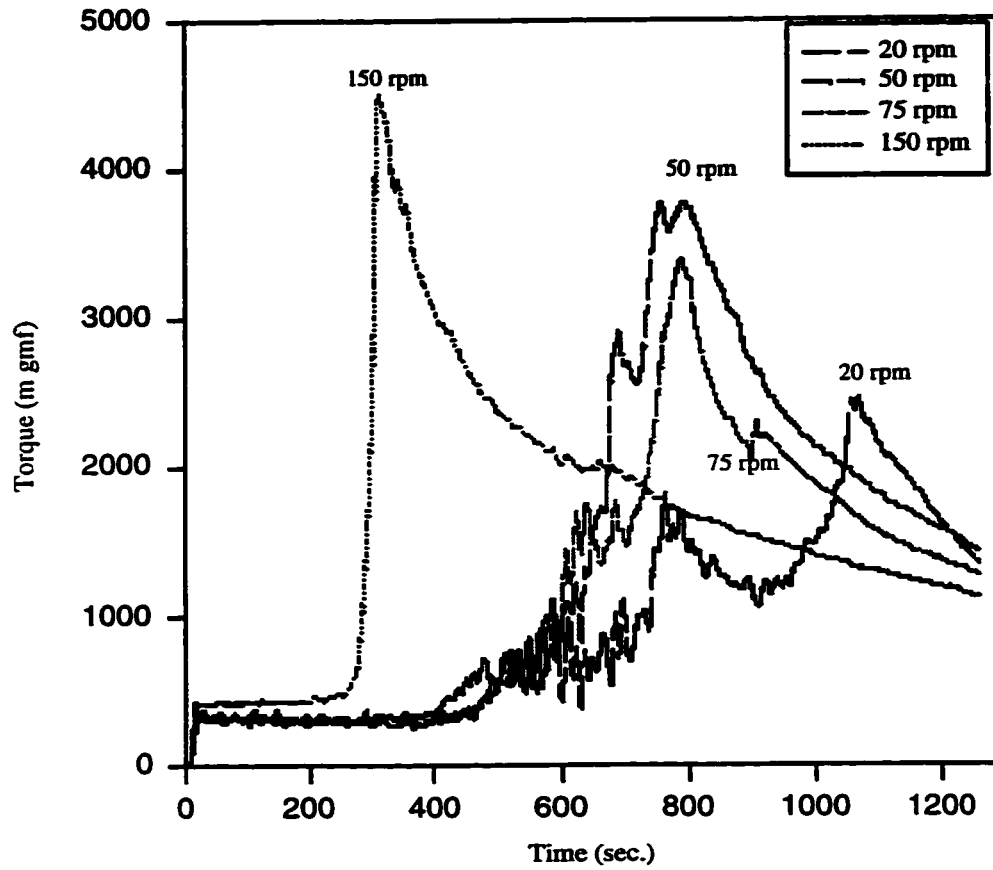


Fig 4.13 (a)
 Effect of shear rate. The torque versus time profile for 80/20 PA330/PS blends mixed at four different rotation rates and ramped from 80-180°C at a rate of 5°C/min.

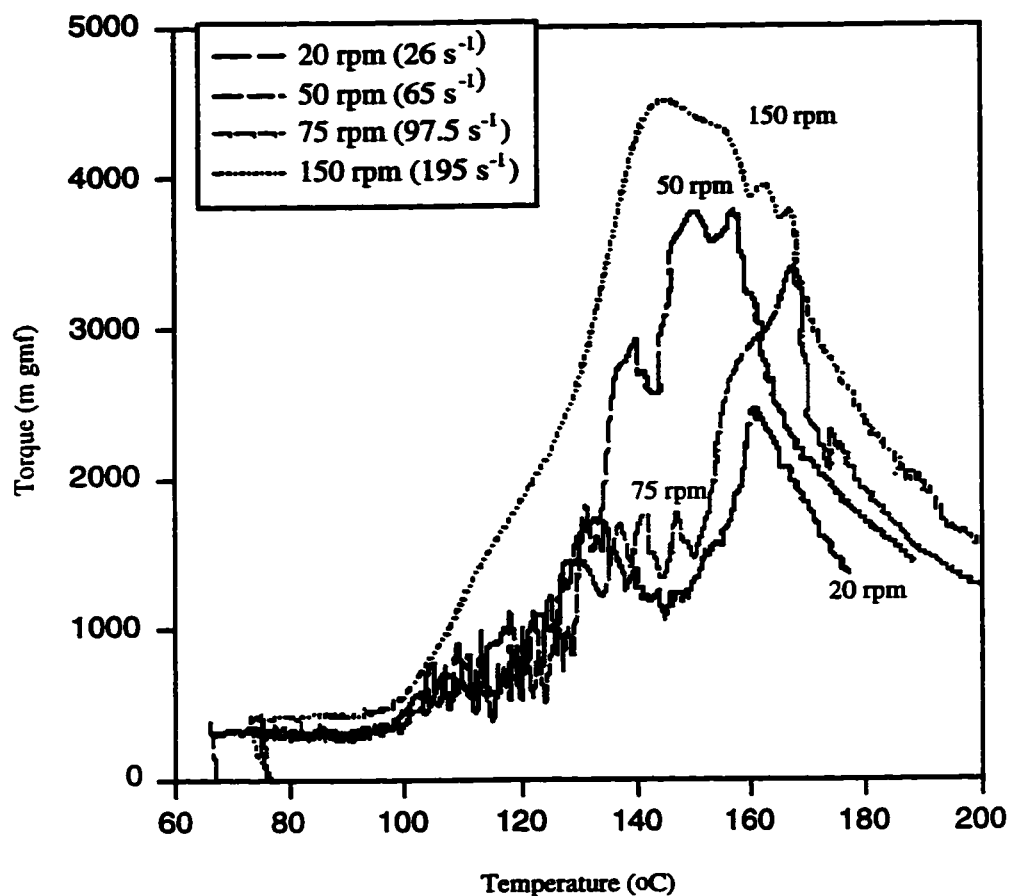


Fig 4.13 (b)
Effect of shear rate. The torque versus temperature profile for 80/20 PA330/PS blends mixed at four different rotation rates and ramped from 80-180°C at a rate of 5°C/min.

The non - phase inverting system studied was a blend of polycarbonate (PC) and polyetherimide (PEI). To clearly observe the melting and break up of the polymers, the temperature was ramped slowly (2°C/min.) and the rotation rate was 10 rpm. This allowed the pellets to be observed in detail. The dispersed PEI pellets were yellow in color and thus, were distinct from the PC pellets. Fig. 4.15 shows the torque and temperature

profiles plotted versus time and Fig. 4.16 shows the photographs of the blend in the mixer at different times during the mixing run.

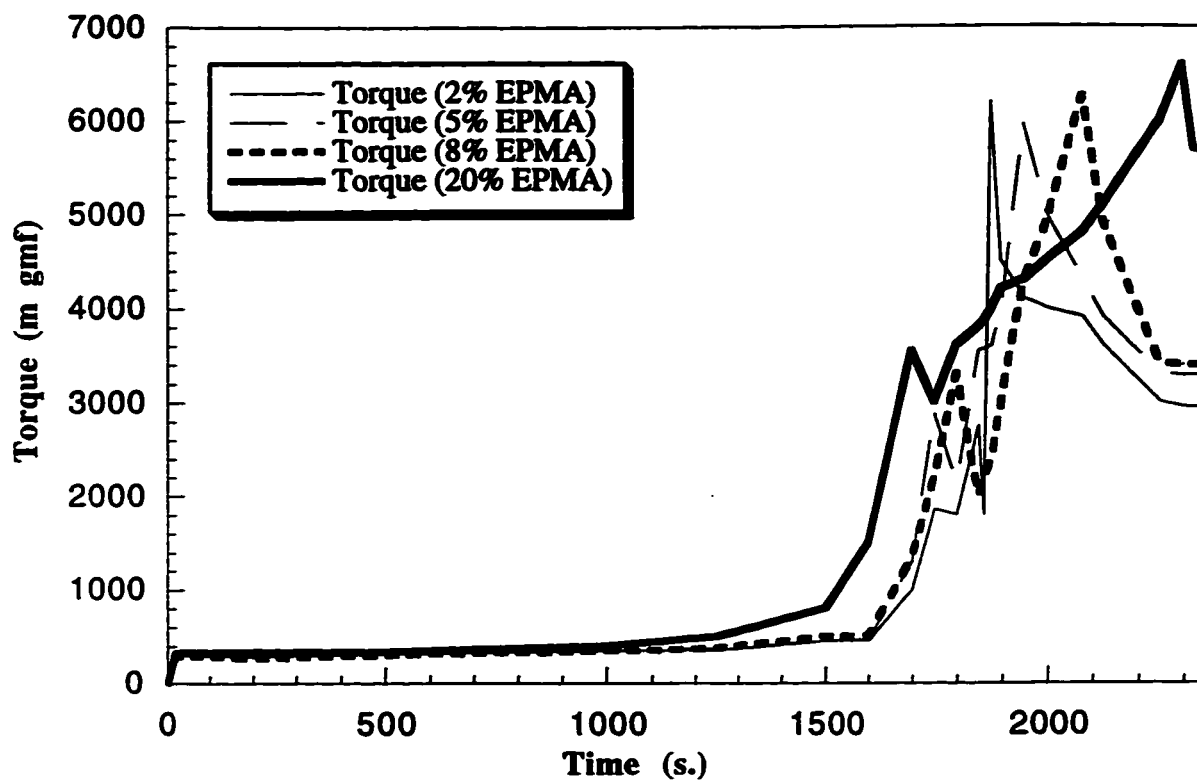


Fig 4.14 Torque profile for the PA330/EPMA blends. The effect of weight fraction of the dispersed phase was studied by changing EPMA concentration. All blends were made at 50 rpm and by ramping the temperature from 90 - 160°C at a rate of 2°C/min.

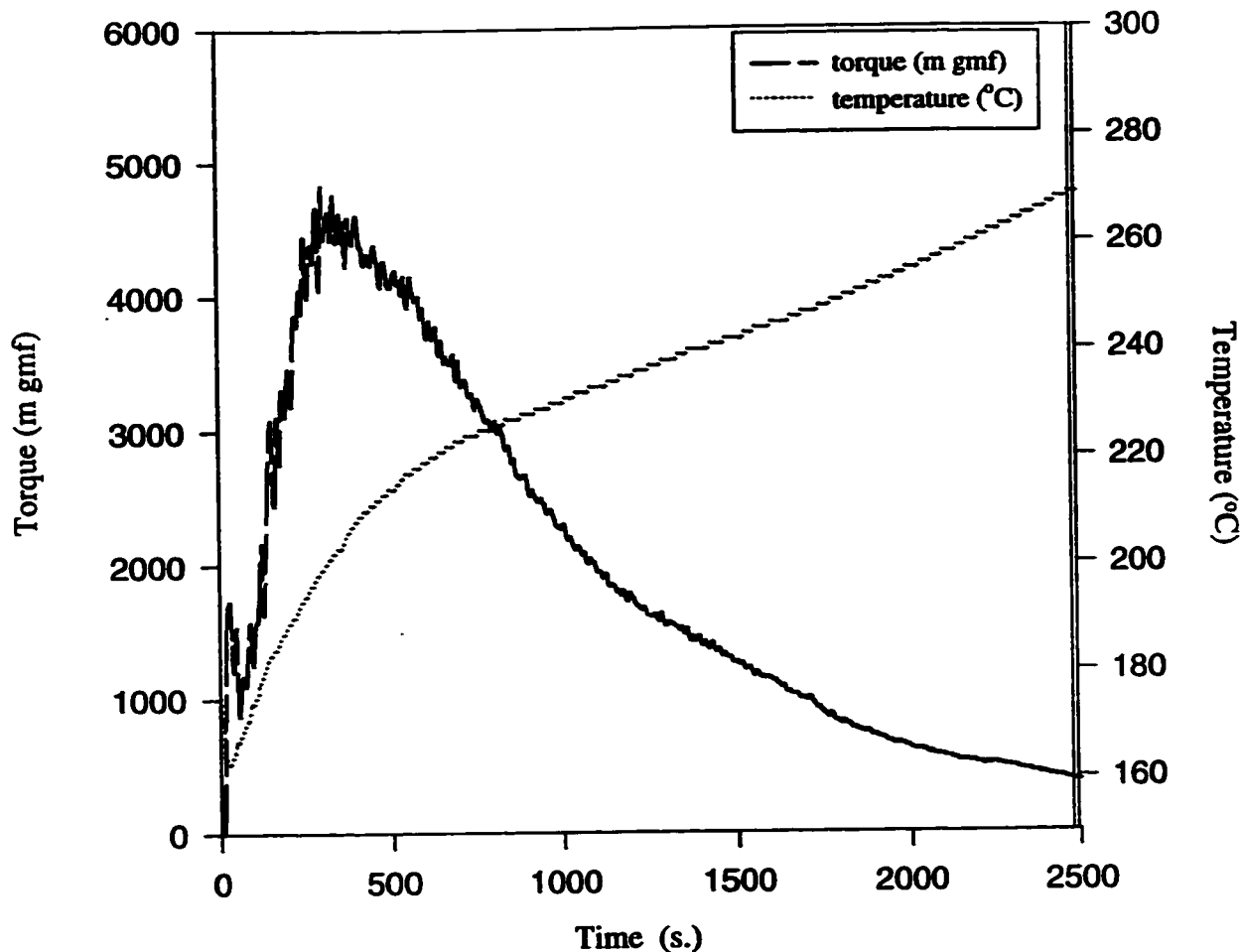


Fig 4.15
Torque and temperature profiles for the PC/PEI blend (80/20). The mixing was done at 10 rpm and the temperature ramped from 200 to 300°C at a rate of 2°C/minute.

4.5. Discussion

The advantage of performing a temperature ramping over an isothermal run is the isolation of torques corresponding to the melting of the two phases. During an isothermal run, the two torque peaks are smeared into one. It is very difficult to observe the melting of the dispersed phase and hence a lot of valuable information is lost. Hence, all the runs were performed by ramping the temperature at a certain rate.

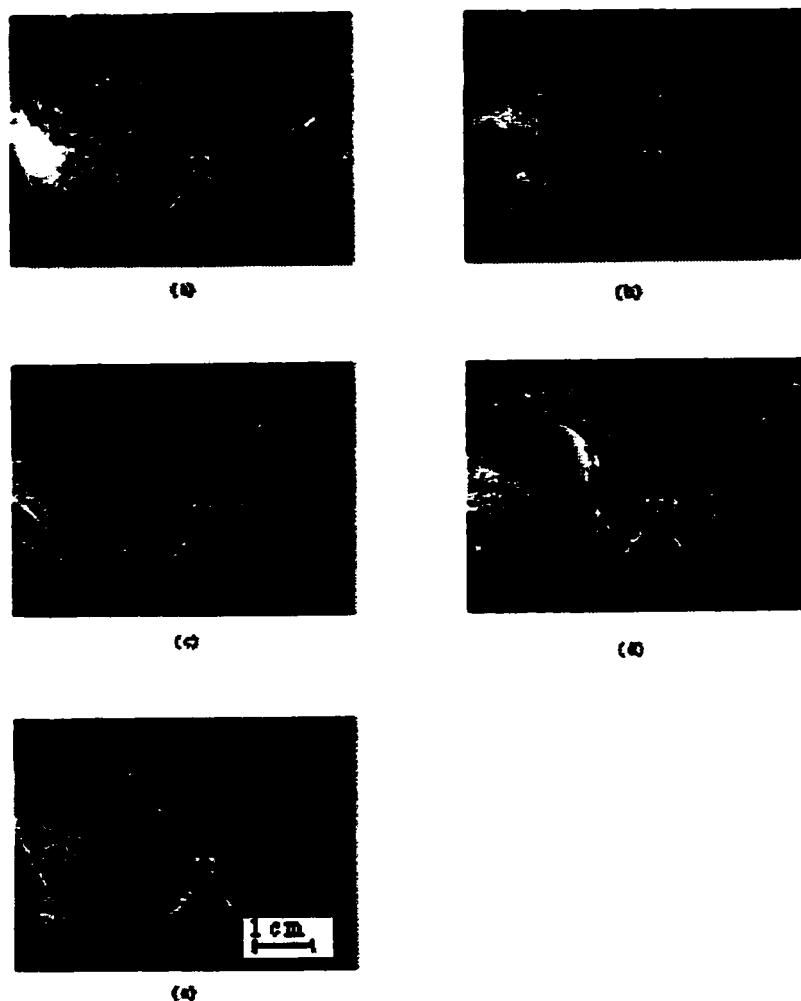


Fig 4.16
 Snapshots of the glass front plate during mixing of an 80:20 PC/PEI blend. The mixing is done at 10 rpm and the temperature ramped from 200-300°C at a rate of 2°C/min. (a) The major phase (PC) is starting to melt, thus forming the major phase (T=190°C). (b) The PS has completely melted and covered the PEI (T=220°C). (c) The PEI has started to soften and this causes some of the pellets to elongate (T=230°C). (d) The PEI is melting and going into the PC phase. Some yellow (PEI) drops can also be seen in the picture. (e) A uniform viscoelastic fluid is observed.

It is very important to understand the step by step morphology development during the phase inversion process since this can be used to set extrusion parameters. Initially both the polymers were added to the mixer in pellet form. The temperature in the mixer was kept constant at 80°C when the material was added. The mixer was kept at 80°C for one minute before ramping. After one minute, the temperature was ramped at a set rate.

As the temperature reached the softening point of PS, there was an increase in torque. PS has a glass transition temperature of 100°C. The pellets start softening at around 95 °C (temperature recorded by the thermocouple). As the PS starts to soften, sheets of PS are pulled off from the pellet surface. The torque rise is dependent on the amount of PS, its viscosity and the shear rate.

PS becomes the continuous phase and pellets of PA are dispersed inside PS. Due to the melting of the polymer, there is increased friction between the material being sheared and the walls of the mixer. This leads to viscous heating of the material and the temperature rises above the set value. When the temperature reaches 125 °C, the PA starts to soften and deforms by the sheeting mechanism. There is a rapid increase in torque since the blend has a majority of PA. The temperature remains nearly constant during the melting of the PA phase. The PA was seen to rapidly deform over a span of less than 15 seconds. At this point, the PS is still the continuous phase but the concentration of PA in the melt is increasing steadily.

The onset of melting of the dispersed phase is different for PS versus PSMA5% (Fig. 4.5). PS melts earlier than PSMA5%. The reactive polystyrene has a glass transition temperature of around 120°C. This is the reason for the lag seen in the torque profiles of the reactive system in Fig. 4.5 and Fig. 4.6. However, the regime of PA melting has the same qualitative behavior for the reactive and the non-reactive system. For the non-reactive system, this transition takes place between 120 and 135°C. However, for the reactive system, the same transition occurs between 145 and 155°C. This is partly because the PSMA melts later than the PS. A molten polymer is a much better conductor of heat than a solid polymer. When the PS melts, it efficiently transfers heat to the PA and hence, the PA reaches its softening point quickly. The torque for the non-reactive system reaches a maximum of around 4000 m.gm-f whereas the reactive system peaks at 4500 m gm-f.

As the PA phase melts, the interaction among the PA particles increases. As more and more of PA particles collide with each other, they start coalescing. After a certain

point, the particles agglomerate to such an extent that PA forms the continuous phase and PS becomes the dispersed phase. The torque profile shows a plateau during this regime. The SEM picture for the non-reactive system (Fig. 4.8(c)) showed that the PS phase had not reached a final dispersed drop structure. The PS was present in the form of elongated fibers and large drops. The PA was the continuous phase but the PS was not dispersed as drops. However, the structure was not co-continuous.

The inversion temperature increased from 150°C for the non-reactive system to around 170°C for the reactive system. The inversion torque peak value also increased from 3800 m gm-f (meter gram force) to about 4600 m gm-f. We observed two peaks during inversion of the reactive system. The first peak observed during the reactive run (Fig. 4.6) is because of the reactive stabilization of the interfacial layer and the second peak is due to the resistance offered by the major phase against inversion. Reaction forms a copolymer at the interface and stabilizes the major phase. When the major phase pieces try to coalesce, the stabilized interface prevents coalescence. Hence, additional mechanical energy is required to overcome the copolymer barrier present. This causes the torque peak to have a higher magnitude than the non-reactive case (Fig. 4.6). The major phase remains as a dispersed phase for a much longer time and the phase inversion is delayed.

The phase inversion occurs at a temperature of about 145°C for the non-reactive case. The non-reactive system shows a dual peak (Fig. 4.6) when torque was plotted versus temperature. This means that the phase inversion is not as rapid and occurs slightly after the melting of the PA phase. One reason for this is the higher viscosity of the PA phase. PA has a viscosity of about 10 kPa.s at a shear rate of 65 s⁻¹ whereas PS has a viscosity of 950 Pa.s at the same shear rate. The PA phase cannot coalesce easily since the polymer is not very mobile. As a result, there is a time interval (after melting) during which the temperature increases due to the viscous heating. The viscosity decreases during this time because of the rise in temperature. This leads to a sufficiently high mobility of the PA phase enabling coalescence and phase inversion to take place. Similar behavior is seen

for the reactive case except that for the reactive system, there is an additional peak due to the reaction.

The morphology of the PA phase immediately after inversion is shown in Fig. 4.9(b). The PA had formed the continuous phase and we could observe holes corresponding to the PS particles which had been dissolved. However, the size of the PS holes was much larger than the final diameter that was observed at the end of the run. In addition, the surface seen in the micrograph is coarse compared to the final morphology. The PS phase is depicted in Fig. 4.8(c). Many elongated fibers were observed which meant that the PS was not in the form of holes. As the shearing continued, the fibers broke up into drops. The final morphology of the blend can be seen in Fig. 4.9(c), which shows the PA phase after 10 1/2 minutes of mixing (a minute after inverting). The size of the dispersed phase (the holes in the micrograph) was very close to the final steady dispersed diameter (1.9 μm).

The effect of temperature ramping rate on the phase inversion was studied for the 80:20 PA/PS system. Fig 4.12(a) and (b) show the torque profiles for the blends made by ramping at three different rates. The curves obtained for all three ramping rates are similar to each other. One common observation among all the three curves was the presence of a shoulder on the torque profile just after the melting of the PS. The shoulder appears at a temperature of 130°C to 140°C which is near the softening temperature of PA. Thus, the small shoulder (Fig. 4.12.(a)) may be the start of the melting process of the PA. The shoulder appears much more clearly in Fig. 4.12.(b) when the torque is plotted versus the temperature. However, this shoulder does not appear at the same temperature for different ramping rates. It is observed that a faster ramping rate shifts the profile to the right, i.e. to a higher temperature or to a later time. This was unexpected since the melting points of the polymers should not change with the ramping rates. So the only conclusion that we can draw is that the melt thermocouple shows a lag in measuring the actual melt temperature inside the mixer. Viscous dissipation causes the melt temperature to be greater than the

temperature near the wall. At a higher ramping rate, the temperature inside the mixer is increasing rapidly and the effect of viscous dissipation is relatively less. For a lower ramping rate the melt temperature will increase greatly due to viscous dissipation and vary from the temperature at the wall. Hence, the thermocouple placed near the wall displays a value lower than that actually inside. Hence, the same material will seem to “melt” at a lower temperature for a lower ramping rate. As a result, the torque profiles are shifted to the left for low ramping rates.

The magnitude of the torque peak decreased with increasing ramping rates. A faster ramping causes a quicker decrease in viscosity. This causes a decrease in the resistance offered by the polymer to the rotating mixer blades and thus a small torque. The torque peak is quite similar for the 1°C and the 2°C per minute ramps but it decreases significantly for the 5°C per minute ramp.

The rotation rate of the mixer also has an affect on the inversion. Fig. 4.13(a) and (b) show the torque versus time and torque versus temperature plots for the PA/PS system ramped at the same rate but at different rotation rates. The melting of the two homopolymers is clearly distinguished for the 20 rpm rotation rate. For the 150 rpm rotation rate, the two peaks are indistinguishable and the mixing more or less resembles that for isothermal mixing.

An interesting phenomenon in the PA/PS system was that the viscous heating caused a huge increase in the melt temperature from the set value. Even though the temperature was only ramped from 80-180°C, the melt temperature reached around 220°C at the end of the run. The large heat generated is due to the high viscosity of the PA (major phase) which is being sheared. The amount of viscous heat generated is greater for a higher rotation rate.

A high shear rate causes more frictional resistance when the polymer starts to melt. Thus, for the 150 rpm rate, the temperature rises at a faster rate as the material starts to melt. As seen in Fig. 4.13(b), the torque peak for the 150 rpm mixing is greater than that

for the smaller rotation rates and the inversion occurs at an earlier time for the higher rotation rates (Fig. 4.13(a)). However, the inversion peak occurs at 160°C for all four rotation rates (Fig. 4.13(b)). The small deviations seen in the melting temperature for the four rotation rates (Fig. 4.13(b)) was probably due to the lag in the measurement of temperature by the thermocouple (as explained earlier).

The effect of weight fraction of the dispersed phase on phase inversion was studied in the PA330/EPMA system. The glass transition temperature of EPMA is -80°C. However, it is a crystalline material and hence, the relevant transition occurs at the melting point of 90°C. As the weight fraction of EPMA increases, the phase inversion occurred at a later time (Fig. 4.14). As the EPMA minor phase concentration increases, the PA330 domains are further separated and cannot coalesce quickly. The magnitude of torque peak during phase inversion is nearly the same for all weight fractions.

The glass plate was used to visualize non-phase inverting systems. The motivation was to observe the break up of the polymer pellets and understand the morphology development in the batch mixer. Fig. 4.15 shows the torque and temperature profiles plotted versus time for the 80/20 PC/PEI blends. The temperature was ramped at a slow rate (2°C/min) and the mixer was rotated slowly to enable better visualization. Fig. 4.16 shows the snapshots of the mixer window at different times. The different melting and mixing regimes have been shown sequentially.

The temperature initially drops and then rises steadily within the first minute (Fig. 4.15). The drop in temperature is due to the addition of cold pellets to the mixer. The torque initially rises when the pellets are fed to the mixer and then decreases sharply. The PC starts softening at a temperature of about 190 °C. Since the ramping is done at a slow rate, it takes time for the entire major phase to soften and break up. Fig. 4.16(a) shows a snapshot of the mixer when the PC is starting to melt while PEI remains rigid. As the pellets melt, they are broken up in the shear field. The PEI pellets are yellow in color and

hence, there is good contrast between the two phases. The PC becomes a sea with the PEI pellets dispersed in it.

All the PC melts at 220 °C and this corresponds to the peak in the torque curve. The PEI is still present as pellets inside the PC matrix (Fig. 4.16(b)). The PEI starts softening at 230°C. The melting of PEI could be determined from the torque profile (Fig.4.15). There is a change in the slope of the torque versus time. Fig. 4.16(c) shows the softening of the PEI pellets. The PEI pellets stretch and elongate. The picture shows irregular shapes of the PEI within a uniform viscoelastic fluid. At this point, the PEI pellets are drawn out and sheets are peeled off from the pellet surface. The torque continues to decrease steadily since increased temperature leads to lower viscosity.

Fig. 16(d) shows the PEI being dispersed into the major phase ($T = 250^{\circ}\text{C}$). The color of the mixture started to turn yellow at this stage. The torque continued to decrease at a constant rate and the temperature continued to increase. The morphology of the dispersed phase at this stage is a mixture of PEI drops, fibers and sheets in a matrix of PC. The final consistency of the blend is shown in Fig.4.16(e). The blend was a homogeneous viscoelastic fluid as the PEI is completely dispersed in PC. The color of the blend was homogeneous and yellow at this stage. The torque reached a steady value of about 500 m. gm-f.

4.6. Conclusions

The glass plate constructed onto the mixer front wall was able to capture the different transition states during phase inversion. The phase inversion could not be clearly distinguished when the blending was done isothermally. Hence, the temperature was ramped at a designed rate so that the melting of each polymer and the different rheological regimes could be distinguished (Sundararaj *et al.*, 1996; Shih, 1992). The phase inversion is delayed as the weight fraction of the dispersed phase increases. Increasing the temperature ramping rate also delays the phase inversion process. The inversion peak was pronounced for the smaller rotation rates.

A large difference was observed in the phase inversion process between reactive and non-reactive systems. Reaction causes the torque peak during inversion to broaden and also causes an increase in magnitude of the peak. The morphology development was analyzed by dissolving one of the phases and observing the other. The transitions between the different regimes visualized during mixing were correlated with changes in the torque curves.

4.7. References

- Bourry, D.; Favis, B. D., 1995 SPE Annual Technical Conference (ANTEC '95), Soc. Plast. Eng. (SPE), 2001 (1995).
- Favis, B. D.; Chalifoux, J. P., *Polymer*, **29**, 1761 (1988).
- Favis, B. D.; Lavallee, C.; Derdouri, A., *J. Mater. Sci.*, **27**, 4211 (1992).
- Fortelny', I.; Kovar, J., *Eur. Polym. J.*, **28**, 85 (1992).
- Jordhamo, G. M.; Manson, J. A.; Sperling, L. H., *Polym. Eng. Sci.*, **26**, 517 (1986).
- Metelkin, V. I.; Blehkt, V. S., *Colloid J. USSR*, **46**, 425 (1984).
- Miles, I. S.; Zurek, A., *Polym. Eng. Sci.*, **28**, 796 (1988).
- Molau, G. E., *J. Polym. Sci., A*, **3**, 1267 (1965).
- Paul, D. R.; Barlow, J. W., *J. Macromol. Sci.-Rev. Macromol. Chem.*, **C18**, 109 (1980).
- Scott, C. E., Ph. D. Thesis, University of Minnesota (1990).
- Shih, C. K.; Tynan, D. G.; Denelsbeck, D. A., *Polym. Eng. Sci.*, **31**, 1670 (1991).
- Shih, Chi-Kai, *Adv. Polym. Tech.*, **11**, 223 (1992).
- Shih, Chi-Kai, *Polym. Eng. Sci.*, **35**, 1688 (1995).
- Sperling, L. H., in "Interpenetrating Polymer Networks and Related Materials" Ch. 2, Plenum press, New York (1981).
- Sundararaj, U.; Macosko, C. W.; Rolando, R. J.; Chan, H. T., *Polym. Eng. Sci.*, **32**, 1814 (1992).^a
- Sundararaj, U.; Macosko, C. W.; Shih, C. K., *Soc. Plast. Eng. Tech. Papers*, **50**, 1802 (1992).^b
- Sundararaj, U., Ph. D. Thesis, University of Minnesota (1994).

Sundararaj, U.; Dori, Y; Macosko, C. W, *Polymer*, **36** (10), 1957 (1995).

Sundararaj, U.; Macosko, C. W.; Shih, C. K., *Polym. Eng. Sci.*, **36**, 1769 (1996).

Utracki, L. A., *J. Rheol.*, **35**, 1615 (1991).

van Krevelen, D. W., in "Properties of Polymers" Chap. 3, Elsevier, Amsterdam, 1976.

CHAPTER 5

FUTURE EXPERIMENTS AND RECOMMENDATIONS

5.1 Future Experiments

5.1.1 Prediction of polymer blend morphology

In Chapter 2, the dispersed phase particle diameters were measured for a number of systems. For the PS/PP system, the weight percent of the dispersed phase and the shear rate were changed, and the dispersed phase diameter was measured. The other systems were studied only by modifying the shear rate but at a constant dispersed weight fraction. All the runs were made at the same temperature. The changing of temperature will have a large effect on the component viscosity and thus will affect the final morphology. A range of temperatures should be chosen and experiments performed under the same conditions of weight percentage and shear rate.

All the blends were prepared on the Haake Rheocord mixer. The results obtained may be dependent on the mixer geometry. The force balance used had only one parameter corresponding to the mixer dimensions, the shear rate. To generalize these results, the same blending studies should be performed on different mixing equipment like a twin - screw extruder. If the results corroborate, the force balance will have even greater credibility.

The force balance was based on several assumptions. One of the assumptions was the replacement of the proportionality constant between the opposing forces with unity. As a result, only a qualitative prediction of the diameter could be obtained. Studies should be undertaken to obtain these proportionality constants. This will also enable us to obtain a predicted diameter for all systems.

5.1.2 Factorial Design to predict particle diameter

The drop diameter was predicted using the force balance. An empirical formula can also be designed to obtain the dispersed diameter. For this, an experimental design should be set up where statistical tools are used to obtain the effects of different parameters. The

design is called as “factorial design” and it is better than a one - parameter design where the effect of each parameter is studied separately. In the factorial design, all the crucial parameters that have an effect on the particle diameter are chosen. A lower (-) and a higher (+) value of each parameter is chosen. The factorial design gives the interaction effects of parameters in addition to single parameter effects. From the magnitude and the importance of each effect, we can design an empirical equation to obtain the particle diameter as a function of all the factors. The factorial design also helps to indicate major trends and so gives a direction for further experimentation (Box *et al.*, 1978).

Some work has been done by our group to obtain a statistical model of the mixing in a batch mixer by studying the PE/PS system. The response studied was the dispersed phase (PS) particle diameter and the parameters affecting the response were shear rate, temperature of mixing and the weight fraction of the dispersed phase. This is called a 2^3 factorial design and Table 5.1 gives the representation of the runs made.

From the measurement of average particle diameters for all the 8 runs described above, we measured the single parameter effects and the interaction effects. These effects are then placed in increasing order and plotted on a normal probability paper. This is called a “normal plot”. If none of the parameters has any effect on the response, then all points will lie on a straight line about zero. Fig. 5.1 shows a normal plot of a PE/PS system as described in Table 5.1.

Table 5.1 Experimental model of a 2³ factorial design for a PE/PS system.

test condition number	temperature (°C)	weight % (% PS)	shear rate (s ⁻¹)
1	-	-	-
2	+	-	-
3	-	+	-
4	+	+	-
5	-	-	+
6	+	-	+
7	-	+	+
8	+	+	+

	Temp. (°C)	weight % PS	shear rate (s ⁻¹)
-	180	2	75
+	220	8	150

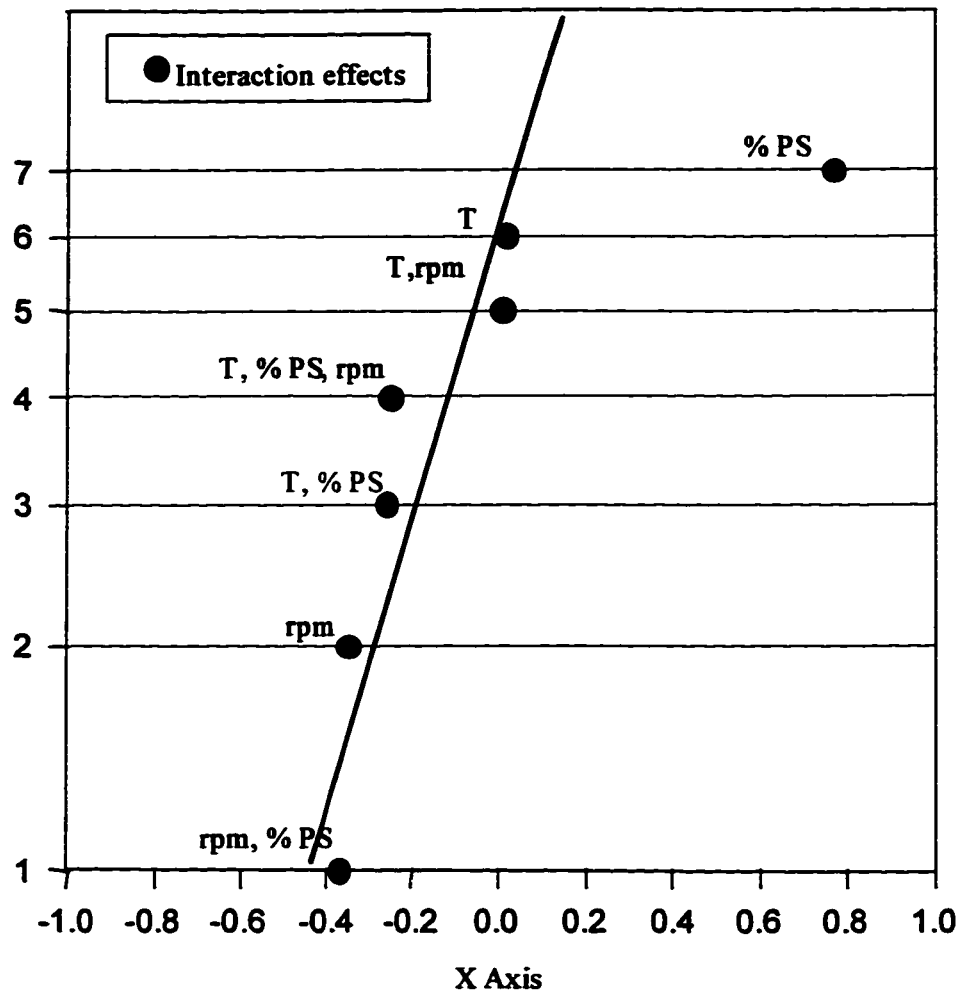


Fig 5.1
Normal Plot for PE/PS system showing the interaction effects.

The biggest effect on drop diameter is due to the weight % of PS. However, there are many parameters that have not been investigated and factorial design can help us determine the important ones.

5.1.3 Partial Least Squares

Another statistical tool that can be applied to obtain a prediction for particle diameter is Partial Least Squares (PLS). This tool can help in determining the factors that have the

greatest influence on the diameter of the dispersed phase. A list of all the factors that are thought to be important is made. From the experimental runs, we obtain the values of each factor and write these values in a matrix form. The matrix equation that we get is of the type:

$$[A] * [X] = [Y] \quad (5.1)$$

where A is an $m \times n$ matrix in which 'n' stands for the number of factors and 'm' stands for the number of experiments; Y is an $m \times 1$ matrix which contains the particle diameter values; and X is the unknown matrix ($n \times 1$) which will give the effect of each factor. PLS is a tool that analyzes this matrix. The solution matrix X (given by PLS) contains numerical values corresponding to the 'n' factors. From the relative values of each factor, we can get the influence that it has on the dispersed phase diameter.

PLS also gives an empirical equation to calculate the dispersed phase diameter. Thus, we can predict the particle diameter (within a certain error margin) given the numerical values of all the relevant parameters. The success of this model depends on the number of data points used in making it, i.e. the more data points used, the better is the model.

5.1.4 Extensional flow

The Haake batch mixer has a complex flow behavior and hence, modeling such a flow is difficult. The force balance used to predict the diameter of the dispersed phase (in Chapter 2) uses only a simple steady shear force for deforming the drop. The steady shear component is given by $\eta_m \dot{\gamma}$ and this is the only force considered in the force balance. However, the polymer also experiences extensional flow and the deformation caused due to this force should also be accounted for more accurate predictions.

In an extensional flow, it is frequently observed that the viscosity increases with increasing extension rate. This phenomenon is referred to as *extensional thickening* (Macosko, 1994). The time-dependent uniaxial extensional viscosity is defined as

$$\eta_u(t, \dot{\epsilon}) \equiv \frac{T_{11}(t, \dot{\epsilon}) - T_{22}(t, \dot{\epsilon})}{\dot{\epsilon}} \quad (5.2)$$

where T_{11} and T_{22} are the principal tensile stresses and $\dot{\epsilon}$ is the steady extension rate. As a result, the extensional force that should be incorporated into the force balance is $\sim \eta_u * \dot{\epsilon} * \pi R^2$, where πR^2 is the cross-sectional area of the particle. These values have to be measured using an extensional viscometer. The incorporation of this force into the force balance should improve the accuracy of the results.

5.1.5 Compatibilization studies

Chapter 3 deals with the effect of order of addition of the blend components on the compatibilization of polymer blends. Four different addition orders were selected and their effects were studied for the PS/PMMA and the PS/LLDPE system. There were three diblocks of PS-PMMA, one diblock of P(S-E/P) and two triblocks of P(S-EB-S). Future experiments should be performed by compatibilizing with other copolymers having different molecular weights so that we can obtain a better understanding of the effect of molecular weight of the compatibilizer.

There is some skepticism about the S-E/P and the S-EB-S compatibilizing the PS/LLDPE system. Even though the PS block may stabilize the PS phase, the EP and the EB blocks may not compatibilize the LLDPE. There is a chance that the compatibilizer may form micelles in PS. To test this, we should perform transmission electron microscopy (TEM) on the PS/LLDPE systems and get a quantitative estimate of the micellization. Ruthenium tetroxide (RuO_4) can be used to preferentially stain the PS.

Even for the PS/PMMA system, a better quantitative estimate of the compatibilization can be achieved by performing TEM. Ruthenium tetroxide (RuO_4)

vapors can be used to selectively stain the PS and not the PMMA. The PS-PMMA diblock may also form micelles. Observation of the compatibilizer via TEM will help determine the amount of copolymer needed for stabilization.

The experiments with different orders of additions provided some understanding of the compatibilization process. It will be interesting to visually observe the melting of the components and the dispersion of the compatibilizer. The visualization experiment was performed even for compatibilized blends, but it was difficult to see the copolymer in the mixture. A very powerful camera that has a strong focus even at very high magnifications is needed. This could be placed in a manner that will help us in observing the compatibilizer as it goes into the mixture.

5.2 Recommendations

5.2.1 Image Analysis

To quantify the morphology, the dispersed phase particle diameter was measured. Some modifications can be made to the algorithm used in measuring this diameter. The NIH software used does not recognize a particle directly from a scanned image of the micrograph. Hence, to measure the particle diameter, the particles from the SEM micrograph were traced. This tracing may introduce some error in the final value of particle diameter. An alternate method to eliminate the tracing procedure is by directly opening the micrograph in the image analysis software. But this job is tedious and may not include all the particles. Other modifications should be devised to get an accurate diameter. Some additional more sophisticated software may enable better particle recognition.

5.2.2 Visualization experiments

The visualization of the mixing operation was done using a glass front plate which was designed by our group at the University of Alberta. Even though the glass plate was successful in observing the dispersion, there were some drawbacks in its design which need to be corrected. The temperature could be more uniform throughout the front plate. There is a temperature gradient which should be eliminated if possible. The temperature at

the center of the mixer (near the indent between the blades) is at a higher value than that near the glass. As a result, some pellets near the glass melt later. This problem can be eliminated by using better conducting material or by putting the heater rods closer to the glass slab.

The glass slab is enclosed on one side by a back plate. There will be some gap present corresponding to the back plate thickness. In our case, this gap is large enough for a pellet to get stuck in between. This will cause some error as there will be a few pellets stuck to the glass which do not get a chance to mix with the entire blend. It is recommended that the design be modified so that the gap is less than 1.5 mm (i.e. too small for a polymer pellet to get stuck in).

5.2.3 General Procedural modifications

The sample from the batch mixer was quenched in liquid nitrogen to freeze the morphology. This quenching process should be as fast as possible to get accurate results. In our experiments, the time between stopping the mixer and the actual quenching of the sample was approximately 15 seconds. Even in 15 seconds, there can be some change in the blend morphology. The maximum amount of time is lost in opening the mixer itself. One recommendation is to use a valve in the mixer front plate itself, which will be closed during the actual run, but when the run stops, a sample can be withdrawn by opening the valve. The use of different blade type (*e.g.* sigma blades) might also aid the mixing process. A comparison of different mixers can be done.

5.3 References

Box, G. E. P.; Hunter, W. G.; Hunter, J. S., "Statistics for Experimenters", Ch.10, John Wiley and Sons, New York, 1978.

Macosko, C. W., "Rheology Principles, Measurements, and Applications", VCH Publishers, Inc., New York (1994).

APPENDIX A

CALCULATION OF SAMPLE WEIGHT

The blends that were made in our research were made by weighing out the pellets of each component before blending. We calculated the sample weights based on the weight fraction of each component. It is crucial to have optimum mixing in the Haake Rheocord mixer. Thus, the volume of polymer pellets added to the mixer is critical.

In order to determine the optimum volume of material to be added, Scott (1990) studied the mixing by adding various masses of polystyrene. At 180°C, the amount of polystyrene that gave optimum mixing was 55g. This corresponded to approximately 54 cm³ volume of material in the mixer. As a result, for all of our experiments, the sample amount to be added to the mixer was calculated with a basis that the total volume at the operating temperature was 54 cm³.

Polymer Densities as Functions of Temperature

The densities of the polymers used in this study were estimated using the methods and data presented by van Krevelen (1976). The molar volumes of the polymers are used to obtain the weights of samples. These molar volumes are calculated by obtaining the molar volume at 25°C and then using the molar thermal expansivity, E, to calculate the molar volume at any desired temperature.

$$E = \left(\frac{\partial \bar{V}}{\partial T} \right)_p \quad (\text{A1})$$

E for polymers does not change to a large extent above and below the glass transition temperature. Therefore, for amorphous polymers which are glassy at room temperature, the molar volume can be calculated using:

$$\text{for } T < T_g: \bar{V} = \bar{V}_g(298K) + E_g \cdot (T - 298) \quad (\text{A2})$$

$$\text{for } T > T_g: \bar{V} = \bar{V}_g(298K) + E_g \cdot (T - 298) + E_r \cdot (T - T_g) \quad (\text{A3})$$

In case of an amorphous polymer which is rubber at room temperature:

$$\text{for } T < T_g: \bar{V} = \bar{V}_r(298K) + E_r \cdot (T_g - 298) + E_g \cdot (T - T_g) \quad (\text{A4})$$

$$\text{for } T > T_g: \bar{V} = \bar{V}_r(298K) + E_r \cdot (T - 298) \quad (\text{A5})$$

\bar{V}_g (298 K) and \bar{V}_r (298) are the molar volumes of the polymer at 298 K, glassy or rubbery. E_g and E_r are the molar thermal expansivities of the polymer in the glassy and rubbery states, respectively.

The sample calculations are given for some of the polymers used during this thesis:

Polystyrene:

At room temperature, polystyrene is a glassy amorphous solid. Beyond its glass transition temperature (100°C), it becomes rubbery. The molar volume of PS at 100°C (373 K), \bar{V}_g , is obtained from the Van der Waals volume, V_w , which is calculated using the group contribution method given by van Krevelen (1978).

$$\bar{V}_g (298K) = 99.48 \text{ cm}^3/\text{g mol}$$

$$E_g = 281 \times 10^{-4} \text{ cm}^3/\text{mol/K}$$

$$E_r = 629 \times 10^{-4} \text{ cm}^3/\text{mol/K}$$

At the processing temperature of 200°C (473 K), the molar volume is calculated as

$$\begin{aligned} \bar{V} &= 99.48 + 0.0281 (473 - 298) \text{ cm}^3/\text{g mol} \\ &= 104.40 \text{ cm}^3/\text{g mol} \end{aligned}$$

Polyethylene:

$$T_g = -78^\circ\text{C} = 195 \text{ K}$$

$$\bar{V}_r (298) = 32.8 \text{ cm}^3/\text{g mol}$$

$$E_r = 205 \times 10^{-4} \text{ cm}^3/\text{mol/K}$$

At the processing temperature of 200°C (473 K), the molar volume is calculated as:

$$\begin{aligned}\bar{V} &= 32.8 + 0.0205 (473 - 298) \text{ cm}^3/\text{g mol} \\ &= 36.39 \text{ cm}^3/\text{g mol}\end{aligned}$$

Polypropylene:

$$\begin{aligned}T_g &= -10^\circ\text{C} = 263 \text{ K} \\ \bar{V}_r(298) &= 49.5 \text{ cm}^3/\text{g mol} \\ E_r &= 307 \times 10^{-4} \text{ cm}^3/\text{mol/K}\end{aligned}$$

At room temperature, PP is a rubbery amorphous polymer. Hence, at the processing temperature of 200°C (473 K), the molar volume is calculated as:

$$\begin{aligned}\bar{V} &= 49.5 + 0.0307 (473 - 298) \text{ cm}^3/\text{g mol} \\ &= 54.87 \text{ cm}^3/\text{g mol}\end{aligned}$$

In a similar manner, the molar volumes of all the polymers used was calculated and at the operating temperature. The formula for PS was also used for the PS-Ox used in Chapter 2. Similarly, the formula for polyethylene was also used for EP and EPMA.

For optimum mixing, the volume of the material added to the mixer should be 54 cm³. The molecular weights of PS and PP are

$$\begin{aligned}M_{PS} &= 104.1 \text{ g/gmol} \\ M_{PP} &= 42.1 \text{ g/gmol}\end{aligned}$$

The total density of the polymer blend is calculated as follows:

$$\frac{M}{V} = \frac{M_{PS}}{w_{PS} \cdot \bar{V}_{PS}} + \frac{M_{PP}}{w_{PP} \cdot \bar{V}_{PP}} \quad (\text{A6})$$

where w_{PS} and w_{PP} are the weight fractions of the polystyrene and polypropylene respectively. The total mass of polymer needed is obtained by

$$M_{total} = 54 \text{ cm}^3 * \frac{M}{v}$$

Thus, we can calculate the weights of each homopolymer that should be added to the mixer.

References

Scott, C. E., Ph D Thesis, University of Minnesota (1990).

van Krevelen, D. W., "Properties of Polymers", Ch. 4, Elsevier, Amsterdam, 1976.

APPENDIX B
CALCULATION OF AVERAGE PARTICLE DIAMETER
OF THE DISPERSED PHASE

One of the key factors in this thesis has been the measurement of the average diameter of the dispersed phase. A sample calculation of average diameter of the dispersed phase is given here. The system studied is PS666D/PP3050 and the SEM micrograph analyzed is for a 92:08 PS666D/PP3050 blend prepared by mixing in the Haake mixer rotating at 75 rpm and at an operating temperature of 200°C.

The SEM micrograph is shown in Fig B1. The picture shows holes and particles of PP dispersed inside a matrix of PS. The two phases are clearly immiscible and we can see the phase separation clearly.



Fig B1
SEM micrograph of a 92:08 PS666D/PP3050 blend prepared at 200°C in a mixer rotating at 75 rpm.

The magnification is shown on the micrograph itself. The dotted line measures 3 cm or 30 mm. Our measurements also include the measuring of hole diameters because the holes represent the particles that have fallen off due to poor adhesion between the phases. In order to measure each diameter, our procedure involved the tracing of each and every particle on a transparency. We have tried to be as accurate and fair as possible in marking out each and every particle. In cases where a particle appeared blurred or unclear in any way, the discretion of the analyzer was used.

Fig B2 shows a scanned image of the SEM micrograph shown in Fig B1 where the particles are marked out on a transparency. Some error is incorporated by this method because of human limitations. However, on an average, this error might be damped because of the huge amount of particles measured for a single sample. Usually, around 200 - 300 particles were measured for a single sample.

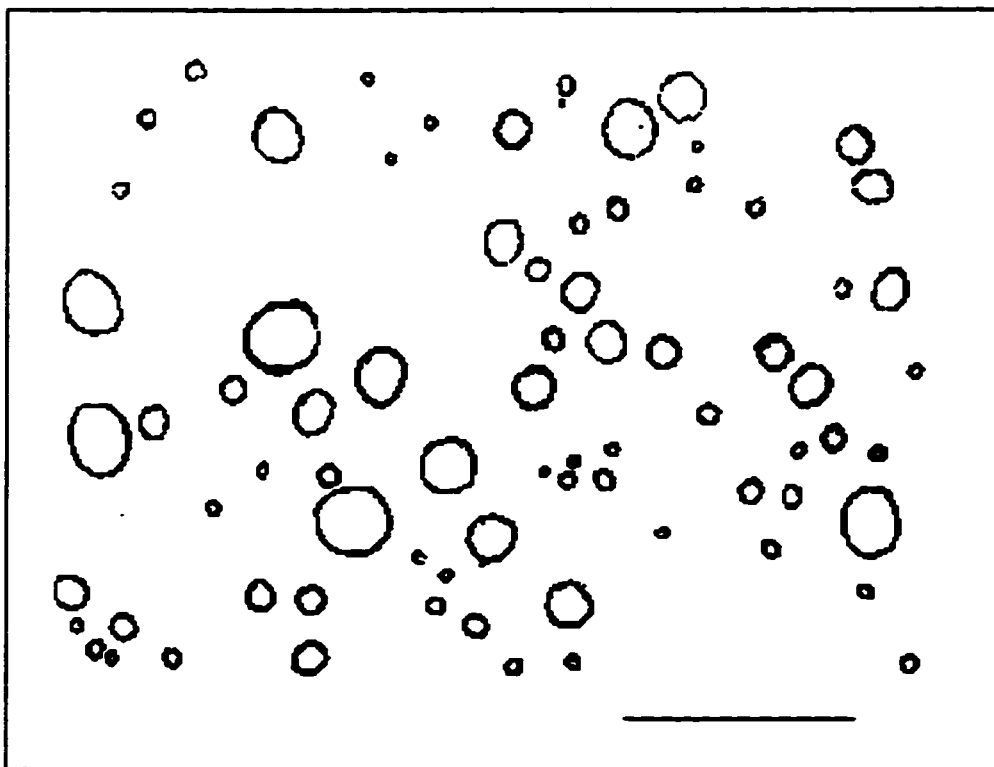


Fig B2
Picture showing the particles marked out from Fig B1.

The image in Fig B2 was analyzed using software in our lab. The software used for analysis is called “NIH Image 1.58b33 f” developed by the National Institute of Health. The straight line shown on the bottom right of Fig B2 is the magnification that was used by the NIH program to measure the area of each particle. The program scans the image, marks the areas occupied by each particle and calculated the area of each particle. To calculate the particle diameter, we have to use a different software because NIH does not measure the particle diameter.

The results from the NIH Image analysis were saved and analyzed using Microsoft Excel. Table B1 shows the calculations done using Microsoft Excel to calculate the particle diameter. The table shows the area and diameter of each particle measured. The average diameter and the standard deviation has also been shown.

Table B1. Area and Average diameter of each particle measured from Fig B2.

Area (μm^2)	Dia. (μm)	Area (μm^2)	Dia. (μm)
0.3039	0.62220074	0.7266	0.96208373
0.251	0.56546019	6.738	2.92975076
0.872	1.05395827	1.5458	1.40327188
0.5417	0.83070072	1.0437	1.15306294
0.0793	0.31783503	4.6109	2.4235837
1.1758	1.22386045	0.3039	0.62220074
3.9767	2.25074651	0.3699	0.68644752
0.5549	0.84076095	0.4624	0.7674924
2.1007	1.63586398	0.2774	0.5944542
0.2774	0.5944542	0.2774	0.5944542
0.0132	0.12967377	0.8059	1.01322466
2.1139	1.6409955	0.1718	0.46781781
0.185	0.4854573	0.687	0.93549946
0.1982	0.50247794	0.4888	0.78909769
0.8323	1.02968674	0.9248	1.08539816

0.3435	0.66149801	0.7134	0.95330468
0.1982	0.50247794	7.9139	3.17512225
0.8059	1.01322466	6.2756	2.8274361
0.502	0.79968147	0.3699	0.68644752
0.5549	0.84076095	3.4483	2.09588617
2.6159	1.82547437	0.251	0.56546019
0.872	1.05395827	0.5417	0.83070072
0.872	1.05395827	0.185	0.4854573
5.5225	2.65236345	0.2642	0.58013835
2.1667	1.66136311	1.8893	1.55137088
0.3171	0.63556986	1.3608	1.31662568
2.1667	1.66136311	3.184	2.01396399
2.497	1.78350546	1.3344	1.30379163
0.8059	1.01322466	0.3699	0.68644752
1.744	1.49052207	0.502	0.79968147
2.0082	1.59944258	1.0702	1.16760957
4.3995	2.36737378	0.938	1.09311685
2.7481	1.87103296	0.3171	0.63556986
0.3567	0.6740882	0.5549	0.84076095
2.7481	1.87103296	1.7968	1.51291678
1.1362	1.20307462	0.5549	0.84076095
2.7613	1.87552116	0.3039	0.62220074
0.4756	0.77837001	0.3831	0.6985882
0.5285	0.82051716		

Average Diameter = 1.1577 μm Standard Deviation = 0.3273 μm

The average diameter measured by this method gives the number average value. There are several other average diameters that can be determined and which become significant depending on the application. For example, one of the averages is the area average particle diameter, D_A . From the above table, an average area is obtained and using this average area, an average particle diameter is calculated.

Another average measured is the volume average particle diameter, D_V . Using the diameter of each particle, the volume of each particle is calculated. An average volume is

obtained from which the average particle diameter can be extracted. The magnitude of all these averages will differ because of the large particle size distribution involved in the case of polymers. We have consistently used the number average dispersed phase particle diameter in all the blends studied and hence the results drawn based on the experiments are harmonious.

APPENDIX C

CALCULATION OF SHEAR RATE IN THE MIXER

In Chapter 2, the average diameter of the dispersed phase was measured experimentally for several different shear rates. The Haake rheocord mixer does not measure the shear rate directly. The mixer only controls the speed of the rotor blades moving inside. The shear rate was obtained from the rotation rate by a simple calculation. The maximum shear rate present in the mixer was used for the calculations. The shear rate will be maximum at the point where the gap for polymer flow is minimum. This was determined assuming drag flow in the gap between the mixer blade and the barrel. Fig. C1 shows one half of the mixer barrel with one rotor. The minimum gap was measured (2 mm).

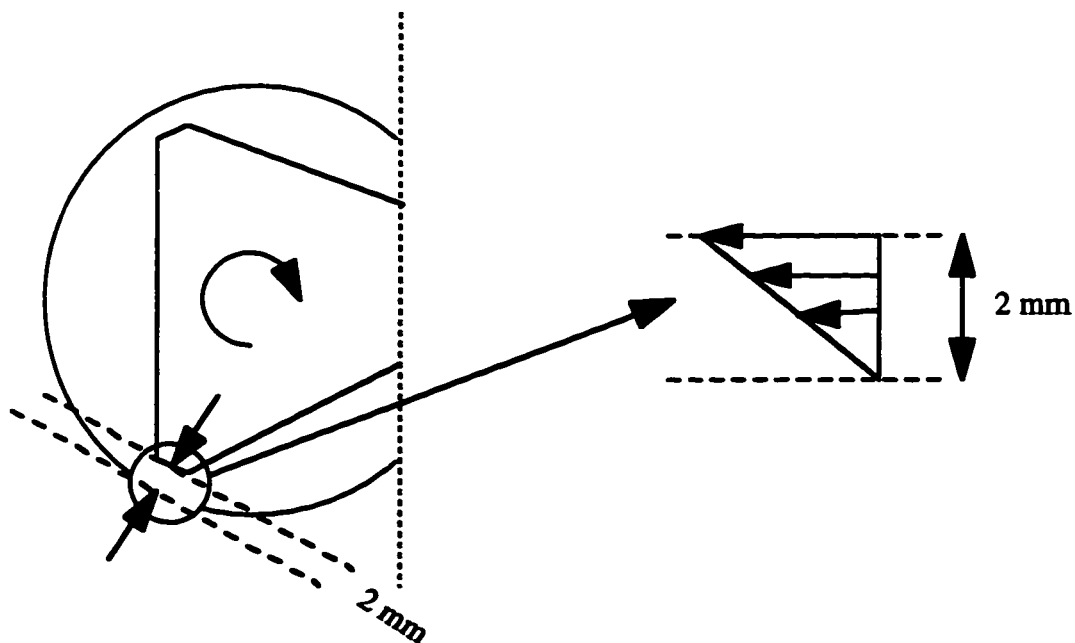


Fig C1
Mixer barrel showing the velocity profile used to calculate the shear rate.

The no slip boundary condition was assumed at the barrel wall and mixer blade surface. The shear rate is obtained by multiplying the rotation rate by 1.3, i.e. for a rotation rate of 50 rpm, the shear rate is 65 s^{-1} .

APPENDIX D

MATERIAL PROPERTIES OF POLYMERS

Tables 2.1, 2.2, 3.1 and 4.1 give the material properties of the different polymers used for blending. The viscosities (η^*) and the elastic moduli of the different polymers were used in the force balance to predict the diameter of the dispersed phase. The measurement of these material properties was done on a Rheometrics Mechanical Spectrometer (RMS - 800). In the RMS, the test geometry appropriate to the material to be tested is selected by the user. A certain torsional shear deformation is given to the sample contained between opposing plateaus. The torque and normal force generated in response to the imposed motion (sinusoidal, in angular direction) on the sample is measured by a transducer. The computer calculates stress from these measurements and combines these values with measured sample motion to calculate strain and to generate values of the selected rheological properties.

To calculate the rheological properties used in the force balance, a rate (frequency) sweep was performed. The user programs the frequency limits in radians/second for dynamic measurements. Before performing any frequency sweep, the strain amplitude should be selected in the linear viscoelastic regime. A strain of 10% was found to be in the linear viscoelastic regime for most of the polymers at the temperature under study. Thus, the frequency sweeps were performed at a strain of 10%.

For carrying out the sweep, a cylindrical disc of polymer having a diameter of 25 mm and a thickness of about 2 mm was prepared using a mold and a laboratory press. The parallel plate test fixture was used for all the frequency sweeps. The parallel plates have a diameter of 25 mm. The RMS chamber is heated to the desired temperature and the sample is inserted between the parallel plates. The frequency limits are set prior to start of the run. These limits were from 0.1 - 100 rad/s. Usually three data points were chosen per decade

of frequency. For a particular frequency, the parallel plates are subjected to an oscillating shear and the transducer measures the torque generated due to this shearing.

The properties that were used in the force balance are the complex viscosity of the polymer (η^*) and the elastic moduli (G' s) of the dispersed and matrix phase. Fig.D1 shows a plot of the complex viscosity versus frequency for two of the polymers used, polystyrene (PS) and polypropylene (PP). Fig. D2 shows a plot of elastic moduli versus frequency for the same polymers.

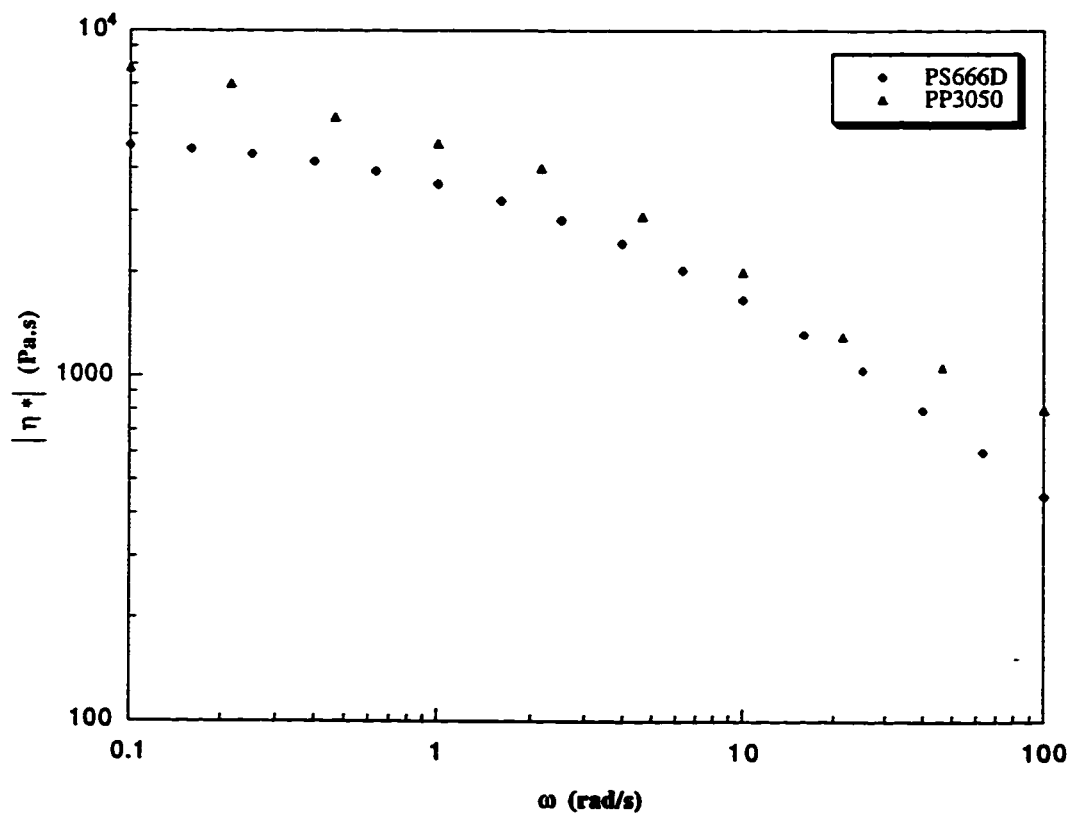


Fig D1
Complex viscosity versus frequency for PS666D and PP3050. The strain used was 10% and the temperature used was 200°C.

The temperature at which these properties were measured is 200°C. From these plots, the values of η^* and G' were evaluated at a value of ω equal to the value of shear rate in the Haake mixer (Chapter 2).

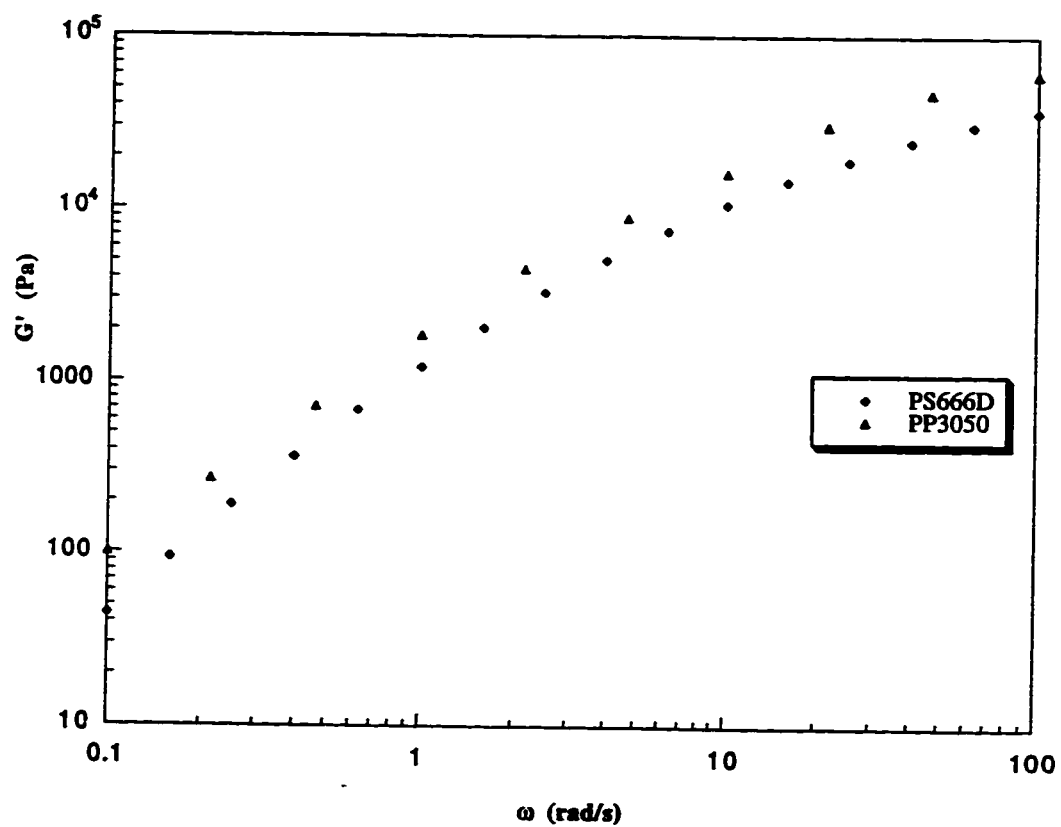


Fig D2
Elastic Moduli (G') versus frequency for PS666D and PP3050. The strain used was 10% and the temperature used was 200°C.

The viscosity measured by the RMS is a dynamic complex viscosity whereas the viscosity used in the force balance is a steady shear viscosity. To compare the two, the Cox - Merz rule (an empirical observation, usually valid) was used. This states,

$$\eta(\dot{\gamma}) \equiv |\eta^*(\omega)| \quad \text{with} \quad \dot{\gamma} \equiv \omega \quad (\text{D1})$$